VŠB - Technical University of Ostrava

Faculty of Safety Engineering

and

1

UFR de physique

DISSERTATION

THESIS COTUTELLE

Ostrava 2010 **Ing. Eva Grigorová**

VŠB - Technical University of Ostrava

Faculty of Safety Engineering

Department of Fire Protection

and

1

UFR de physique

Laboratoire de Physique des Lasers, Atomes et Molécules

Dissertation

Spectroscopic Methods for Concentration Measurements and Calibration of Reactive Gases

Student:	**Ing. Eva Grigorová**
Supervisor (VŠB-TU Ostrava):	**doc. Ing. Zdeněk Zelinger, CSc.**
Supervisor (University of Lille 1):	**prof. Georges Wlodarczak**
Co-Supervisor (University of Lille 1):	**Dr. Stéphane Bailleux**
Study program (VŠB-TU Ostrava):	**Fire Protection and Industrial Safety**
Field of Study (VŠB-TU Ostrava):	**Fire Protection and Safety**
Study program (University of Lille 1):	**, du rayonnement et de l'environnement**
Field of Study (University of Lille 1):	**Optique et Lasers, Physico-Chimie, Atmosphère**
Date of Dissertation submission:	**07. 09. 2006**
Date of Dissertation transmission:	**14. 07. 2010**
Date of defense:	**15. 12. 2010**

Declarations

I affirm that I have written the dissertation myself and have not used any sources and aids other than those indicated.

In Ostrava 14. 7. 2010

…..…….

Signature of student

Acknowledgements

First I would like to acknowledge my supervisors doc. Ing. Zdeněk Zelinger, CSc. and Prof. Georges Wlodarczak, and Dr. Stephane Bailleux for expert and patient guidance of this dissertation, their valuable advice and suggestions; thanks to them a larger scheme originated from tiny results that brought new scientific knowledge to the field of atmospheric chemistry, astrochemistry, and plasma chemistry, and that allowed me to try and understand several spectroscopic methods that I shall deal with in this dissertation.

I would also like to thank other workers and friends from VŠB - Technical University of Ostrava and J. Heyrovský Institute of Physical Chemistry, Academy of Sciences of the Czech Republic in Prague, primarily to RNDr. Ing. Michal Střižík, PhD, Ing. Václav Nevrlý, PhD, Ing. Petr Bitala, Ing. Tomáš Hejzlar, Ing. Hlaváčová Irena, PhD, doc. RNDr. Svatopluk Civiš, CSc., RNDr. Martin Ferus, RNDr. Petr Kubelík, RNDr. Petr Pracna, CSc., Ing. Jan Skřínský, then to Ing. Patrik Kania, PhD, Dr. Roman Matyenko, Prof. Jean Demaison and others who always created pleasant work atmosphere, and were precious mentors to me also. Great thanks also belong to my dear family - Marie, Jiří, Ivana, Tomáš, and Zuzanka Grigorov, and to Mr. Libor Basler for tolerance, support and patience, then to my friends, above all to Bc. Martina Přečková, Jana Holoušková and Libuše Olašinová, Ing. Jerry Newman, M.A.

Abstract

The topic of my dissertation is focused on utilization of spectroscopic methods for detection and measurement of various molecular systems that are interesting from the point of view of their reactivity and role that they play in atmospheric chemistry, astrochemistry, human body, or in simulated plasma processes.

Description of the work is divided into four thematic parts describing four independently performed experiments.

The very first analyses of the asymmetrical vibration ν_4 band and the symmetrical ν_2 band of the $FCO_2^{\cdot}$ radical, that belong among significant intermediate products of degradation processes of halogen hydrocarbons, were performed within this work. The detailed analysis led to determination of rotational constants, centrifugal distortion constants, and fine splitting constants of both bands.

For the first time in history we performed the spectroscopically unambiguous identification of the molecular radical ion $CS^{\cdot+}$ using the microwave spectroscopy with high spectral resolution in the frequency range of 414 to 622 GHz. The complex analysis allowed us to exactly determine the values of the rotational constant and fine splitting constant.

It was also designed and performed experiments including measurements of spectra of cyan BrCN and CH_3CN species using the time resolved Fourier transform infrared spectroscopy. It was studied behavior of these molecules and their disintegration products in the low temperature plasma environment.

Finally, I have studied the ecological impact of ammonia on the environment and influence of trees on the amount of ammonia in the air, and designed and assembled the optoacoustic cell for the experimental arrangement of the laser optoacoustic detection method for measuring trace amounts of ammonia and other gaseous species.

Keywords: spectroscopy, radical, ion, atmosphere, astrochemistry, human health, plasma

Abstrakt

Téma mé disertační práce je zaměřeno na využití spektroskopických metod pro detekci či měření koncentrace rozličných látek, které jsou zajímavé z hlediska jejich reaktivity a role hrající v atmosférické chemii, astrochemii, v lidském těle nebo v simulovaných procesech plazmatu. Popis vlastní práce je rozdělen do čtyř tematických celků, které popisují čtyři nezávislé, uskutečněné experimenty.

Vůbec poprvé byla provedena analýza asymetrického vibračního pásu ν_4 a symetrického pásu ν_2 $FCO_2^{\cdot}$ radikálu, patřícího mezi významné meziprodukty degradačních procesů halogenovaných uhlovodíků. Detailní analýza vedla k určení rotačních konstant, centrifugálně distorzních konstant a konstant jemného štěpení pro oba pásy.

Historicky poprvé byla uskutečněna také první spektroskopicky jednoznačná identifikace molekulového radikálového iontu $CS^{\cdot+}$ pomocí mikrovlnné spektroskopie s vysokým spektrálním rozlišením ve frekvenčním rozsahu 414 až 622 GHz. Celková analýza umožnila přesné určení hodnoty rotační konstanty a konstanty jemného štěpení.

Dále byly navrženy a uskutečněny experimenty zahrnující měření spekter kyanových látek BrCN a CH_3CN časově rozlišenou infračervenou spektroskopií s Fourierovou transformací. Bylo studováno chování těchto molekul a jejich rozkladné produkty v prostředí nízkoteplotního plazmatu.

Nakonec byl studován ekologický dopad amoniaku na životní prostředí a vliv stromů na množství amoniaku v ovzduší a byla navržena a sestavena optoakustická kyveta experimentálního uspořádání metody laser optoakustické detekce pro měření stopových množství amoniaku a dalších plynných látek.

Klíčová slova: spektroskopie, radikál, iont, atmosféra, astrochemie, lidské zdraví, plazma

Synthèse

Le sujet de ma thèse concerne l´application des méthodes spectroscopiques utilisées pour la détection et la mesure de concentration des espèces différentes intéressantes du point de vue de leur réactivité et le rôle dans la chimie atmosphérique, l´astrochimie, dans le corps humain ou dans les process simulés du plasmat.

La description de la thèse elle- même est divisée en quatre ensembles thématiques, décrivant quatre expériences indépendantes.

Pour la première fois a été mise en oeuvre l´analyse de la bande de vibrations asymetrique ν_4 ainsi que de la bande de vibrations du radical ν_2 $FCO_2^{\cdot}$, un des produits intermédiaires importants des process de dégradation des carbures d´halogène. Le résultat de l´analyse détaillée a permis de déterminer des constantes de rotation, des constantes de distorsion de centrifuge ainsi que des constantes de la fine scission pour les deux bandes.

Historiquement pour la première fois a été également effectuée l´identification spectroscopiquement univoque de l´ion de molécule radicale $CS^{\cdot+}$ à l´aide de la spectroscopie de microondes, à différenciation spectrale très élevée et la gamme de fréquence de 414 à 622 GHz. L´analyse globale avec les données infrarouges disponibles a permis de déterminer précisément les valeurs de la constante de rotation et de la constante de structure fine.

Ensuite ont été proposées et effectuées des expériences incluant les mesures des spectres des matières de cyane BrCN et CH_3CN à l´aide de spectroscopie infrarouge différenciée, avec la transformation Fourier. J´ai étudié le comportement de ces molécules ainsi que leurs produits de décomposition dans le milieu du plasma à basse température.

Finalement, j´ai étudié l´impact écologique de l´ammoniaque sur l´environnement ainsi que l´impact des arbres sur la quantité de l´ammmoniaque dans l´atmosphère. Une cuve opto-acoustique de la classification expérimentale de la méthode laser de la détection opto-acoustique a ainsi été conçue pour mesurer les concentrations de l´ammoniaque et d´autres gaz présents en très faible quantité.

Mots- clé : spectroscopie, radical, ion, atmosphère, astrochimie, santé humaine, plasma

Dissertation content

Goals

Dissertation was written in cooperation declared by an international agreement among the VŠB-TU Ostrava, Faculty of Safety Engineering and the 1 in France.

The work consists of a theoretical part with basic principles of spectroscopy and quantum physics outlined, and from a part describing my own work that I performed during my doctorate studies. The theoretical part of dissertation should prove useful to students of VŠB - Technical University of Ostrava and other people interested in spectroscopy experiments that have not encountered this topic before and are interested in study of it.

The first part of the dissertation was done at the 1, in the Laboratoire de Laser, Atomes et Molecules (PhLAM), under supervision of Prof. G. Wlodarczak and Dr. S. Bailleux. The target was to measure and analyze the microwave spectrum of $CS^{\cdot+}$ radical cation, and to analyze the asymmetrical ν_4 and the symmetrical ν_2 rotational-vibrational bands of the $FCO_2^{\cdot}$ radical that are molecules significant from atmospheric and astrophysical point of view.

The second part of my dissertation was done in cooperation between VŠB – TU Ostrava, Faculty of Safety Engineering and J. Heyrovský Institute of Physical Chemistry, AS CR. It was focused on the study of species (NH_3, BrCN, CH_3CN, HCN, and HNC) that are significant from the point of view of astrochemistry, atmospheric chemistry, and human health, by using spectroscopic methods. Target of this part of the work was assembling of the optoacoustic cell for laser optoacoustic detection, whose sensitivity would enable the measurements of even trace amounts of gaseous pollutants and also investigation of decomposition products CH_3CN and BrCN by the time resolved Fourier transform infrared spectroscopy. My supervisor in the Czech Republic was doc. Ing. Z. Zelinger, CSc.

Introduction

All objects found in the Universe, including ourselves and the space around us, consist of atoms that join into molecules through chemical bonds, and that rearrange themselves by various chemical reactions.

These processes usually work through complicated chemical mechanisms. Their progress then depends on properties of atoms that enter the reactions - their structures, especially the structure of the electron cloud that determines a possibility of creation of a chemical bond, and then on their chemical stability.[1]

If we consider atmospheric processes, for example, intermediate products with characteristics of reactive gases (radicals or ions) are often created during chemical changes. These gases encourage surrounding molecules to reactions by their increased reactivity, therefore they play important role in chemical processes that take place in the earth atmosphere and in space, during combustion and also within human body.

As far as the environment, effects of these species are most significantly shown in stratosphere and troposphere that compose the main transport medium of our planet - physical, chemical, and also chemical-biological. Their negative effect can be shown on global scale by the greenhouse effect, by decrease of stratospheric ozone, climatic changes, further by acidification of the environment, material corrosion, cultural monument erosion, loss of biodiversity and yield of agricultural plants, and by health endangerment.[1]

Monitoring of the chemical phenomena in atmosphere and in space became by now an indisputable necessity that can be performed well by using spectroscopic methods that allow non-destructive analyses of species, and also by a long-distance detection of gases (so called remote sensing).[2]

For this reason fundamental research of chemical species, primarily reactive ones, that contributes to determination of their structure, lifetime and understanding of reaction mechanisms these species participate in, brings knowledge significant from the point of view of human health protection, environmental protection, processes taking place in space, and also helps to expand experimental investigation methodology that can be further utilized in similar experiments.

In my work I focus on four independent experimental or analytical tasks using various sensitive spectroscopic methods like microwave spectroscopy, Fourier transform infrared spectroscopy and method laser optoacoustic detection. These methods were used for detection or measurements of concentrations of species that are interesting from the point of view of their reactivity and role that they play in atmospheric chemistry, astrochemistry, human body or simulated plasma processes.

Specifically, in my work I dedicated myself to analyses of the asymmetrical vibration ν_4 belt and the symmetrical ν_2 belt of the $FCO_2^{\cdot}$ radical that belong among significant intermediate products of degradation processes of halogenated hydrocarbons.

I also summarize results of the first spectroscopically unambiguous identification of the $CS^{\cdot+}$ molecule radical ion using the microwave spectroscopy with high spectral resolution in the frequency range of 414 to 622 GHz. From the analysis results we can expect help in looking for this radical in the universe.

Than I have also performed experiments that include measurements of the BrCN and CH_3CN cyan species spectra by time resolved Fourier transform infrared spectroscopy. It was studied behavior of these molecules and their disintegration products in the low temperature plasma environment.

At the end I describe the study of ecological impact of ammonia – a species that belongs among primary atmospheric pollutants - on environment, and influence of trees on the amount of ammonia in the air. In the follow up to these questions we have designed and constructed an optoacoustic cuvette - experimental layout of the laser optoacoustic method for measurement of the amount of ammonia and other gaseous species.

Description of the work itself has been divided to four thematic sections that describe the above mentioned tasks. Obtained results are then discussed in individual conclusions.

Individual tasks were very inspiring for me and I am happy that they included, although sometimes marginally, both problems of the earth atmosphere, and questions related to distant universe or human health. Because I do realize that universe systems and parts are very much related, more than we can possibly imagine today.

1. Theory

Since this work primarily deals with application of selected laser spectroscopic methods, it will be useful to shortly describe some basic principles used directly in the area of spectroscopy and related to the topic of this dissertation here. There is a lot of high quality literature on the given topic. I used mostly the book by J. Fišer dedicated to the basics of quantum mechanics in this section.[3]

1.1. Origin and Development of Spectroscopy

Spectroscopy is a method of quantitative chemical analysis that investigates experimentally measured spectra and provides information about investigated species (structure and composition, temperature, etc.) non-destructively.

Although we know the colored spectrum that occurs on rain drops lighted by the sun since time immemorial, we date the origins of spectroscopy to the 17th century.

Figure 1: Rainbow [4]

We can consider the Czech doctor, physicist and astronomer Jan Marek Marci of Kronland (1595 - 1667), who, in 17th century, fifteen years ahead of the famous physicist Isaac Newton, first performed and described decomposition of sunlight to its colored parts by a glass prism, a founder of spectroscopy.

Figure 2: Portrait of Jan Marek Marci [5]

Boundaries between individual colors were not exact; they were determined exactly by physicists Bunsen and Kirchhoff in 1859.

In 1800 J. F. W. Herschel shown by his experiment that sun radiation does not fall just to the visible part of the spectrum, but also to the infrared one. Similarly J. W. Ritter expanded general public knowledge to the ultraviolet area.

At the beginning of 19th century many other scientists, for example, W. H. F. Talbot, C. Wheatstone, A. J. Angstrom, D. Alter, and J. B. L. Foucault studied spectra of different origin to find out that these sources emit clear emission lines, characteristic for chemical species contained in these sources. Also W. H. Wollaston and J. von Fraunhofer should be mentioned, since they independently discovered, using a narrow slot, sharp and dark absorption lines in the spectra of space objects that appear in wave lengths characteristic for atoms and molecules that absorb sunlight. The theoretical explanation of origin of these lines, nowadays called Fraunhofer lines, was offered later by G. R. Kirchhoff who, together with R. Bunsen, performed the first chemical analysis of the sun atmosphere. They discovered two, until then unknown, elements Cesium and Rubidium during experiments with alkaline metal spectra in 1861.[3][6]

Fast expanding production technologies and emergence of electronics primarily contributed to large expansion of spectroscopy after the Second World War.[2] Spectroscopic experiments became more effective mostly due to use of computers that enabled automation of experiments, electronic records of measured data, their storage and comparison with previous experiments, or chemical databases during the process of measured data identification. Discovery and use of the laser sources and synchrotron devices also increased use of spectroscopic methods.[3] Today spectroscopy belongs among significant scientific disciplines that focuses on determination of chemical composition and molecular structures and enables us to analyze earth and star objects. This is also the only method for the study of chemical elements in stars of our galaxy.[2]

1.2. Origin and Development of Quantum Mechanics

The origin of quantum mechanics, to which foundation stones were laid by E. Schrödinger and W. Heisenberg in 1925 - 1927, is narrowly connected to the development of spectroscopy.[7]

As opposed to classical physics that deals with large particles (macro particles) the quantum mechanics studies questions related to small size particles - structure of atomic

nuclei, atoms, and molecules (micro particles) and solid species, and large amount of otherwise unexplainable experimental data.[3] Probability description, quantification, and discreteness and discontinuity of energy and some other quantities, that in classical mechanics are continuous, is typical for quantum mechanics. [6][7]

M. K. E. L. Planck's, who in 1900 formulated the hypothesis that energy that emanates from radiating body does not flow continually, but in certain quantities - quantums, study preceded the origin of quantum mechanics. He then thought that energy quanta are directly proportional to radiation frequencies, i.e., indirectly proportional to their wave length, and thus formulated a law later called the Radiation Law after him. [8][9]

In 1905 inspired by then marginalized Planck theory of light quanta A. Einstein proposed a hypothesis that energy quanta that occur during interaction of light and matter have momentum, and so we can perceive them as particles.

We call these particles photons.

The energy carried by one photon is proportionate the radiation frequency f.

$$\mathbf{E} = \mathbf{h} \cdot \mathbf{f} \qquad (1)$$

Where *h* is the Planck constant, a basic constant of the quantum physics,

Another important step during development of the quantum physics was creation of the Hydrogen model by N. H. D. Bohr in 1913. Basic idea was that electron runs around the nucleus along orbits, i.e., trajectories with exactly defined diameters. The model was not satisfactory, however, since it was not useful for atoms with more than one electron (and also it was in variance with uncertainty principle).

The last cornerstone of the quantum mechanics is the L. de Broglie's hypothesis about dual character of matter, according to which matter has both corpuscular (particle), and wave properties. Its mathematical expression is de Broglie's equation that assigns a particle with the momentum P and the wavelength λ.

$$\lambda = \frac{\mathbf{h}}{\mathbf{p}} \qquad (2)$$

The de Broglie's wave can be described by the wave function Ψ. The wave function does not correspond to any specific physical quantity.

The square of absolute value of the wave function $|\Psi|^2$ specifies probability density of a micro particle occurrence, in other words it says that the given particle appears at a certain location at a certain time with a certain probability. Since $|\Psi|^2 d\tau$ represents the probability of finding a particle in the volume element $d\tau$, the integral $\int |\Psi|^2 d\tau$ specifies the probability of finding of the particle anywhere in space.

The wave function Ψ must be unique and continuous, and the expression $\int |\Psi|^2 d\tau$, where we integrate over all allowable values of all variables the wave function depends on, must have a finite value.

The wave function is a solution of the Schrödinger's equation.[10]

The stationary Schrödinger's equation, i.e., equation for states with energy independent of time, can be written in the following form:

$$\hat{\mathbf{H}} \cdot \Psi = \qquad (3)$$

where $\hat{H}$ is the Hamilton operator (Hamiltonian),

E is the energy of the system described by the wave function Ψ.

Hamiltonian, the total system energy operator, consists of the kinetic energy operator $\hat{T}$ and the potential energy operator $\hat{V}$, and thus it can be written as:

$$\hat{\mathbf{H}} = \hat{\mathbf{T}} + \hat{\mathbf{V}} \qquad (4)$$

Individual components of the Schrödinger's equation can be seen as follows:

$\hat{\mathrm{H}}$ = electron kinetic energy + energy of nuclear repulse - energy of the attraction of electrons by nuclei + energy of electron repulsion

The Schrödinger's equation has the exact solution for the system with one electron only. We have to use approximation while solving for systems with more electrons.

Since atom nuclei have their mass 4 or 5 orders higher than electrons, they move on the average much slower. Thus we can investigate molecule properties approximately, i.e., we consider nuclei in zero approximation as motionless, and in higher

approximations we can explain movement of the nuclei by the disturbance theory methods. This procedure is called the Born-Oppenheimer or adiabatic approximation.

Further simplification of the Schrödinger's equation happened thanks to work of physics, mathematicians and programmers on development of computer programs for its calculation after entering of input data that contained information about atomic structure of a molecule.

By solving the Schrödinger's equation we can conclude that several states, characterized by three quantum numbers ($n,\ l,\ m_l$), correspond to one energy value. These states have the same main quantum number n and further differ by the quantum numbers l, and m_l. We call these states degenerative, and the number of energetically equivalent states is called the degenerative degree.

Quantum chemistry deals almost exclusively with stationary states of molecules. Finding of the wave equation Ψ for a particle (or particle system) that moves within a field of external forces is much more complicated.[3]

1.3. Atoms and Molecules

Everything consists of atoms - tiny particles that are in constant movement and that are mutually attracted if they are farther apart, and repulsed if we push them too close together.[11]

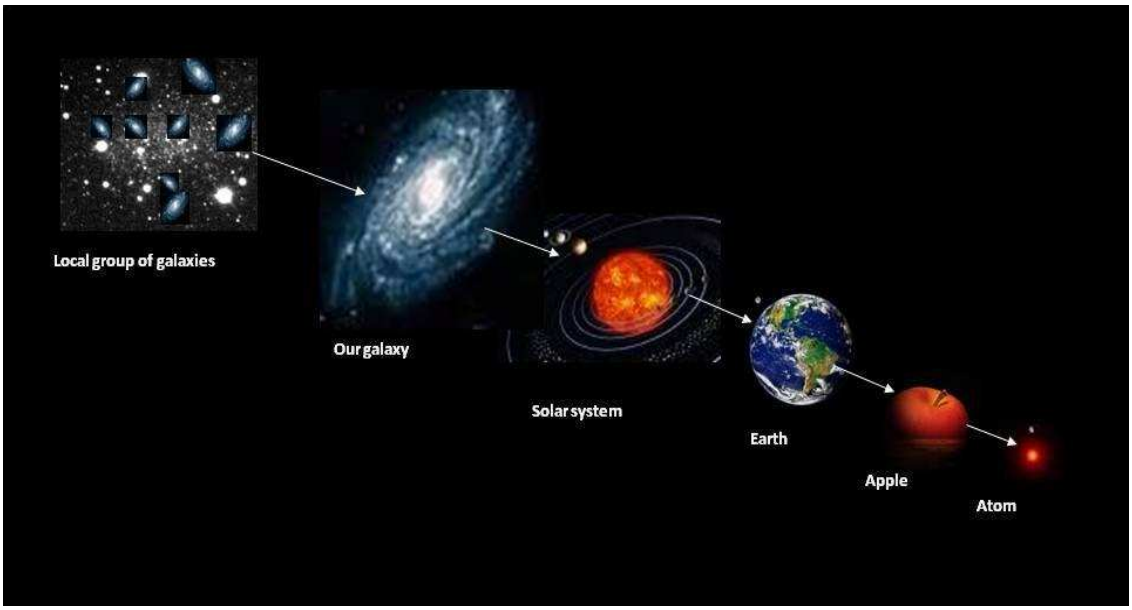

Figure 3: Illustration - everything consists of atoms

Atoms can be considered basic elements of matter that determine properties of a given chemical element. They consist of a nucleus that contains neutrons and protons and from cloud with electrons.

The atom nucleus is, as opposed to electrons, positively charged and its diameter is 10^{-15} m, which is about 100 000 times less than diameter of the whole atom. It is very small and concentrates practically the whole atom mass (99.9 %).

From the point of view of quantum mechanics atoms and molecules exist only in discrete quantum states with the appropriate energy - in the lowest energy state, so called ground state E_0, or in the higher energy state E_x.

There is absorption or emission of energy during transition between these states. For absorption or emission of energy in the form of electromagnetic radiation the following is valid [3]:

$$E' - E'' = \Delta E = h \cdot f = \frac{h \cdot c}{\lambda} = h \cdot c \cdot \sigma \qquad (5)$$

where E' is the energy of the higher energy state, and

E'' is the energy of the lower state

σ is the wavenumber

c is the speed of light in vacuum,

Electromagnetic radiation propagates in vacuum by the speed of light c with the value $c = 2.997\ 924\ 58 \cdot 10^8\ m \cdot s^{-1}$.

Atoms and molecules can accept and give out energy in the form of radiation in completely specific frequencies.

A species can be transferred to an excited state by several ways: adding of heat, by electrical charge, bombardment by accelerated particles with large energy, or by the electromagnetic radiation effect, or absorbing of energy quanta - photons.[13]

During the change of molecule energy state electronic state can be changed, or there may be a change in the vibrational or rotational movement of the molecule, possibly a change in the spin orientation of electron or nucleus. If we disregard energy changes related to the spin orientation, we can decompose the total energy change into electron, vibrational and rotational contributions.

$$\Delta E = \Delta E_e + \Delta E_v + \Delta E_r \qquad (6)$$

It is valid that:

$$\Delta E_e \gg \Delta E_v \gg \Delta E_r \qquad (7)$$

The change in electronic state is usually accompanied by the vibrational and rotational changes, the change in vibrational state by a change in the rotational state.

Occupancy of individual molecule states in a large set of molecules is described by the Boltzmann distribution law. A molecule can revert to the original state after absorption of an energy quantum by emission of radiation or by non-radiant transfer during collisions with other molecules (see Figure 4). A probability of transition is further limited by selection rules that follow the quantum mechanics and are closely related to the molecule symmetry.[3]

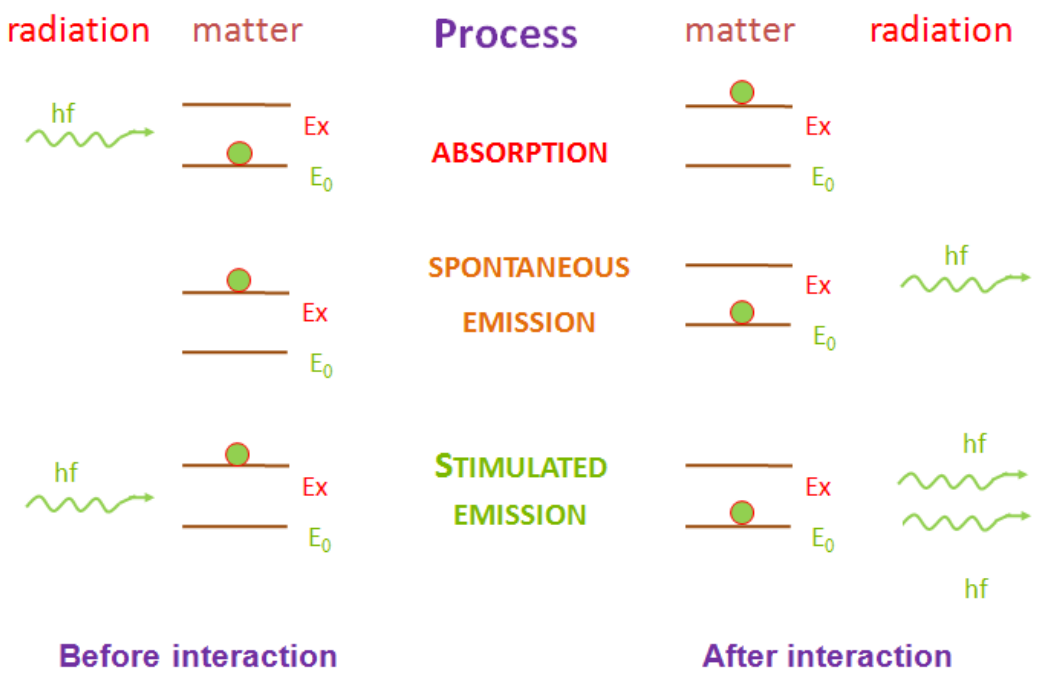

Figure 4: The processes in atom or molecule [13]

1.4. Atomic Orbital

The atomic wave function that is a solution of the Schrödinger's equation and is determined by the values of the quantum numbers n, l and m_l is identified as the Atomic Orbital (AO). This orbital designs an area that has the highest probability of a given electron occurrence. The quantum numbers are used to describe the electron distribution and the structure of the orbital (see Table 1).[14]

Table 1: The illustration of quantum numbers

QUANTUM NUMBERS	SYMBOL	VALUE	DESCRIBE
Principal	n	1,2,3,…	electron position – its distance from nucleus
Orbital (azimuthal)	l	0,1,2,3,…(n-1)	orbital shape size of orbital momentum
Magnetic orbital	m_l	0,+-1,+-2…+-l	space orbital orientation - z-component
Magnetic spin	m_s	+-1/2	projection of spin momentum into a certain direction, e.g. direction of z axis

Orbital are marked according to the general formula: **A** type^{B}

where **A** corresponds to the orbital energy, marked by the principal quantum number n.

B is the number of electrons in an orbital, while each orbital has 2 electrons that differ by their spin. As opposed to hydrogen atoms (or one electron ions) the orbitals of multiple electron atoms with the same n and different l have a different energy due to electron repulsion.[3]

Individual orbitals are usually occupied by electrons according to increasing energy of the orbital. Order of occupation of atom orbitals (AO) in electroneutral atoms is according to the increased energy:

$$ls < 2s < 2p < 3s < 3p < 4s < 3d < 4p < 5s <\ldots \qquad (8)$$

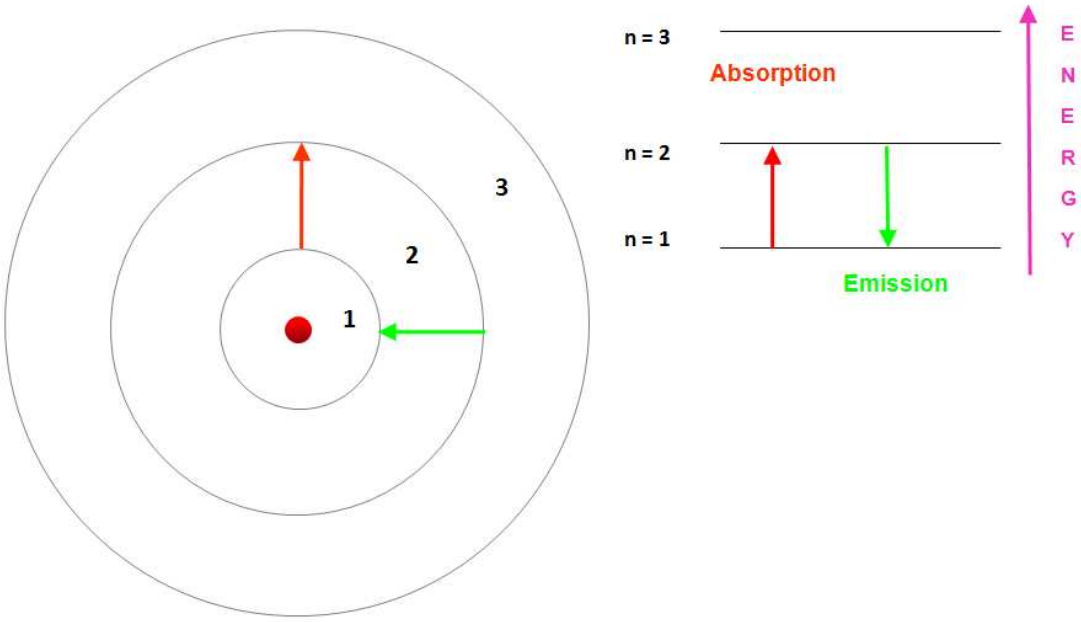

Figure 5: Illustration – s orbital and energy levels

There are molecule orbitals in molecules, whose occupation by electrons determines the electron structure of a multiple atom particle, and consequently physical properties and reactive capabilities of the molecule.

The molecule orbitals are one-electron wave functions that by their square affect distribution of charge density in a particle. Electrons in the molecule orbitals move in the field of several atom nuclei.

There are certain rules and limitations in quantum number values that are defined by the Pauli Exclusion Principle and the Hund's rule.[14]

- The Pauli principle: Each orbital can be occupied by maximum of two electrons with the opposite spin. This means that the two electrons in a given orbital must differ by the spin quantum number m_s; for one electron is $m_s = +1/2$, for the other $m_s = -1/2$.

- The Hund's rule: Degenerated orbitals are occupied by electrons, so the number of electrons with parallel spins is at its maximum (the rule of maximum spin multiplicity).[3]

1.5. Spin

The spin is a basic characteristic of elementary particles, composite particles (hadrons), and atom nuclei. The spin is the intrinsic momentum that can be interpreted as a consequence of momentum of the particle acting around its own axis. Similarly as the orbital momentum spin is quantized also. In quantum mechanics it is not possible to determine its three components, only its size and one of the other ones (normally we select its z component), whose admissible values are determined by values of the spin number s and the magnetic spin number m_s. A size of the spin is obtained from the equation (9), on the left sides of the equations (9-11) analogy relationships for the orbital momentum of a particle are shown.

$$|\mathbf{l}| = \hbar \cdot \sqrt{l \cdot (l+1)} \qquad |\mathbf{s}| = \hbar \cdot \sqrt{s \cdot (s+1)} = \hbar \cdot \frac{\sqrt{3}}{2} \qquad (9)$$

$$l_z = \hbar \cdot m_l \qquad s_z = \hbar \cdot m_s \qquad (10)$$

where m_l is the magnetic orbital quantum number

m_s is the magnetic spin quantum number

With the given s the projection of spin into the axis z can have the following values:

$$m_l = -l, -l+1, \ldots, +l \qquad m_s = -s, -s+1, \ldots, +s \qquad (11)$$

in total then $2 \cdot s + 1$ values.

A spin number s can be an integer (including zero) or half-integer.

According to the value of spin the particles are considered as:

- **Fermions** - particles with a half-integer spin (most particles - electrons, protons, neutrons, mions, etc.)
- **Bosons** - particles with the whole number spin (photons, π, K-mesons and others).

The spin value determines the symmetry of system state considering rotation in space, i.e., the manner in which wave functions that correspond to the different values of angular momentum projections mutually transform themselves during turning of a coordinate system.

In the quantum description of a particle with spin a wave function must not determine only probability of different positions of its occurrence in space, but also the probability of different spin orientations. The wave function then does not depend on three space coordinates, but also on a spin variable that gives the value of a spin projection to a different direction in space (the axis z is normally selected) and gains a limited number of discrete values.[15]

The directional limitation of electron orbital and spin angular momentum vectors for l=2 and s=1/2 is shown in Figure 6.

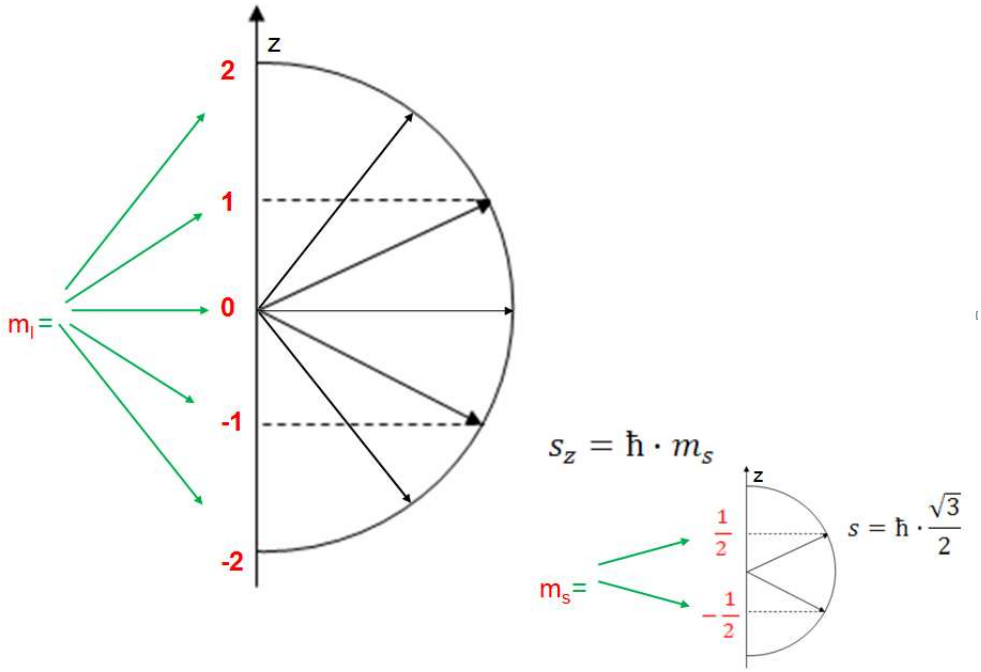

Figure 6: The directional limitation of electron orbital and spin angular momentum vectors for l=2 and s=1/2[14]

1.6. Radicals and Ions

Currently, many definitions of radicals exist. One of the most common describes radicals as molecules that have one or more unpaired electrons in its valence orbital. However, this definition is far from exact, since then it would include many molecules

that we do not consider radicals due to their relative reaction stability (e.g. O_2, NO, and NO_2). For this reason it is useful to expand this definition and consider reactive particles that have one or more unpaired electrons, and whose reactivity predeterminates them to a short lifetime, as radicals. Each electron (with its own spin) behaves like a small magnet. In radicals electron spins are not paired, therefore radicals show paramagnetic properties. This paramagnetic behavior of radicals is used for their identification in spectroscopy. Another important radical property is increased spin multiplicity of electronic states. So, once we summarize properties of radicals as particles, we can say that a radical is a reactive, paramagnetic particle that has a high multiplicity of electron quantum states and a spin magnetic momentum.[16]

Ion is a particle (atom, molecule, molecule fragment, molecule cluster, aerosol particle, macroscopic object – drop of liquid - etc.) that carries one or several elementary electric charges with positive or negative polarity. However, there are some particles that belong here also (usually dielectric material powder ones, but also metal ones) that carry both local positive and negative charges, and, in spite of this, appear electrically neutral to their surroundings.

Some radicals, called ion-radicals, also belong among ions. Ions in the air behave differently from ions in water solutions. Under influence of water, every species that is an ion crystal in solid form (e.g. NaCl), becomes an ion. These processes do not occur in gases.[17]

Radicals and ions are created by breaking of a chemical structure of a molecule, mostly by pyrolysis, photolysis, or by an electric discharge.

One of the first techniques, by which a radical was created, was based on the flash photolysis using pulse lamps. In 1955 Low and Ramberg produced the $OH^{\cdot}$ radical in the continuous electric discharge. Rotational spectra of radical were measured in the Walter Gordy laboratory for the first time, when a microwave discharge was used to create the $SO^{\cdot}$ radical.[18][19] The first rotational spectrum of a molecular ion (specifically CO^{+} produced using an electric discharge) was measured in 1975 by Dixon and Woods.[18]

Studies of radicals and ions are much more complicated than studies of other stable molecules. The reason is their problematic creation in sufficient amounts for detection. Their vigorous reactivity often does not allow it. We need a very sensitive method with high spectral resolution to efficiently study these species. The high sensitivity

requirement is given by short lifetimes and low concentrations of detected particles in comparison with high concentrations of stable molecules. The microwave, laser diode and Fourier transform infrared spectroscopies have suitable properties to detect these species.

1.7. Electrical Discharge and Plasma

The plasma is considered as the fourth form of matter, the quasi-neutral form of electrically charged and neutral particles.

In case of neutral gas, particles collide only during collisions that later determine a movement of the particle. However, plasma also has charged particles that can create spatial charges that lead to origination of an electric field. Due to the Coulomb's force the charges in plasma can influence each other over long distances. Particle movements then do not depend only on local conditions, but on a state of plasma at longer distances, therefore on a collective behavior of all present particles.[20][21]

We can encounter high temperature plasma in the Universe; in laboratory conditions we encounter it, for example, during thermonuclear fusion. The electric charge low temperature plasma is one of the ways of creation of radicals and ions. It is excited by high voltage (by application of a high energy electric field to gas located between a system of electrodes).

The following electric field types are used to produce radicals and ions for spectroscopy studies [22]: continuous (DC); low-frequency (AC); radio-frequency (RF), and microwave (MW) discharges.

The electric discharge can be generated inside of a hollow cathode. The cathode should be in this case cooled by liquid nitrogen or by a water flow system. The technique of concentration modulation, sometimes also called population modulation or on-off modulation, is very useful during application of the hollow cathode at the same time. Advantage of this procedure lies in using of modulated AC (on the order of tens to thousand Hz) discharge, while the signal from a detector is processed using a phase sensitive (lock-in) amplifier that analyzes only 1f harmonic component of the signal equal to the modulation frequency of the charge. This achieves a significant increase in signal to noise ratio. The experimental arrangement for the concentration modulation was described for example in the works. [23][24] The method of direct differentiation of charged and neutral samples in electric charges is so called speed modulation.[25][26][27]

During use of this technique the electrode polarity is periodically changed inside of the charge cell, which influences the direction of propagation of the electrically charged samples. This way it is possible to differentiate ions from neutral samples and also recognize positively charged cations and negative anions.

1.8. Electromagnetic Radiation

The electromagnetic radiation (or Maxwell's rainbow) includes a range of all possible frequencies of the electromagnetic waves. The electromagnetic waves consist of electric and magnetic components. In case of waves polarized in a plane, vectors of the electric field intensity (E) and magnetic induction (B) always oscillate in one plane, while the E and B vectors are always mutually perpendicular and, at the same time, perpendicular to the wave propagation (see Figure 7). In case of unpolarized waves the mutually perpendicular E and B vectors can have any direction perpendicular to the wave propagation.[3]

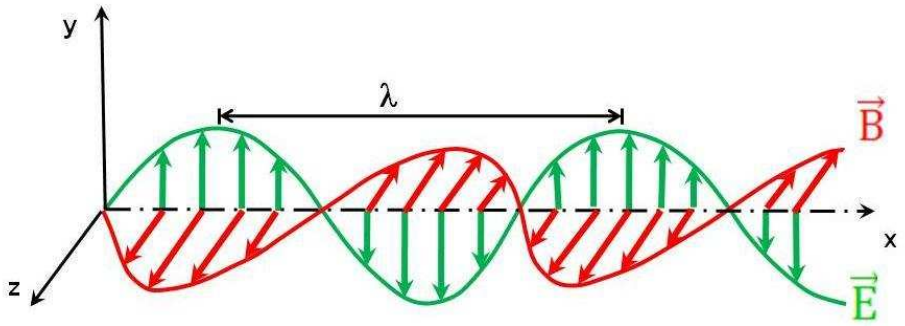

Figure 7: Electromagnetic Waves

E - *oscillating electric field in the xy plane,*
B - *oscillating magnetic field in the xz plane*;
wave (photon) moves in the direction of the x axis.

The distance between two maximums of the curve, that describes oscillations of the electric field intensity, is the wavelength. Number of wave per second is the frequency. Number of waves per unit of distance in direction of the x axis is a wavenumber.

From the point of view of quantum mechanics we can consider electromagnetic radiation to be both a wave, and at the same time a flow of discrete particles (photons).

We can divide electromagnetic waves into several groups according to their wavelengths or frequencies (see Figure 8):

Radio waves are the longest used electromagnetic waves. The radio waves are divided to the long (approx. 150 – 500 kHz, i.e., 200-60 m), medium (approx. 500-2000 kHz), short (approx. 2-30 MHz), and very short (30-1000 MHz) waves.

Next in row is the **microwave region** that can be divided to three parts, namely submillimeter, millimeter, and centimeter waves. In connection with this area we talk about the microwave spectroscopy.

Table 2: Microwave region of the electromagnetic radiation

	Wavelength [mm]	**Frequency [GHz]**
Centimeter	100-10	3-30
Millimeter	10-1	30-300
Submillimeter	1-0.1	300-3000

The infrared radiation (IR) is known as the heat radiation that is transmitted by each subject heated to the temperature higher than 0 deg. K. The higher is the subject temperature, the higher is the intensity of infrared radiation, and the radiation maximum moves towards shorter wave lengths. In higher temperatures (above approx. 600 °C) hot subjects emit also visible light.

The visible light is a part of the electromagnetic spectrum that is visible to human eye. The electric component of the electromagnetic field that reacts with human retina causes that we can see this part of the spectrum. It extends from the wave lengths of approx. 750 nm (we can see it as the red light) to approx. 360 nm (violet light).

The ultraviolet radiation (UV) follows immediately after the (violet) visible light towards shorter wave lengths or higher frequencies. **The X-ray radiation** has even shorter wave lengths (and higher frequencies) than UV radiation. **The Gamma radiation** is the "hardest" electromagnetic radiation with the shortest wave lengths and highest frequencies.[17]

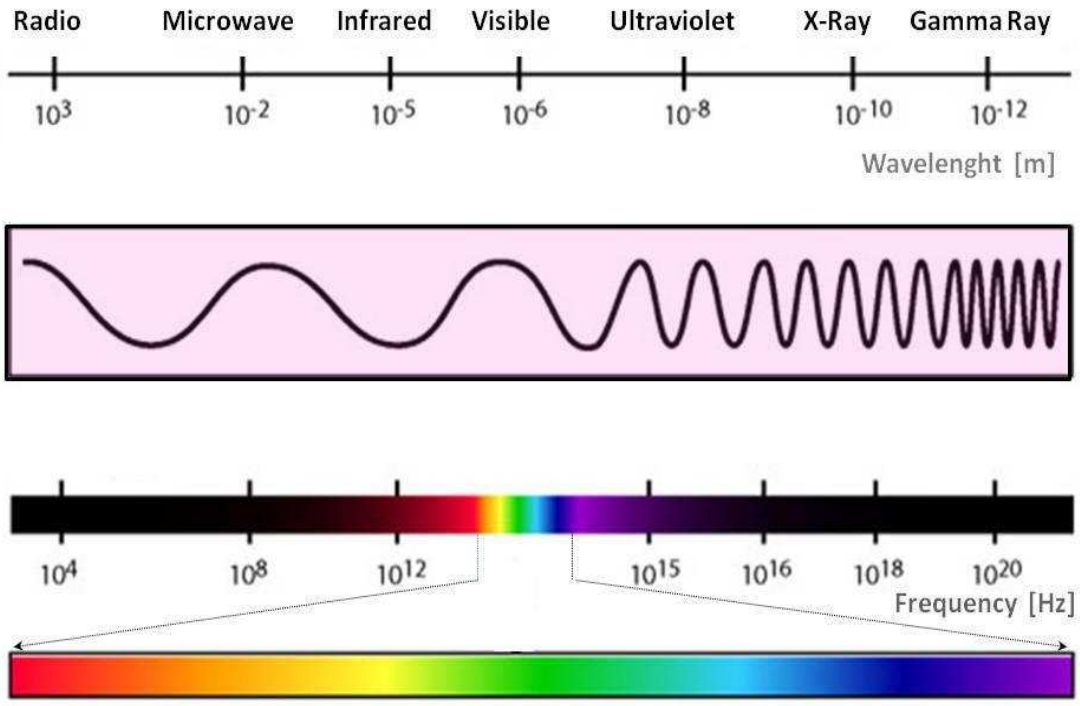

Figure 8: The electromagnetic spectrum

Each species has its own specific spectrum that is always at a certain, unchanged location from the point of view of electromagnetic radiation wavelengths. Thanks to this knowledge we can, based on comparison of individual measured lines and lines characteristic for a certain species, uniquely identify a certain species.

There are two basic types of spectra: emission or absorption, depending on whether the species absorbs or emits the electromagnetic radiation that is transmitted to it.

Absorption and emission spectra of the same species lie in the same wavelengths.

Atomic spectra differ from the molecular ones. The atomic spectra are lines, opposed to this the molecular spectra contain bands that consist of many lines lying next to each other. These bands are caused by the vibrational and rotational molecular states.

Each of the absorption spectrum lines reflects absorption of energy by a system of molecules and transition of molecule parts from a state with lower energy to the state with higher energy. The lines are always shaped as so called "peaks", which comes out of the Heisenberg uncertainty principle (the natural expansion of absorption lines):

$$\tau \, \Delta E \sim h \qquad (12)$$

where ΔE is the uncertainty of a level energy,

τ is the lifetime of a particle in this level,

The level uncertainty, and as a consequence, the natural width of a line is indirectly proportional to the particle lifetime in the original state. The Heisenberg uncertainty principle refers to an important fact that in the microworld the energy E cannot be determined exactly during a finite measurement time $\Delta\tau$.

The spectral lines, however, are additionally expanded due to mutual particle collisions (pressure expansion of spectral bands), by influence of electric and magnetic fields, and due to the Doppler's effect. During the Doppler's expansion of lines frequencies, at which absorptions occur, move as a consequence of multidirectional movement of atoms and molecules. The frequency shift $\Delta\nu$ is directly proportional to the speed of an atom or a molecule.[29]

1.9. Spectroscopic Experiment

The base of spectroscopic methods is monitoring of interaction of electromagnetic radiation with the investigated species with the goal of utilization of observed phenomena for a proof of the species presence, study of its structure, or determination of its concentration.[12] During interactions of radiation with the investigated species there is either exchange of energy between the investigated species and radiation, or the species only influences properties of passing radiation in certain way without exchange of energy.

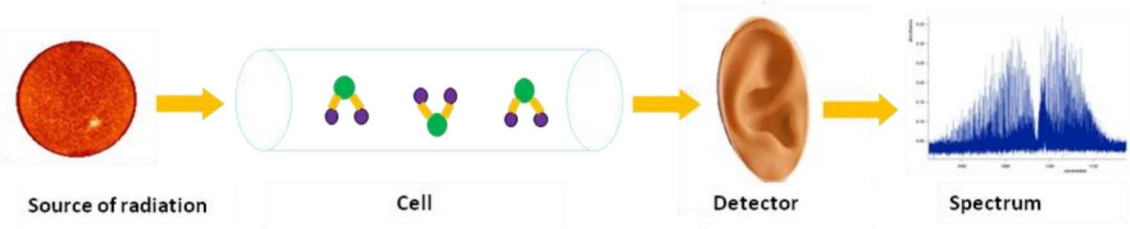

Figure 9: Simplified schematic of spectroscopic experiment

The Figure 9 shows the simplified schematic of spectroscopic experiment.

A source, or the species itself, emits radiation. The radiation passes through a sample that absorbs, or emits radiation (on certain frequencies only) and then this radiation comes to the detector that determines a change in the radiation flow and converts it to the electric signal. We should mention also scattering of the radiation

which is defined as the deflection of the incoming radiation in all direction. Its value during spectroscopic experiments performed during my PhD studies was small and could be neglected.

The signal intensity on the detector depends on the frequency of electromagnetic radiation. The graphic representation of the intensity dependence of the passed radiation on the frequency of electromagnetic waves is an absorption, or emission, spectrum (graph) that shows dependency of transmittance T or another quantity (e.g. absorbance A) on a wave length, wavenumber or frequency of used radiation.[3]

In practice we use a monochromatic (i.e., with very limited range wave lengths), or polychromatic radiation source, which, however, needs a dispersion system (prism, grid, or Michelson's interferometer) for delimitation of a monochromatic ray.

The individual spectrometer parts can differ significantly according to the range of electromagnetic radiation wave lengths emitted by the source.

The molecular spectra and the types of spectroscopy are summarized in Table 3.

Table 3: The molecular spectra and the types of spectroscopy [3]

Used radiation	Wave length [m]	Studied phenomenon	Processes in molecule	Spectroscopy
Radio waves	10^{-1}-10^{-2}	Absorption in magnetic field	change of orientation in nuclear spin	Nuclear magnetic resonance (NMR)
Microwaves	10^{-3}-10^{-1}	Absorption in magnetic field	change of orientation of electron spin	Electron spin resonance (ESR)
		Absorption	change of rotational state of molecule	Microwave
Infrared (IR)	10^{-6}-10^{-3}	Absorption	change of vibration and rotation state of molecule	Infrared
Visible and ultraviolet (UV)	10^{-7}-10^{-6}	Absorption	change of electronic state of molecule	Electron or electronic
	10^{-9}-10^{-7}	Emission after previous excitation	change of electronic state of a molecule	Luminescent
	10^{-10}-10^{-9}	Inelastic scatter	change of vibration and rotation state of a molecule	Raman's
	10^{-12}-10^{-10}	Change of propagation speed and absorption of polarized radiation	change of polarisability of a molecule	Optical rotational dispersions (ORD) of circular dichroism (CD)
Vacuum ultraviolet	10^{-9}-10^{-7}	Photoemissions of electron	loss of valence electron	Ultraviolet photoelectron (UPS)
X-ray	10^{-10}-10^{-9}	Photoemissions of electron	loss of internal electron	X-ray photoelectron (XPS, ESCA)
γ	10^{-12}-10^{-10}	Absorption	change of atomic nucleus state	Mössbauer's

1.10. Division of Spectroscopy

Spectroscopy can be divided based on two criteria:

1. Division according to the used experimental technique, i.e., according to the area of electromagnetic spectra which we measure. This division depends on the used radiation source in absorption spectroscopy or on the type of radiation emitted by the species (e.g. microwave, sub-millimeter, infrared, electron spectroscopy, etc.).
2. Division according to the type of induced process in an atom or molecule
    - Electron spectroscopy
    - Vibration spectroscopy
    - Rotational spectroscopy
    - Ionization spectroscopy

1.11. Rotational Spectroscopy

The rotational spectroscopy deals with the study of spectroscopic transitions between molecule quantum states that only differ by rotational quantum numbers (J-quantum number of the total angular momentum, k - quantum number of the projection of angular momentum into rotational axis in a fixed molecule coordinate system) namely by spectroscopic transitions, in which there is no change of any vibration or electron quantum number.

The rotational spectroscopy is the spectroscopy mostly within ground vibrational and ground electronic states.

The rotational spectroscopy is typical for the microwave part of the spectrum (MW).

In order for the investigated molecule to have rotational spectrum, it must be sufficiently free, so the rotational movement of the whole molecule is not hindered. So, this is primarily spectroscopy of gases or species that can be introduced into gaseous phase for at least a short while. The necessary condition for origination of rotational spectra is the existence of a permanent electric dipole moment in a molecule.

Deeper analyses of the rotational spectroscopy can be found in many publications.[29][30][31][32][33]

1.12. Rotational Movement of a Molecule

We can analyze rotational and vibration movements of molecules independently, based on the Born-Oppenheimer approximation. The rotational movement of a two-atom molecule can be described the simplest by the solid rotor model. Atoms within this model are represented as two balls with masses m_1 and m_2, connected by a thin massless coupling with the length r (see Figure 10, $r = r_1 + r_2$). The distance between individual atoms (balls) and angle sizes do not change during rotation of this model.

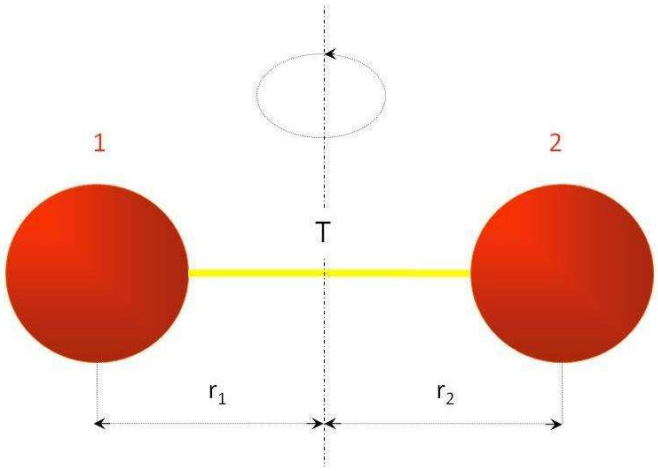

Figure 10: Rigid rotor model

Molecule rotation is characterized by the moment of inertia and angular momentum. The moment of inertia of the system shown on the Figure 10 around axis that passes through its center of gravity T and is perpendicular to the link between the balls expressed by the following relationship:

$$I = \frac{m_1 \cdot m_2}{m_1 + m_2} \cdot r^2 = m_r \cdot r^2 \qquad (13)$$

Where m_r is the reduced mass

The value of the rotational energy of molecules is obtained by decomposition of the molecule rotation to the turning of three mutually perpendicular main axes passing through the center of gravity. The axes are designated a, b, and c, and can be identified with the axes x, y, and z, according to three clockwise I^r, II^r, III^r and three anti-clockwise representations I^l, II^l, III^l.[34] The axes are selected so the moment of inertia of the molecule around one of them would be the highest and around one of them the lowest:

$$I_a \leq I_b \leq I_c \qquad (14)$$

If a molecule has *n*-fold axis of symmetry that is larger or equal to two, then we consider it the main axis with the maximum fold.

By solving the Schrödinger's equation for the case of rotational movement of two-atom molecule we obtain the following relation for individual rotational energy levels:

$$E_r = \frac{h^2}{8 \cdot \pi^2 \cdot I} \cdot J \cdot (J+1) \qquad (15)$$

where J designates rotational quantum number that can only have the values $J=0, 1, 2, \ldots$

Transferred to the frequency units:

$$F(J) = \frac{E_r}{h} = \frac{h}{8 \cdot \pi^2 \cdot I} \cdot J \cdot (J+1) = B \cdot J \cdot (J+1) \qquad [Hz] \qquad (16)$$

And to the wavenumber units:

$$F(J) = \frac{E_r}{h \cdot c} = \frac{h}{8 \cdot \pi^2 \cdot I \cdot c} \cdot J \cdot (J+1) = \frac{B \cdot J \cdot (J+1)}{c} \qquad [cm^{-1}] \qquad (17)$$

Based on the sizes of the appropriate moments of inertia I_a, I_b, I_c, the molecules in spectroscopy split into several categories (see Table 4).

Table 4: Types of molecules in spectroscopy

Model	Components of inertia momentum	Rotational constants	Example of a molecule
Linear molecules	$I_b = I_c$, $I_a = 0$	B=C, A = ∞	
Spherical	$I_a = I_b = I_c$	A=B=C	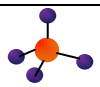
Symmetrically prolate	$I_a < I_b = I_c$	A>B=C	
Symmetrically oblate	$I_a = I_b < I_c$	A=B>C	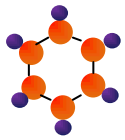
Asymmetrical	$I_a < I_b < I_c$	A>B>C	

the A, B, C constants in the table are rotational constants, for which is valid:

$$A = \frac{\hbar^2}{2 \cdot I_a} \quad [\mathrm{J}] = \frac{h}{8 \cdot \pi^2 \cdot c \cdot I_a} \quad [\mathrm{Hz}] \qquad (18)$$

$$B = \frac{\hbar^2}{2 \cdot I_b} \quad [\mathrm{J}] = \frac{h}{8 \cdot \pi^2 \cdot c \cdot I_b} \quad [\mathrm{Hz}] \qquad (19)$$

$$C = \frac{\hbar^2}{2 \cdot I_c} \quad [\mathrm{J}] = \frac{h}{8 \cdot \pi^2 \cdot c \cdot I_c} \quad [\mathrm{Hz}] \qquad (20)$$

$\hbar$ is the reduced Planck constant.

The rotational constants have the following relationship:

$$A > B > C \qquad (21)$$

Each category is characterized by selection rules.

1.12.1. Linear Molecules

By solving the Schrödinger's equation for linear molecules we obtain the relationship for rotational level energy:

$$E_J = B \cdot J \cdot (J+1) \qquad (22)$$

For the energy difference between two rotational levels in case of the linear molecule it is valid that:

$$\Delta E = E' - E'' = \frac{h^2}{8 \cdot \pi^2 \cdot I} \cdot f \cdot [J' \cdot (J'+1) - J'' \cdot (J''+1))] \qquad (23)$$

J´ describes the rotational quantum number of the top state

J´´ describes the rotational quantum number of the bottom state

Only transitions that meet the selection rule apply in the microwave, millimeter, and infrared spectra:

$$\Delta J = J' - J'' = \pm 1 \qquad (24)$$

1.12.2. Symmetrical Rotor Type Molecules

We can describe rotation of the symmetrical rotor type molecule using two quantum numbers:

- quantum number *J* of the total molecule angular momentum that can have only integer values 0, 1, 2, 3, ...
- quantum number *k* of the molecule angular momentum around its symmetry axis with the highest frequency. The *k* number can only be a positive or negative whole number, and for a given value of *J* can *k* have altogether *2J* + 1 values: *-J, ..., J* - 1, *J*. Statuses with values $k \neq 0$ are therefore twice degenerated.

The energy of the symmetrical rotor does not depend on a sign of the quantum number *k*, therefore we often use the symbol *K* that is defined as

$$K = |k|. \quad (25)$$

While only the transitions that meet selection rules apply in the spectrum:

$$\Delta J = \pm 1, \Delta K = 0 \quad (26)$$

Symmetrical molecules have either the prolate rotor type, or the oblate rotor type.

Symmetrical Molecule of prolate rotor type

By solving the Schrödinger's equation for prolate rigid rotor type we can obtain the following relationship for energy:

$$E_{J,k} = B \cdot J(J+1) + (A - B) \cdot k^2 \quad (27)$$

Symmetrical Molecule of oblate rotor type

By solving the Schrödinger's equation for oblate rigid rotor type we can obtain the following relationship for energy:

$$E_{J,k} = B \cdot J(J+1) + (C - B) \cdot k^2 \quad (28)$$

The specified relationships for energy and its change are valid only for the rigid rotor models, and can be used only for slow rotations with a low value of J. With actual molecules the situation looks differently. There are centrifugal distortion effects during rotation, which change inter-nuclear distances and angle sizes among atoms. The rotation energy can then be determined by adding the energy that corresponds to centrifugal distortion to the energy of rigid rotor.

$$E_{J,k} = E_{J,k}^{rotational} + E_{J,k}^{centrifugal\ distortion} \quad (29)$$

where

$$E_{J,k}^{centrifugal\ distortion} = -D_J \cdot [J \cdot (J+1)]^2 - D_{J,k} \cdot J(J+1)k^2 - D_k k^4 + \\ +H_J[J \cdot (J+1)]^3 + H_{J,k}[J \cdot (J+1)]^2 k^2 + H_{k,J} \cdot J \cdot (J+1) \cdot k^4 + H_k \cdot k^6$$

(30)

where D_J, D_{Jk}, D_k are the quartic centrifugal distortion constants

$H_{J,k}$, $H_{k,j}$, H_k are the sextic constants.

These constants are much smaller than rotational ones.[33]

1.12.3. Asymmetrical Rotor Type Molecules

Rotational spectra of the asymmetric rotor molecule types are very complicated; there are no generally valid relationships for spectral line wavenumbers. The spectra of individual species must be processed as individual cases.

To describe asymmetry or a measure of symmetry of a molecule we use the Ray's asymmetry parameter κ that assumes the values from +1 to -1:

$$\kappa = \frac{2 \cdot B - A - C}{A - C} \qquad (31)$$

+1 for symmetrical prolate rotor

-1 for symmetrical oblate rotor

The wave function of asymmetrical rotor is a linear combination of wave functions of prolate and oblate rigid rotors. A value of energy of asymmetrical rotor rotational state can then be found between the energy values of prolate and oblate rotors.

To describe this model we use the quantum numbers k_a – that corresponds to the wave function of the prolate symmetrical rotor – and k_c that corresponds to the wave function of the oblate symmetrical rotor.

The selection rule for the change of quantum number J in asymmetrical rotor is:

$$\Delta J = \pm 1 \qquad (32)$$

There are three types of rotational transitions (see Table 5) for asymmetrical rotor, depending which component of dipole moment in the direction of main axes is not equal zero.

Table 5: Types of transitions in rotational spectroscopy together with selection rules [54]

Type of transition	Non-zero component μ	Δka	Δkc	Position of electric dipole moment
Type a transition (parallel)	$\mu_a \neq 0$	0, ±2, ±4,…	±1, ±3, ±5, …	Along axis with smallest inertia momentum
Type b transition (perpendicular)	$\mu_a \neq 0$	±1, ±3, ±5, …	±1, ±3, ±5, …	
Type c transition	$\mu_a \neq 0$	±1, ±3, ±5, …	0, ±2, ±4,…	Along axis with largest inertia momentum

It also must be valid that

$$J = k_a + k_c \quad (33)$$

or $J + 1 = k_a + k_c$. (34)

Rotational levels are marked with the symbol J_{KaKc},

where $K_a = |k_a|$ (35)

and $K_c = |k_c|$ (36)

In literature there is sometimes alternative labeling k_{-1} and k_1 instead of k_a and k_c.

There is centrifugal distortion of the asymmetrical rotor type during rotation of molecules described in Hamiltonian using the centrifugal distortion constants, just like with the symmetrical rotor. In order to get the rotational distortion constants out of measured data, we need to modify the Hamiltonian by reduction of adjustable parameter number. This is ensured by so called "reductions", e.g. the A-reduction and the S-reduction. The A-reduction is much more common than the S-reduction

For completeness sake we need to say that constants obtained from the Hamiltonian in the A-reduction are generally linear combinations of the unreduced Hamiltonian parameters.[34]

1.13. Fine and Hyperfine Structures in Rotational Spectra

The presence of an unpaired electron in a molecule is represented by the electron spin-rotational interaction. This interaction causes a split of rotational level, with the exception of $N = 0$, into two sublevels (the unpaired electron has two possible orientations), and we can observe so called fine splitting of the spectra:

The total angular momentum is then given by the following relationship:

$$J = N + S \tag{37}$$

$$J = N + ½ \text{ and } J = N - ½, \tag{38}$$

where N is angular momentum of the molecule skeleton without the spin included,

S is the electron spin angular momentum,

J is the angular momentum after pairing of N and S and describes so called fine splitting of rotational levels.

If there is the nucleus with non-zero nuclear spin I in a molecule that has the spin angular momentum equal to

$$I = \hbar\sqrt{I \cdot (I + 1)} \tag{39}$$

The result of pairing of nuclear spin and rotational angular momentums is the total angular momentum $\boldsymbol{F}$:

$$F = J + I \tag{40}$$

where F gains the values

$$F = J + I, J + I - 1, \ldots, |J - I| \tag{41}$$

The principle of hyperfine structure is pairing of the nuclear spin angular momentum I with the rotational angular momentum J (see Figure 11) and related electromagnetic interaction between the nuclear magnetic momentum, or the nuclear electric quadruple with magnetic and electric field that is generated by the rest of the molecule system.

Various combinations of the mentioned interactions cause hyperfine splitting to sublevels that are observable by the high resolution spectroscopy techniques only.

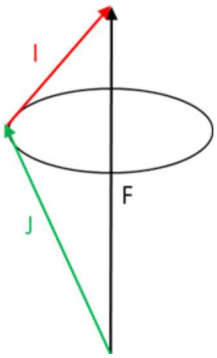

Figure 11: Vector contributions of rotational (J) and nuclear (I) spin angular moments to the total angular momentum F [36]

1.14. Stark and Zeeman Effects

Splitting and shift of energy levels and, in consequence, splitting and shift of spectral lines, occur in rotational spectrum also due to outside electric or magnetic fields.

The splitting of energy levels caused by the outside electric field is called **Stark effect**, and is caused by the reaction of a permanent electric dipole molecule momentum with an outside electric field applied.

The splitting caused by an outside magnetic field reacting with the magnetic field of an unpaired electron is called the **Zeeman effect**. The Zeeman effect is used for identification of radical spectra. If it is not a radical than the splitting of spectrum does not occur, and we can immediately conclude that the investigated spectral line does not belong to a radical. The Figure 12 shows the practical application of Zeeman effect during experiment.

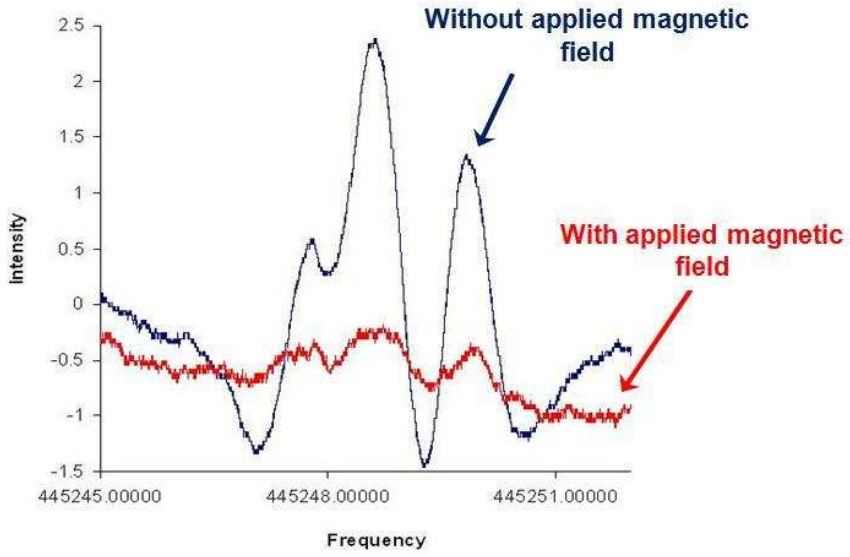

Figure 12: The testing of $CH_2Br^{\cdot}$ radical by application of magnetic field

1.15. Vibrational Spectroscopy

The vibrational spectroscopy studies absorption (or emission) transitions between two different vibrational levels within the same electronic state.

Energy differences that correspond to changes of vibrational levels are usually characteristic for the **infrared region** of the spectrum.

A vibration frequency of the biatomic molecule depends on the atomic attraction force, i.e. on a type of chemical bond, on the type (mass) of vibrating atoms, and on molecular geometry.

Vibrational of the multiple atomic molecule is a complicated form of oscillating movement that can be described as the sum of simple harmonic movements, so called normal vibrations. Position of N atoms bonded in a molecule can be described by $3N$ independent coordinates. The system can perform $3N$-6 (non-linear molecule) or $3N$-5 (linear molecule) normal vibrations. A molecule then has $3N$-6, or $3N$-5 vibration degrees of freedom and the same number of normal vibrations.

During normal vibration all atoms in a molecule vibrate with the same frequency and phase, but with different amplitudes. The vibrations during which the length of a bond changes are called valence vibrations (symmetrical or asymmetrical); if a bond angle changes then these are deformation vibrations.

We can determine a strength constant from the frequency that corresponds to the middle of a spectral band, and molecule moments and length of a bond from the distance of rotational lines. This way we can obtain data about a molecular structure from the fine structure of the infrared spectrum.

Similarly, as with the rotational spectrum, the electric dipole moment of a molecule has critical significance for origination of the vibration spectrum: Only the vibrations, during which a periodic change of dipole moment occurs, will appear in the spectrum. Therefore we will not be able to observe the vibrational spectrum of homonuclear two-atomic molecules.[19]

1.16. Molecular Vibrations

Small vibrations of a two-atom molecule can be best described using the linear harmonic oscillator model, where the molecule is represented by two balls with m_1 and m_2 masses connected by a spring (see Figure 13).

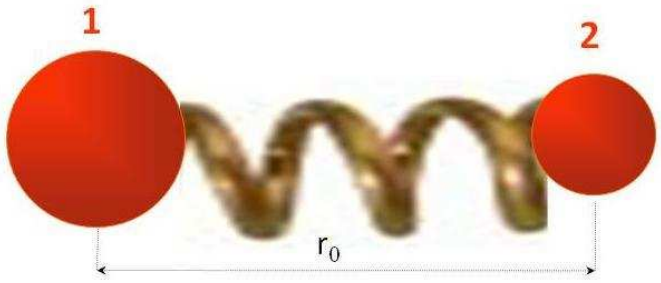

Figure 13: Oscillating molecule model

The counterforce F that is proportionate to the extension of the spring affects the balls during the spring extension.

$$F = -k(r - r_0) = -kx \qquad (42)$$

This relationship is called the Hook's law

where r is the length of the spring during extension

r_0 corresponds to the equilibrium

$$x = r - r_0 \qquad (43)$$

By solving the motion equation of a given system, we will find out that the harmonic oscillator oscillates with the frequency *f*:

$$f = \frac{1}{2 \cdot \pi} \cdot \sqrt{\frac{k}{m_r}} \qquad (44)$$

The proportional constant *k* (strength constant) characterizes the spring rigidity or the strength of a bond on molecular scale.

By solving the Schrödinger's equation of this system we will obtain discrete values of a vibration energy that can be gained by the harmonic oscillator:

$$E_v = h \cdot f \cdot (v + \frac{1}{2}) \qquad (45)$$

where v is the vibration quantum number with the following values

$v = 0, 1, 2, 3$ (46)

This equation demonstrates that even for the lowest vibration state ($v = 0$) the energy E_v is not zero.

The potential curve that shows the dependency of potential energy on deviation from the equilibrium position and allowed vibration level of the linear harmonic oscillator is shown on Figure 14 in red.

The mentioned simplified description can be used for only very small molecule oscillations, and therefore for their lowest energy states. When the spring (bond) is compressed or extended during vibrational pass a certain limit, the Hook's law becomes invalid. The molecule then does not behave as a harmonic oscillator any more.

Dependency of the potential energy on internuclear distance in actual molecules is then better explained by the empirical relationship proposed by P. M. Morse:

$$V = D_e \cdot [1 - e^{-a(r-r_0)}]^2 \qquad (47)$$

D_e is the molecule spectroscopic dissociation energy,

the constant *a* characterizes a given molecule electronic state.

The Morse's curve that shows the dependency of potential energy on deviation from equilibristic position and allowed vibration level of a two-atom molecule is shown on Figure 14 in green.

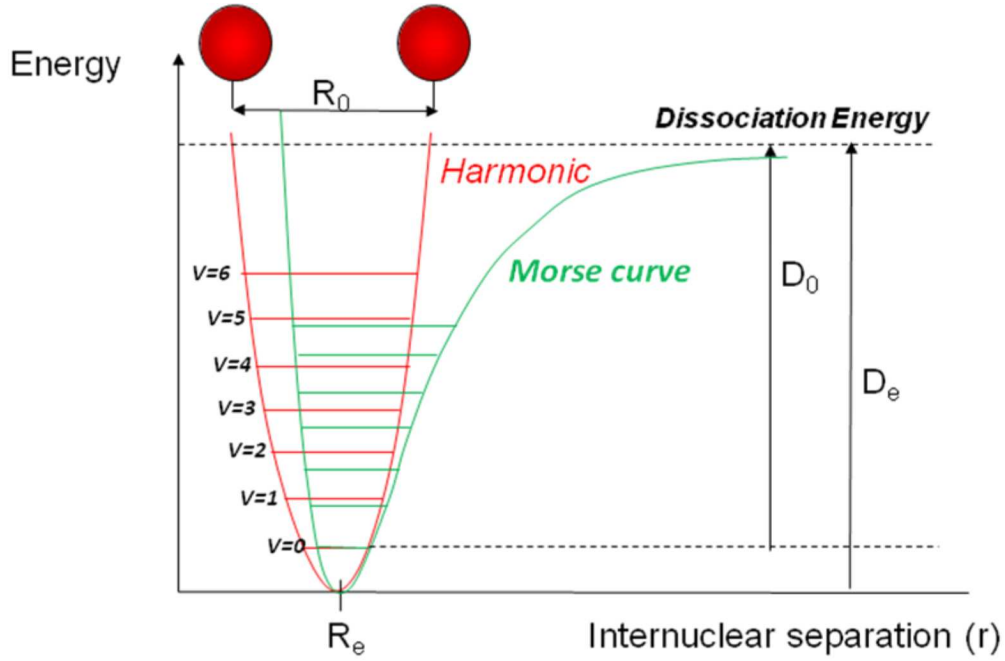

Figure 14: Potential curves

For transitions between the non-harmonic oscillator levels is valid that:

$$\Delta v = \pm 1, \pm 2, \pm 3, \ldots \qquad (48)$$

Intensity of spectral transitions decreases quickly with the increasing value of $|\Delta v|$.

The spectrum indeed, beyond so called fundamental bands, has much less intensive upper harmonic bands (overtones), hot bands (see Figure 15), and sometimes also combination bands.

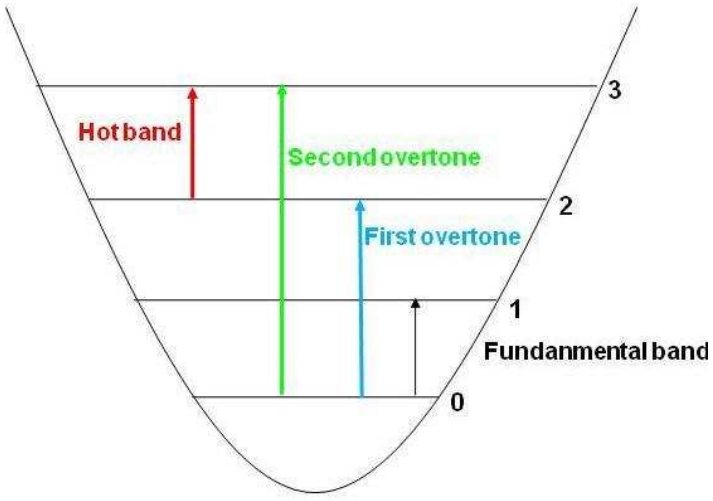

Figure 15: The types of vibrational transitions [36]

By solving of the Schrödinger's equation of such system we gain a series of energy values that get closer to one another with increasing quantum value in:

$$E_v = h \cdot \mathrm{f} \cdot \left(\mathrm{v} + \frac{1}{2}\right) - \frac{\mathrm{h}^2 \cdot \nu^2}{4 \cdot \mathrm{D_e}} \cdot \left(\mathrm{v} + \frac{1}{2}\right)^2 \qquad (49)$$

With the increasing number of atoms, problems related to mathematical analysis of vibrations also increase.

1.17. Rotational-Vibrational Spectroscopy

It is important to realize that the deceleration of molecular rotation, or possibly its complete stop usually occurs only in liquids, solid species, and partially also in compressed gases - that is, in condensed samples. Then we can talk about purely vibration spectroscopy of species. The rate of rotational deceleration depends on the size and the type of molecular interactions and also on the temperature of a sample.

During absorption of medium (MIR) and near (NIR) infrared radiation by a molecule coincidental a change of molecule vibrational and rotational states occurs. The resulting molecule rotational-vibrational energy is then given by the sum of the vibrational energy E_v and the rotational one E_r.

During the first approximation we can assume that the rotations and vibrations are mutually independent and write the following for the energy of molecule with neglecting of non-harmonicity and the correction for elasticity of the rotor:

$$E_{v,r} = h \cdot \nu \cdot \left(v + \frac{1}{2}\right) + \frac{h^2}{8 \cdot \pi^2 \cdot I} \cdot J \cdot (J + 1) \qquad (50)$$

We can characterize each rotational-vibrational level by the quantum number $\boldsymbol{\nu}$ and the rotational quantum number J.[37]

The following rules are valid for **linear molecules** with the permanent dipole moment directed along the axis of symmetry:

$$\Delta \mathrm{J} = \pm 1 \qquad (51)$$

The following rules are valid for **linear molecules** with the permanent dipole moment directed along the axis perpendicular to the axis of symmetry:

$\Delta J = 0, \pm 1$ (52)

The following rules are valid for **symmetrical rotor molecule types** with the permanent dipole moment directed along the axis of symmetry:

$\Delta J = 0, \pm 1 \quad \Delta K = 0 \quad \text{for } K \neq 0$ (53)

$\Delta J = \pm 1 \quad \Delta K = 0 \quad \text{for } K = 0$ (54)

The following rules are valid for **symmetrical rotor molecule types** with the permanent dipole moment directed along the axis perpendicular to the axis of symmetry:

$\Delta J = 0, \pm 1 \quad \Delta K = \pm 1$ (55)

The following selection rules are valid for **asymmetrical rotor molecule types**:

$\Delta J = 0, \pm 1$ (56)

In conjunction with admissible values of J given by the selection rules, we can distinguish the following line bands in molecular spectra (see Figure 16):

Branch P with selection rule $\Delta J = -1$ (57)

Branch R with selection rule $\Delta J = +1$ (58)

Branch Q is the middle of the band,
where the $\Delta J = 0$ is valid. (59)

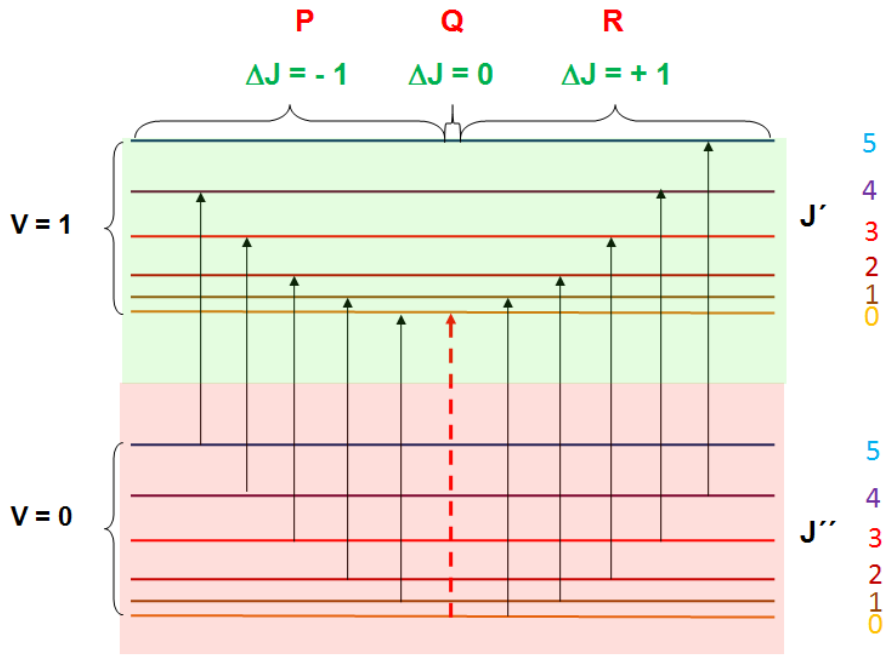

Figure 16: Schematic representation of the rotational vibration energy levels

1.18. Electronic Spectroscopy

I am going to talk about the electronic spectroscopy only shortly, since it is not a topic of this work. The electron spectroscopy studies the transitions between two different electronic levels. There is a change in molecule energy during the electron transitions that leads to the change of electronic state, i.e., to the change of electron orbitals of molecule. Differences in energy that correspond to these electron level changes correspond to the energy of photons of visible and so called ultraviolet areas of a spectrum and also to the X-ray area.

Electron spectra are measured both in absorption, and emission arrangements. Energy values of molecule electron levels can in part represent a type and strength of a chemical bond, in part characteristics of individual atoms in a molecule.

The energy difference between two molecular energy states is usually many times larger than between vibration states, and there is usually a change of the vibrational and rotational states during a change of the electronic state at the same time. Electronic spectra are provided by all molecules, since changes in the electronic distribution are always accompanied by the changes in its dipole moments.

Selection rules related to the symmetry of wave functions describing upper and lower electronic states are applied.

1.19. Spectroscopic Methods Used in This Work

- Microwave spectroscopy (MW)
- Fourier transform infrared spectroscopy (FTIR)
- Optoacoustic spectroscopy (PAS)

1.19.1. Microwave Spectroscopy (MMW)

The microwave spectroscopy uses the absorption of electromagnetic radiation related to the change of only rotational movement of a molecule that takes place within one vibration state and one electronic state.

This method is practically useful only in a gaseous phase, since in this phase molecules can move freely and rotate. In liquids or in solid phase the rotational movement is eliminated due to weak intermolecular interactions, or presence of a molecule grid.

The beginnings of the microwave spectroscopy can be connected to the names of Cleeton and Williams [38], who performed the first spectroscopic measurement in the microwave area in 1933. The first microwave high resolution spectrometer with tunable monochromatic source of radiation was designed by Bleaney and Penrose in 1945. They obtained the first high resolution microwave spectrum of ammonia using this spectrometer.

A classical microwave experimental arrangement consists of a radiation source, a cell, and a detector. The radiation sources are clystrons, magnetrons and carcinotrons.[40]

The carcinotrons, better known under their English name of [39] "*backward-wave*" *oscillators (BWO oscillators),* are based on the interaction of an electron beam with an electromagnetic wave slowed down in suitable periodic structures in the form of the planar microstructures or helixes from conductive materials. Advantages of these sources are a relatively high input of up to 100 mW and a possibility of continuous frequency tuning within a wide range, on the other hand there are disadvantages like a high price, need of a strong magnet, high-voltage source, and higher instability in

comparison with klystrons. The frequency instability can be eliminated by a phase tie to a frequency source with higher frequency stability. [2]

The above mentioned sources are today gradually replaced by solid-state oscillators that use semiconductor elements, mostly Gunn diodes, since they show much lower noise, are tunable across a wide frequency range and have long lifetimes. Even here they need to be frequency stabilized using the phase lock loop. An important property of all mentioned microwave sources is generation of the linearly polarized radiation.

So called *bolometers* and also *diode crystals* are mostly used as radiation detectors.

The frequency and amplitude modulations are used to obtain better signal to noise ratio, and thus an increase in measurement sensitivity. It is valid that the frequency modulation is more sensitive than the amplitude one. On the other hand the frequency modulation introduces a deformation of a spectrum through the instrumental function and a decrease in resolution.[2]

1.19.2. Fourier - Transform Infrared Spectroscopy (FTIR)

The FTIR spectroscopy uses the Michelson interferometer, where source radiation passes onto semi-permeable beam splitter that lets through half of the rays toward a movable mirror, and reflects the other half to a fixed mirror. The rays reflect back from both mutually perpendicular mirrors and the partial waves are summed together or subtracted at the beam splitter according to the position of the movable mirror. What happens here is interference. Obtained signal is mathematically transformed – by the Fourier transform – to the infrared spectrum.

The time resolved Fourier transform infrared spectroscopy that I have used in the experimental part is a very suitable technique to study dynamics of chemical processes. The basic principle of the time resolved Fourier transform infrared spectroscopy is switching on a pulse charge in time intervals defined by the position of interference maximum of the HeNe laser (100 - 200 μs). During the time the charge is switched on and there is a signal recorded from a detector in a selected time interval (1 - 6 μs). From the obtained data matrix - the signal intensities I within given time t and trajectory difference δ - we obtain interferograms that correspond to the time t $I(t,\delta)$ that are separately recalculated to the spectrum corresponding to the certain time t $S(t,v)$ using the Fourier transform.[40][42] FTIR spectrometers have high light sensitivity in comparison with the classical dispersion ones. The huge advantage is a high resolution

that depends on the size of used optical trajectory difference. The resolution can be increased by a large movement of the mirror. The limitation of this method is the sensitivity of the infrared FT emission technique, as well as the considerable time required to obtain the data.[43]

1.19.3. Laser Photoacoustic Detection Method (PAS)

The laser photoacoustic spectroscopy (PAS) is a quantitative analysis method physically based on the photoacoustic phenomenon.[44]

The principle of the photoacoustic spectroscopy lies in the following phases:

1. Excitation of a molecule to the higher energy level by absorption of electromagnetic radiation.
2. Radiation less relaxation of the excited state demonstrated by increased temperature and pressure in a cell.
3. Modulation of laser intensity to the acoustic frequency demonstrated by periodical changes of pressure and temperature – the pressure is observed as an acoustic signal.
4. Detection of the acoustic signal by a sensitive microphone.[45] [46][47]

The experimental arrangement generally consists of a radiation source (e.g. CO_2 laser), an optoacoustic cell, and a radiation detector.

The molecular gas CO_2 laser that operates on rotational-vibration transitions of a CO_2 molecule serves as a radiation source, and contains three basic parts [48]

- Active laser environment, where the radiation is amplified
- A source for excitation of the active environment
- A resonator that creates the feedback between the radiation and active environment that leads to laser oscillations

If the active environment with an inversion content of the levels is enclosed in an optical resonator (created by two plan-parallel mirrors), the laser radiation feedback enables creation of the electromagnetic oscillation generator. If light amplification in the active environment exceeds losses during one passage between the mirrors, the laser will start emitting radiation with the wave length characteristic of the given active environment. One of the mirrors is partially permeable in order to release the laser beam out of the resonator.[47]

Three basic types of acoustic modes (see the Figure 17) can originate within cylindrically enclosed cell, the space, in which there is the interaction between the particles of the flow through gas and the laser radiation.

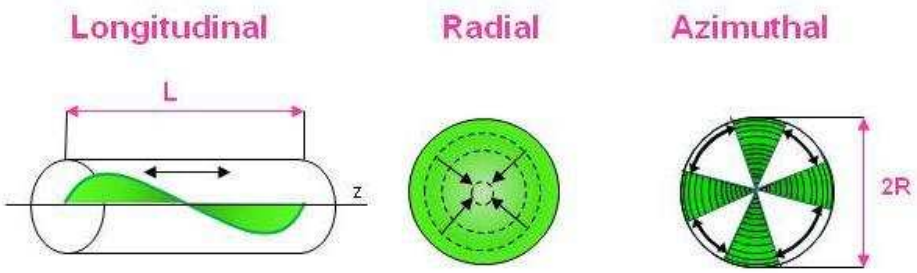

Figure 17: The basic acoustic mode types

Nowadays there are a lot of optoacoustic detection method modifications that enable analysis of gaseous and condensed species.[49] This method enables even the trace detection of gaseous species in the order of concentrations of ppbV to ppmV, i.e., 10^{-9} to 10^{-6} of volume ratios. It is used for monitoring of atmospheric harmful species, during monitoring of dangerous chemical production products, during detection of explosives and drugs [45]. The versatility of using the OA laser detection is given by the possibility to tune the laser. The last but not least advantage of this method is also mobility of the analyzer, which does provide a possibility to perform measurements in laboratory, and also in certain distances from a source. [45][46][47]

The main disadvantage of this method is a comparatively high acquisition price and repair and maintenance of the CO_2 laser.[47]

2. Performed Spectroscopic Studies

The work itself has been focused on the studies of selected species significant by their influence on human health, atmospheric chemistry and environment, phenomena taking place in Universe, and progress and study of phenomena taking place in a simulated environment of the discharge plasma. The following species (NH_3, HCN, HNC, BrCN, CH_3CN, $FCO_2^{\cdot}$, $CS^{\cdot+}$) were investigated by various spectroscopic methods.

The very first analyses of the asymmetrical vibration ν_4 band and the symmetrical ν_2 band of the $FCO_2^{\cdot}$ radical that belong among significant intermediate products of degradation processes of halogen hydrocarbons were performed within presented dissertation. The detail analysis led to the determination of the rotational constants, centrifugal distortion constants, and fine splitting interaction constants of both bands. For the first time in history we performed the spectroscopically unambiguous identification of the molecular radical ion $CS^{\cdot+}$ using the microwave spectroscopy with high spectral resolution in the frequency range of 414 to 622 GHz. The complex analysis allowed us to exactly determine the values of rotational constants as well as the fine structure constants.

We designed and performed experiments including measurements of spectra of the cyan BrCN and CH_3CN species by the time resolved Fourier transform infrared spectroscopy. The behavior of these molecules and their disintegration products in the low temperature plasma environment has been studied.

Finally we have studied the ecological impact of ammonia on the environment and influence of trees on the amount of ammonia in the air and assembled the optoacoustic cell of experimental arrangement of the laser optoacoustic detection method for measuring of trace amounts of ammonia and other gaseous species.

Each performed experiment had been preceded by the research of literature in the area of given problematics, or selection of a precursor suitable for generation of unstable compounds (spectroscopically investigated products) and the study of the conditions of their origination. Radicals are often extremely reactive species, whose laboratory identification is often possible only through finding a suitable precursor and correct experimental conditions. Finding a stable molecule, from which a given radical can be created in the amount sufficient for detection, is in many cases very complicated.

Not always was a started experiment finished by finding of the sought species, and different conditions of creation of investigated species had to be selected, or the experiment had to be finished. Analyses of measured spectra followed the experimental work. Quantum numbers were found for individual lines of measured spectra by iterations using exclusion and comparison methods. Thus was achieved unique identification of the investigated molecules and obtained information about individual energy levels at the same time. The atomic lines in the spectra were assigned by comparison with the lines published in databases (e.g. www.nist.gov) and in the available literature.

The situation was much more complicated in cases of some molecules, especially radicals in the interest area that were never investigated. So called *ab initio* calculations were performed in cooperation with quantum chemists. Input parameters for these prediction calculations were the characteristic chemical properties of molecules coming out of number of atoms, lengths of bonds, molecular symmetries, electronegativity and spin statistics, and approximate positions of the lines were obtained as the resulting information.

2.1. Analysis of $FCO_2^{\cdot}$ Radical Infrared Spectrum

In 1995 Prof. G. A. Argüello et all. at Berchische Universität in Wuppertal (Germany) measured several fundamental and combination bands (ν_6 ~735 cm^{-1}, $2\nu_5$ ~948 cm^{-1}, ν_2 ~970 cm^{-1} and ν_4 ~1094 cm^{-1}) of the infrared spectrum of the $FCO_2^{\cdot}$ radical in the spectral area of 600-1400 cm^{-1}. The infrared spectrometer with the Fourier interferometer Bruker HR 120 was used for the measurement with the spectral resolution of 0.003 cm^{-1} in the order of the Doppler width. [50]

In my dissertation I have occupied myself with analyses of two vibrational bands obtained from this measurement. They were the ν_2 symmetrical and ν_4 asymmetrical excited vibrational bands of the ground electronic state $\tilde{X}^2B_2$. This is the very first study of these vibrational bands of vibration-rotationally resolved structure of this radical. Figure 18 shows these two investigated bands.

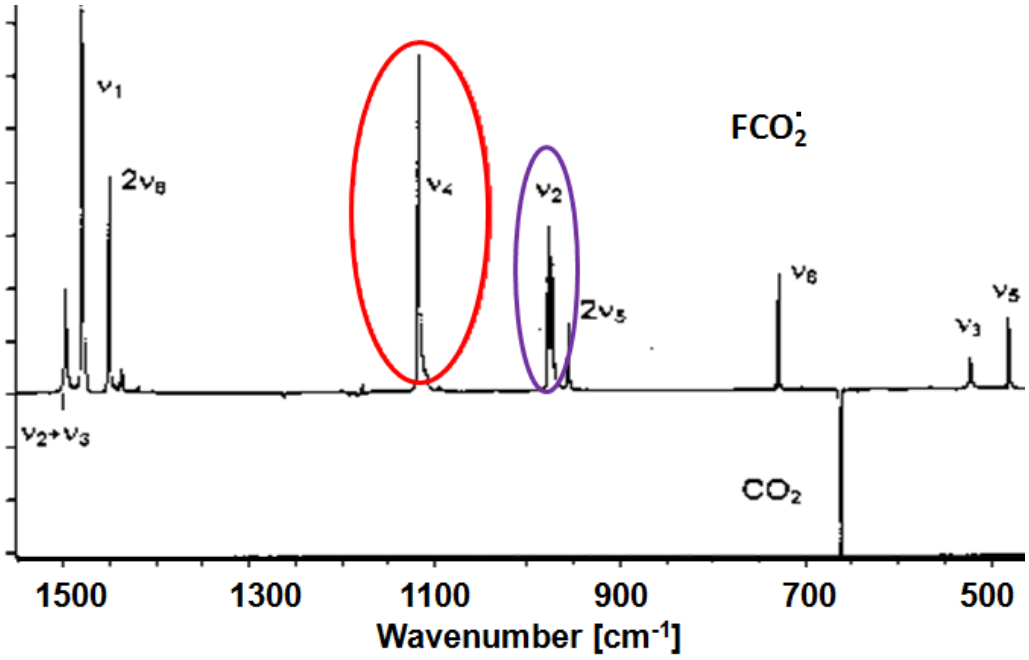

Figure 18: The infrared spectrum of $FCO_2^{\cdot}$ radical obtained in the Matrix experiment [50]

A thorough study of this molecule, analysis of its molecule structure and symmetry (necessary for determination of the wave function), and derivation of the selection rules applied in the spectrum preceded its infrared spectrum analysis.

2.1.1. The $FCO_2^{\cdot}$ Radical Symmetry

Fluoroformyloxyl is a radical that consists of four atoms: ^{19}F, ^{12}C, and two identical atoms ^{16}O. Basically, this is a CO_2 molecule with a fluorine atom attached to carbon one.[51] Bond lengths and angles calculated based on chemical calculations are specified in the Table 6. The molecule center of gravity lies at the connection of CF atoms, closer to the carbon one. The molecule contains an unpaired electron that causes the open valence system.

Table 6: The bond lengths and angles of the $FCO_2^{\cdot}$ radical [52]

Samples	re (CF) / pm	re (CO) /pm	re (XC) / pm	angle (OCO) / deg
$FCO_2^{\cdot}$ X^2B_2	131.02	123.44	10.18	118.8

X is the center of gravity.

The $FCO_2^{\cdot}$ radical is an asymmetrical rotor with the planar structure. Because I am going to deal with the symmetry of this molecule in the following chapter, it should be correct to mention symmetry operations in short here. We perform an appropriate symmetry operation on the **symmetry elements**.

We divide molecules into exactly defined point groups according to their symmetry.

A point group is a group of symmetry elements, whose operations leave at least one space point unmoving.

In a state of equilibrium $\tilde{X}^2B_2$ this radical belongs to the point group C_{2v}, which means that it is symmetrical along two-fold symmetry axis, and also along two, mutually perpendicular, symmetry planes (see Figure 19).

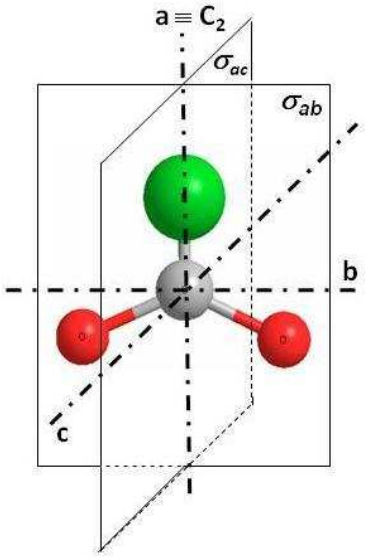

Figure 19: The $FCO_2^{\cdot}$ molecule model

In agreement with previous studies[53] the representation I^r (a=z, b=x, c=y) was selected, so that the principal axis a, along which the permanent dipole moment lies, became the axis of symmetry, and also the axis of the smallest moment of inertia (I_a).

The elements and operations of $FCO_2^{\cdot}$ radical symmetry are summarized in Table 7.

Table 7: The elements and operations of $FCO_2^{\cdot}$ radical symmetry

Symmetry element	Symbol	Symmetry operation
Identity	E	nothing happens
Axis	C_2	turn by 180°($2\cdot\pi/2$)
Plane	σ_{ab}, σ_{ac}	Reflection
Center of symmetry	I	Reflection through the center of symmetry

Table 8 shows the characteristics of the point group C_2v.

Table 8: Characteristics of the point group C_2v [54]

C_2 v	E	C_2	σ_{ab}	σ_{ac}	Vibration	
A1	1	1	1	1	ν_1, ν_2, ν_3	**Symmetrical vibration**
A2	1	1	-1	-1		
B1	1	-1	1	-1	ν_4, ν_5	**Asymmetrical vibration**
B2	1	-1	-1	1	ν_6	

Letters A and B in the Table 8 signify symmetry and mean:

A1 means that molecule is symmetrical according to all symmetry elements

A2 means that molecule is symmetrical according to the identity and two-fold symmetry axis, but it is not symmetrical according to planes

B1 means that molecule is symmetrical only by the identity and the plane σ_{ab}

B2 means that molecule is symmetrical only by the identity and the plane σ_{ac}, so the values

+1 demonstrate that there was no change after the symmetry operation, and

-1 that there was a change after performing of the symmetry operation

Nuclear spins of carbon and oxygen atoms are equal to zero (I (^{12}C) = 0, I (^{16}O) = 0), which means that they are bosons. Only fluorine (^{19}F) has the nuclear spin equal to ½, which makes it so called fermion.

Presence of two identical bosons (interchangeable oxygen atoms) in the $FCO_2^{\cdot}$ radical predetermines that the molecule wave function follows the Bose-Einstein's wave statistic. Based on the Pauli's principle that says that the wave function of two identical bosons must be symmetrical, we can derive that the **total wave function of the $FCO_2^{\cdot}$**

radical is symmetrical. This means that if we mutually exchange two oxygen atoms in this radical, the total wave function will not change the sign ($\Psi \rightarrow \Psi$ (+1)).

In accordance with the characteristic table of the point group it corresponds to the total wave function of the $FCO_2^{\cdot}$ radical of the **A1 and A2 representation**.

We can write the total wave function Ψ as the product of electron Ψ_{el}, vibration Ψ_{vib}, rotation Ψ_{rot}, and nuclear spin Ψ_{ns} wave functions:

$$\Psi = \Psi_{el} \cdot \Psi_{vib} \cdot \Psi_{rot} \cdot \Psi_{ns} \qquad (60)$$

We have to analyze the individual wave functions in the next step. The wave function of the electronic state $\tilde{X}^2B_2$ has the B2 symmetry, and the wave function of the ground vibrational state has the A1 symmetry.

The rotation wave function depends on the combination of even and odd values of quantum numbers K_a, and K_c (see Table 9), for which the following selection rules are valid:

$$K_a + K_c = N \text{ or } N + 1 \qquad (61)$$

Table 9: The Ka, Kc symmetry [55]

Ka	**Kc**	**Representation of Ψ_{rot}**	
Even number	Even number	A1	Symmetrical
Even number	Odd number	A2	
Odd number	Even number	B1	Asymmetric
Odd number	Odd number	B2	

The quantum numbers K_a and K_c are projections of rotational angular momentum into the axis z for the limit cases of prolate and oblate rotors.

Each of these functions must be transformed according to one irreducible representations of the group C_2v, i.e., it must have one of the A1, A2, B1, or B2 symmetries.

The nuclear-spin wave function is given by the sum of spins of all nuclei, and is completely symmetrical as well. (A1).

Once we substitute to the equation $\Psi = \Psi_{el} \cdot \Psi_{vib} \cdot \Psi_{rot} \cdot \Psi_{ns}$ (62)

we will obtain: $1 = (-1) \cdot 1 \cdot \Psi_{rot} \cdot 1$ (63)

$$\Psi_{rot} = -1 \qquad (64)$$

and find out that the **total wave function of the ground vibrational state is symmetrical only and just for the odd numbers of the quantum number K_a.**

The same way we will find out that for the first excitation vibration state is valid that the vibration wave function depends on the character of the vibration band.

For ν_4 asymmetrical vibration band the vibration wave function is asymmetrical, and therefore the total wave function of the ν_4 band is symmetrical for even values of K_a only, and the other way round for the **ν_2 symmetric vibration band the vibration wave function and the total wave function are symmetrical only for odd values of K_a**.

The influence of unpaired electron in a spectrum shows itself by splitting of electron levels to two sublines (except of N=0) by so called fine splitting. The effect of nuclear spin of the fluorine atom demonstrated by splitting of this two sublines to further two sublines - so called hyperfine splitting is much smaller that the fine splitting (see Figure 20), and can be observed only through measuring techniques that enable to sensitively monitor very small energy changes (e.g. microwave spectroscopy); we do not observe this hyperfine splitting in the infrared spectrum (it is joined together).

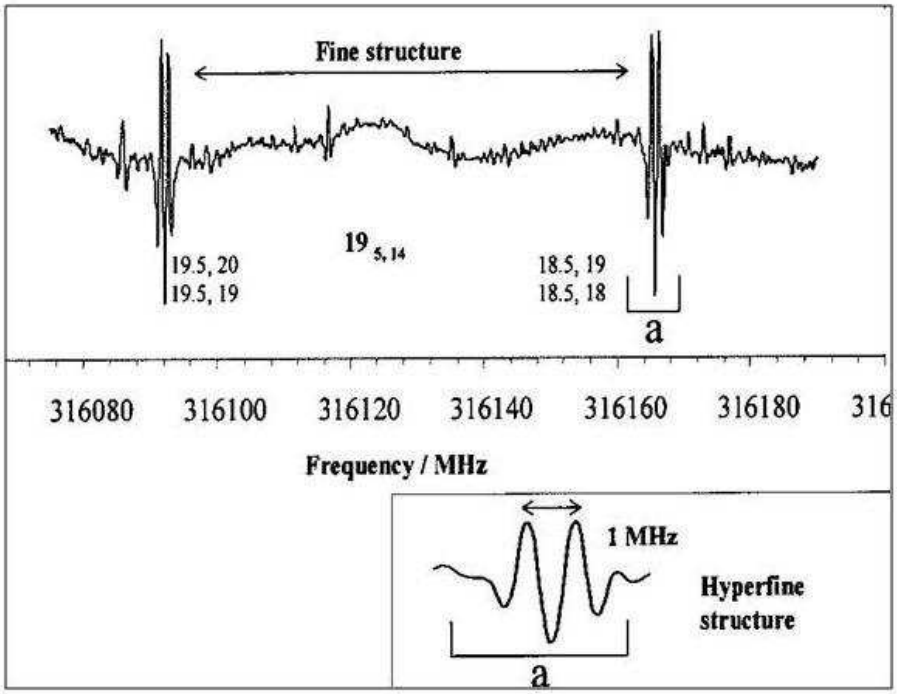

Figure 20: Example of fine and hyperfine structures from the microwave spectrum of $FCO_2^{\cdot}$ radical [53]

2.1.2. Chemistry of the $FCO_2^{\cdot}$ Radical

The $FCO_2^{\cdot}$ radical occurs during the stratospheric degradation of fluorized hydrocarbons (HFC- hydrofluorocarbons) and hard and soft freons (CFC-chlorofluorocarbons, HCFC-hydrochlorofluorocarbons).[56] [57]

Its production is in small amounts influenced by alternate extinguishing agents with chemical mechanism of extinguishing that are a significant source of the fluorine species emissions (e.g. CF_2O), from which CFCO is created. A principle of these extinguishing agents is that during combustion the hydrofluorocarbons change F into HF and also CF_2O, and thus reduce concentration of species necessary for propagation of flame (H and $OH^{\cdot}$). So, this is an interesting molecule, both from the point of view of stratospheric chemistry, and spectroscopy and fire chemistry.

From the physical and chemical property point of view this radical is very similar to the isoelectron radical NO_3. This is demonstrated by similar electron absorption spectra and reactivity of these samples in comparison with atmospheric trace gases.[51]

It differs from the molecules like XCO_2, where *X = Cl, Br, I,* especially by a stronger bond in the connection of a halogen element with Carbon. As opposed to

chlorine, bromine and iodine that are bonded with Carbon by the weak van der Waals bonds there is a covalent bond between fluorine and Carbon in the $FCO_2^{\cdot}$ radical with the dissociative energy of 11.5 kcalmol^{-1}

Thanks to this difference the $FCO_2^{\cdot}$ radical belongs among "longer living radicals" with the lifetime of 3 s at the temperature of 296 K and the atmospheric pressure.[53] With lower temperatures and pressures in stratosphere its lifetime is probably much longer; and it can participate in many chemical reactions.

The following reactions of this radical in atmosphere are most significant [57]:

$$FCO_2^{\bullet} + NO \rightarrow FNO + CO_2 \quad (65)$$

$$FCO_2^{\bullet} + NO_2 \rightarrow FNO_2 + CO_2 \quad (66)$$

Further atmospheric reactions are:

$$FCO_2^{\bullet} + HO_2^{\bullet} \rightarrow HF + CO_2 + O_2 \quad (67)$$

$$FCO_2^{\bullet} + FCO^{\bullet} \rightarrow CF_2O + CO_2 \quad (68)$$

$$FCO_2^{\bullet} + F^{\bullet} \rightarrow FCO_2F \quad (69)$$

Degradation of HCFC and HFC and theoretically possible intermediate products are shown in Figure 21.

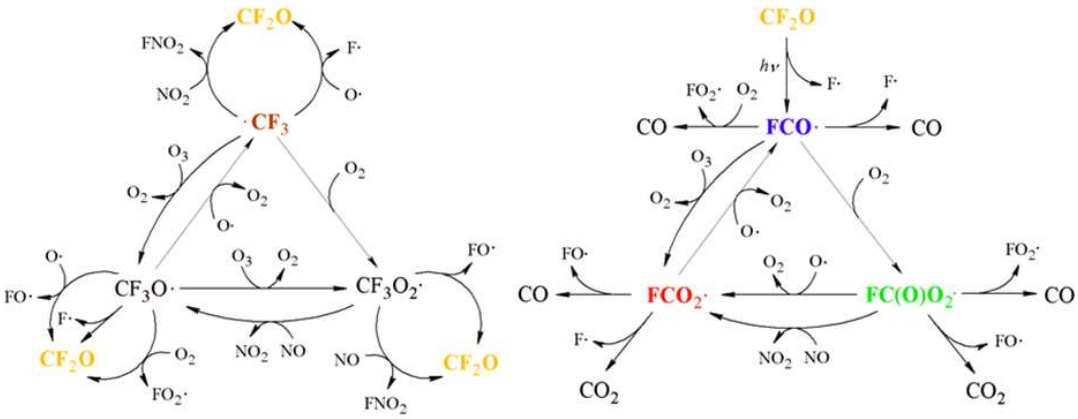

Figure 21: Degradation of HCFC and HFC and theoretically possible intermediate products [35]

It was found that this radical does not practically cause ozone loss.[52][57][35]

2.1.3. Previous Studies Related to this Work

Recent interest on the fluorocarboxyl radical, $FCO_2^{\cdot}$, is motivated because it is assumed to participate in atmospheric processes such as the degradation of hydrofluorocarbons that have been considered as chlorofluorocarbon substitutes.[56][68] However there still exists rather little information on the spectroscopic properties of the $FCO_2^{\cdot}$ radical.

J. S. Francisco et al. led the first theoretical considerations that predicted existence of this fluoroformyloxyl radical $FCO_2^{\cdot}$ in 1988.[59] [60] Maricq et al. first observed the highly structured absorption in the visible area in 1993, and the transition $X^2B_2 \rightarrow B^2A_1$ of the radical was assigned.[57] Argüello et al. performed the Matrix experiment in the the visible spectrum and the IR spectrum of natural $FCO_2^{\cdot}$, $FC^{18}O_2^{\cdot}$ and $F^{13}CO_2^{\cdot}$ isolated in noble gas matrices was reported [50]. In this study the free $FCO_2^{\cdot}$ radical was prepared by vacuum flash pyrolysis of bis(fluoroformy1) peroxide, FC(O)OOC(O)F, diluted in N_2, Ar, or Ne and, the six fundamental vibrational states for $FCO_2^{\cdot}$ in the ground X^2B_2 electronic state were assigned. For $FCO_2^{\cdot}$ isolated in Ne the ν_1, ν_2 and ν_3 modes are at 1475, 960, and 519 cm^{-1} (A_1 symmetry), ν_4 and ν_5 at 1098 and 474 cm^{-1} (B_1 symmetry), and ν_6 at 735 cm^{-1} (B_2 symmetry).

Zelinger et al. performed first gas-phase detection of the $FCO_2^{\cdot}$ radical by millimeter wave in the spectral region of 240-380 GHz[52] and 210-245 GHz[61] (see Figure 22). High resolution infrared spectroscopy was performed guided by *ab initio* calculations. In this way the observed infrared bands ν_1 (1478 cm^{-1}), ν_2 (970 cm^{-1}) and ν_4 (1094 cm^{-1}) were identified.

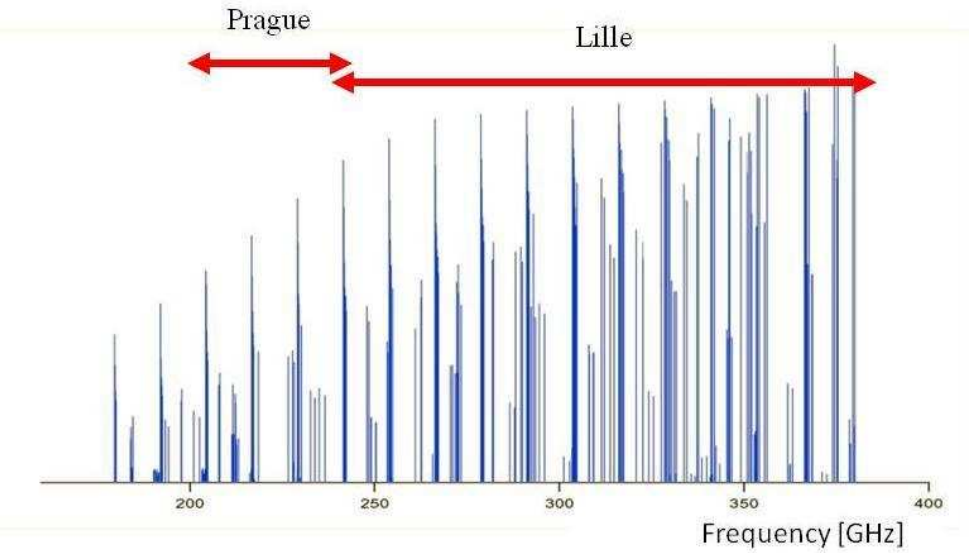

Figure 22: Investigated spectral range of $FCO_2^{\cdot}$ radical in Lille and Prague [61]

The rotation constants, quartic centrifugal distortion constants, and fine and hyperfine splitting constants of the ground vibrational state were determined.

No rotational- vibration band spectra were analyzed till now. This work presents the very first analysis of vibration bands $v_4 = 1$ and $v_2 = 1$ of the $FCO_2^{\cdot}$ radical infrared spectrum measured by FTIR.

2.1.4. Description of the Investigated Bands

Below are depicted the investigated vibration bands of the infrared spectrum, schematics of the $FCO_2^{\cdot}$ radical vibration bands, and descriptions of the individual bands.

The ν_4 asymmetrical vibration bands measured in the 1040 – 1130 cm^{-1} spectral

region

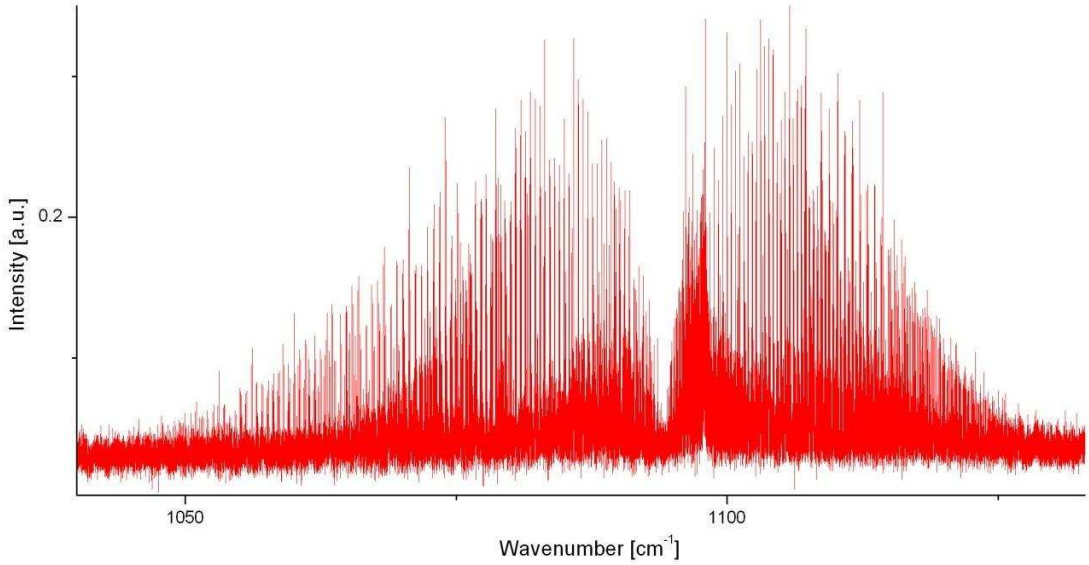

Figure 23: An overview of the ν_4 band spectrum obtained by FTIR spectroscopy

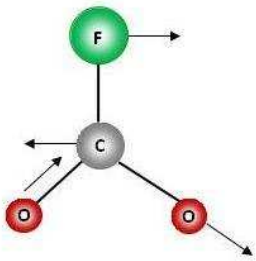

Figure 24: Schematic of ν_4 vibration band

Band Description

- Asymmetrical fundamental
- CO stretched
- b type, perpendicular

} band

The change of electric dipole moment during vibration occurs along the main axis b.

The ν_2 symmetrical vibration band measured in the 600–1400 cm^{-1} spectral region

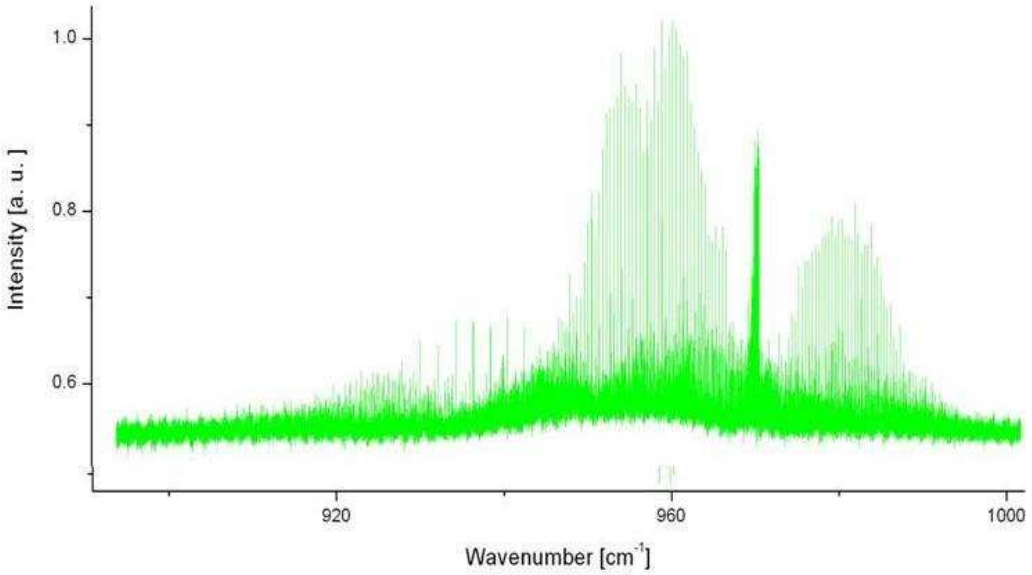

Figure 25: The overview of the ν_2 band spectrum obtained by FTIR spectroscopy

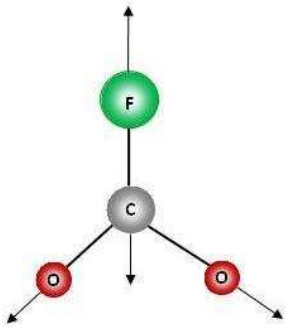

Figure 26: Schematic of ν_2 vibration band

Band Description

- Symmetrical fundamental
- CF stretched
- a type, parallel

} band

The change of electric dipole moment during vibration occurs along the main axis a.

2.1.5. Partial Results and Discussion

This work presents the very first analysis of vibration bands $v_4 = 1$ and $v_2 = 1$ of the $FCO_2^{\cdot}$ radical infrared spectrum. Its rotational-vibrational spectrum was difficult to interpret spectroscopically, because this is the very first study of rotationally resolved structure of vibrational bands of this asymmetrical rotor type radical. As it came up during the solution this spectrum exhibits very complex character.

The Table 10 has very short descriptions of the individual investigated bands, band centers, selection rules, and Hamiltonian models used for fitting. This information is located in Table 10 columns for comparison of the two bands.

Table 10: Characterisations of investigated bands

	The ν_4 band of electronic state $\tilde{X}^2B_2$	The ν_2 band of electronic state $\tilde{X}^2B_2$
- Lines P and R were grouped into clusters - Distance between two individual clusters corresponds to the value of 2C - Individual line distances of clusters are equal to $2N\text{-}K_c$		
Band Description	- unperturbed band - in IR spectrum, separated from other bands - creates very dense spectrum - P and R medium intensity branches dominate the spectrum - Q branch smoothly flows into P and R branches - regular cluster transitions - each line is created by a double caused by spin-rotational interaction (fine splitting) - assigned almost all spectral lines	- From N≥40 strongly influenced by energy levels 2ν5 of the dark overtone - connected with 2ν5 band by Fermi-resonance - P and R branches have strongest lines that contain low Ka values, but lines overlap significantly - Q branch is overloaded by lines - where the strongest lines have K_a=J and very low K_c - fine splitting was observed only in the weak lines (low K_a or K_c) of P and R branches and Q (high K_a) - some lines were impossible to assign - they probably belong to hot bands - ν_5 and ν_3
Band center	1094 cm^{-1}	970 cm^{-1}
Selection rules	Only even K_a $K_a + K_c = N$ or $N + 1$ $\Delta N = + / - 1$	Only odd K_a $K_a + K_c = N$ or $N + 1$ $\Delta N = + / - 1$

Used Hamiltonian	The lines were fitted using Hamiltonian that consisted of the Watson',rotational Hamiltonian.[63][64]The A reduction was selected that included the quartic centrifugal distortion parameters and the spin-rotational Hamiltonian[63][65] that contained the spin-rotational centrifugal distortion parameters.	The lines were fitted using Hamiltonian that consisted of the Watson's rotational Hamiltonian [66] (the A reduction was selected), the spin-rotational Hamiltonian, and part that included the Fermi resonance. [67][68]

Based on theoretical knowledge of molecular geometry of the $FCO_2^{\cdot}$ radical in equilibrium state (equilibrium structure), a spectral prediction was made, and individual lines were gradually assigned quantum numbers N, K_a, K_c, and J. With the number of correctly assigned lines the predicted spectrum, that gained the shape of the experimentally obtained spectrum, improved.

This analysis has been carried out by using the ground state combination differences (GSCD) from the IR, together with the microwave transitions from the previous measurement, and led to obtaining of a first complete set of excited vibration molecular parameters for determination of rotational and centrifugal distortion constants and then fine and hyperfine constants, i.e., the parameters that provide information about molecular geometry and dynamics - behavior of a molecule during the vibration movement in selected vibration modes of this atmospherically significant molecule.[50]

The GSCD method is suitable for estimate of ground state parameters in case that the upper state has been determined (by data from IR measurement) and for verification of line assignment of the upper energy state levels in the IR spectrum, if parameters of the ground state are very exactly defined (e.g. from MW).

The Figure 27 shows the basic principle of GSCD method.

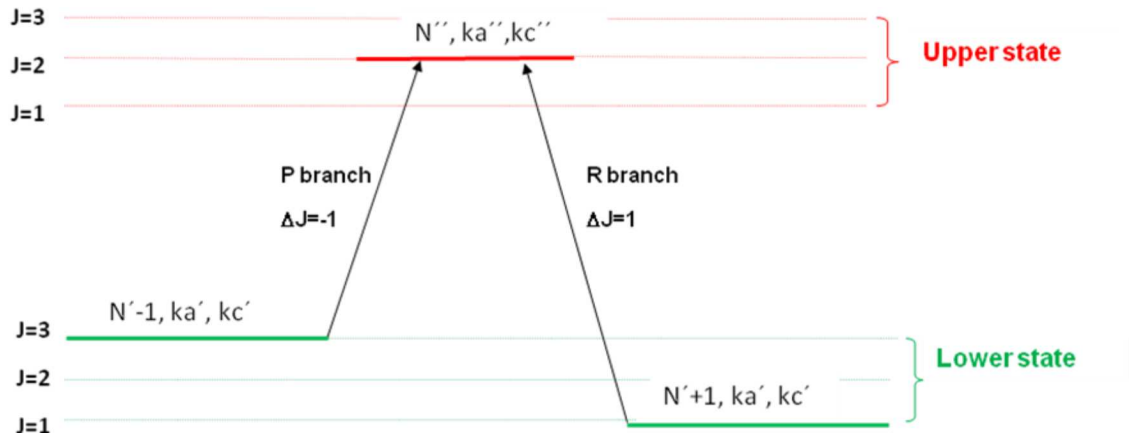

Figure 27: GSCD method principle

The analysis consisted from several parts that could be summarized to four steps.

1. Preliminary spectrum simulation using the ground vibration state constants from the previous study for the upper and lower energy levels (see Figure 28)
2. Assignment of first weak, but well isolated, lines

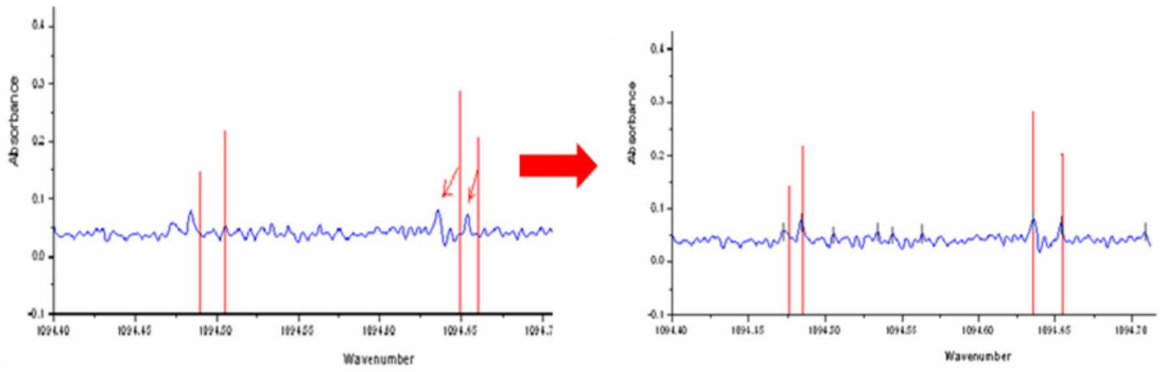

Figure 28: The first simulation vs. the final simulation

3. In case of the ν_4 band (in the vibration state $v_4 = 1$) the first rough analysis of P- and R- branches enabled us to estimate the rotational constant C and also the middle of the ν_0 band. By the consequent analysis of transitions in the weak Q - branch near the middle band, where the spectrum is not so dense, it was possible to estimate rotational constants A and B, and the spin-rotational constants ε_{aa} and ε_{bb}.

   In case of the ν_2 band (in the vibration state $v_2 = 1$) the situation was much more complicated, since the Q branch of spectrum was strongly saturated by lines and, at the same time, the vibration band of the second vibration state

ν_5=2 was affecting the spectrum. The lines of middle and low values of N, and K_a were assigned first and the C constant of the band center was determined.

4. The fitting iterations leading to optimization of the spectroscopic constants, assignment of other lines based on the predictions of positions and intensities, and at the same time to the improvement in spectrum prediction, continued. The iterations continued long enough to sufficiently assign the spectrum.
   The CALPGM fitting program was used for the ν_4 band analysis [69]. Mrs. Agnes Perrin developed a program used for analysis of the ν_2 band.
5. Molecule constants of the vibration states v_4 = 1 and v_2 = 1 of the $FCO_2^{\cdot}$ radical, and the first excited vibration states of this radical in the ground electronic state $\tilde{X}^2B_2$ were determined.

The results of this analysis are more than satisfactory, as can be seen from the size of the main deviation specified in the lower part of the Table 11.

Future interpretation of these constants will lead to closer understanding of geometry of the $FCO_2^{\cdot}$ radical both in base, and excited states, and thus to understanding of its reaction mechanism.

2.1.6. Partial Conclusion

Fluoroformyl oxy and peroxy radicals play a role of crucial importance in atmospheric fate of fluorinated hydrocarbons including the emission from refrigeration units, air conditioning and fire extinguishing systems, etc. Due to its relatively long atmospheric lifetime, $FCO_2^{\cdot}$ radical is the suitable candidate for remote sensing and in-situ monitoring of this pollutants in atmosphere. Substantial progress towards such the efforts was achieved in the frame of this Ph.D. thesis. I would like to point out and appreciate my cooperation with many experts in the field of molecular spectroscopy. The rovibrational analysis of FTIR spectra of $FCO_2^{\cdot}$ radical provides the practical application of the theoretical background and spectroscopic knowledge.

For the case of the ν_4 asymmetrical vibration band

Quantum numbers with N values up to 56 and K_a up to 38 were assigned to 3300 rotational-vibration lines. The exact value of the band center was determined at 1094.142207(61) cm^{-1}. Fifteen parameters that allowed us to make an exact prediction

of all spectrum lines were determined exactly. The three components of the electron–spin rotation tensor ε in the principal inertial axis system have also been accurately determined together with three parameters describing their centrifugal distortion correction. The most remarkable observed variation is that the spin–rotation interaction term ε_{aa} magnitude increases by 114 %, when the ν_4 vibration is excited, while the A rotational constant decreases slightly.

It can be assumed strong influence of the Jahn-Teller effect from large difference of the centrifugal distortion parameters between the first vibration and the ground state from a position of this vibration in low spectral frequencies in comparison with other vibrations [57]. This effect is caused by interaction of the ground electron band and the near electron band $\tilde{B}^2A_1$ (1.630 eV) with different symmetry than the one of the ground electron band during asymmetrical vibration ν_4, and both electronic states $^2B_2$ and $^2A_1$ correlate with A representation.

In other words during the stretch of vibration around the b_2 axis there is a change of the molecule symmetry that already falls into the A representation of the C_s point group, which means that it is no longer symmetrical according to the symmetry axis, does not behave as a rigid rotor, but according to the mirroring plane, and it is not possible to exactly identify which plane it is.

The vibronic interaction can lead to stabilization of the lower symmetry nuclear arrangement and destabilization of the higher energy one.[70][71]

For the case of the ν_2 symmetrical band

The very first analysis of the ν_2 symmetrical vibration band of the ground electronic state of the $FCO_2^{\cdot}$ radical was performed.

The quantum numbers N up to 55 and Ka up to 39 were assigned to 2377 lines. The exact center of this band was determined to be at 970.20822(18) cm^{-1}. The ν_5 band of the second excited vibration band (overtone) falls into the ν_2 band. Coupling of the energy levels 5^2 and 2^1 expresses itself more significantly at higher values of N (N> 40). These two bands are connected by so called Fermi-resonance. At this moment it is very hard to perform the exact analysis of the resonant 5^2 band and calculate rotational constants, since there is no high definition study of this band.[68]

Table 11,12 and 13 summarize obtained result of the analysis.

Table 11: Band origin, rotational and quartic centrifugal distortion constants [cm^{-1}] for the ground vibrational and the $v_4 = 1$, and $v_2 = 1$ states of FCO_2 in $\tilde{X}\,^2B_2$

	$v_4 = 1$ (4^1)	$v_2 = 1$ (2^1)[68]	$2v_5$ (5^2)[68]	$v = 0$ (0)[61]
v_0	1094.142207(61)	970.20822(18)	965 ±2 cm^{-1}	
A	0.45332718 (40)	0.45791846(250)	0.460609(130)	0.45872654(21)
B	0.37798015 (43)	0.37618883(100)	0.379831(110)	0.37726869(18)
C	0.20596570 (14)	0.206146680(570)	0.20887147(910)	0.20656958(19)
Δ_K	0.65448 (69) ×10^{-6}	4.2771(620)×10^{-7}	#	5.231(52) ×10^{-7}
Δ_{NK}	-0.15605 (83)×10^{-6}	97.94(450)×10^{-9}	#	
Δ_N	0.25952(22) ×10^{-6}	2.08360(400)×10^{-7}	6.3592(260)×10^{-7}	2.5654(60) ×10^{-7}
δ_K	0.32457 (22) ×10^{-6}	3.8698(190)×10^{-7}	#	3.5658(1134) ×10^{-7}
δ_N	0.11967 (12) ×10^{-6}	0.81826(300)×10^{-7}	#	1.1047(31) ×10^{-7}
H_K		5.671(770)×10^{-11}		#
H_{KN}		-6.862(990)x10^{-11}		#
h_K		-3.972(500)x10^{-11}		#
σ(fit)	0.50 x10^{-3}	1.7 x10^{-3}		2.2349 x10^{-6}

The values in parentheses apply to the last digit and denotes uncertainty 1 σ.

(Example: If value of band origin is indicated as ν_4= 1094.142207 (61)

then value is 1094.142207 cm^{-1}

accuracy is 0.000061 cm^{-1})

From the Table 11 it is apparent that the spin-rotational constants of the ν_2 band (2^1) are close to the spin-rotational parameters of the ground vibration state, and therefore

fine splitting is observable only for weak transitions of the medium K_a and K_c values in the P and R branches.

Not all lines of the ν_2 symmetrical band spectrum were possible to assign. It is assumed that these lines belong to hot bands.

Table 12: The fine splitting constants, nuclear spin-rotation constants of the FCO_2 radical [cm^{-1}]

	$\nu_4 = 1$	$\nu_2 = 1$ [68]	$2\nu_5 (5^2)$ [68]	$\nu = 0$ (0) [61]
ε_{aa}	-5.9540(80) x10^{-3}	-2.7732(160) x10^{-3}	#	-2.67628(27) x10^{-3}
ε_{bb}	-2.85027 (48) x10^{-2}	-2.73083(150) x10^{-2}	#	-2.65055(20) x10^{-2}
ε_{cc}	-1.5845 (44) x10^{-3}	-1.39817(670) x10^{-3}	#	-1.4733(3) x10^{-3}
Δ^S_N	0.1362(18) x10^{-6}	#	#	-0.1370(34) x10^{-6}
Δ^S_{NK}	-0.245(14) x10^{-6}	#	#	-0.389(57) x10^{-6}
Δ^S_K	0.437(18) x10^{-6}	#	#	0.549(18) x10^{-6}

The values in parentheses apply to the last digit and denotes uncertainty 1 σ.

Table 13: Coupling constants [cm^{-1}] [68]

Fermi :	$5^2 \Leftrightarrow 2^1$
J^2	$h^{1\ F}_{55,\ 2} = 1.8283(480)\text{x}10^{-4}$
J^2_{xy}	$h^{2\ F}_{55,\ 2} = 4.862(490)\text{x}10^{-5}$

2.2. The First High Definition Spectroscopic Study of the Rotational Spectrum of $CS^{\cdot+}$ Cation Radical

Figure 29: Orion Molecular Cloud Complex – possible occurrence of $CS^{\cdot+}$ [72]

The rotational spectrum of $CS^{\cdot+}$ radical cation in its ground electronic state $X^2\Sigma^+$ was measured for the first time in history in a flowing positive column discharge in a CS_2 /Ar mixture partially cooled with a limited flow of liquid nitrogen.[73]

The $CS^{\cdot+}$ cation radical is a molecule that interests many astrophysics and spectroscopic scientists. It is mainly because although its existence in Universe has been predicted, and its reaction mechanisms leading to its origination proposed, it was not found in the Universe yet. Beyond other things a low value of ionization potential of CS[74] suggests its existence, and also the fact that a CS molecule with similar structure, and a CO^+ molecule with similar reaction mechanisms were found in the Universe already. The CS molecule was discovered in several astrophysical environments like dense clouds, star forming regions[75][76][77][78] diffuse clouds[79], circumstellar envelopes[80], shocked molecular gas associated with the supernova remnant IC 443[81], Carbon rich stars[82], and comets[83][84]. The CO^+ molecule is found in different photo-dissociation regions of the Universe (NGC 7027 and M17 SW[85][86][87]; Orion bar[86][87]; NGC 7023[87][88]; Mon R2 and G29.960–02[89]; S140 and NGC 2023[90], including towards the original star-explosion galaxy M82[91]). The CO^+ was also experimentally

recognized in the X-ray area towards nuclei of the Cygnus galaxy [92], and its creation in M82 was thus ascribed to X-ray radiation[93].

Although spectra of the $CS^{\cdot+}$ radical were measured by vibration and electron spectroscopy in the past, the obtained data did not allow detailed description of the molecule. Thus the detection of the $CS^{\cdot+}$ radical cation was not possible, primarily because the absence of high resolution experimental data measured in laboratories. Also relatively small dipole moment made detection of this radical in the Universe harder.

Only the experiment performed by us at the prestigious Université Lille 1 (Laboratoire de Physique des Lasers, Atomes et Molécules, PhLAM) in France helped to obtain the first rotational spectra of this radical in the microwave area that enabled us to describe structure of this molecule in detail.[73]

2.2.1. Structure of the $CS^{\cdot+}$ Molecule

The $CS^{\cdot+}$ radical cation is a molecule consisting of two atoms: Carbon C^{12} and Sulfur S^{32}(see Figure 30). There is a polar covalent bond between the atoms. Sulfur carries positive charge.

The distance between atoms of C^{12} and S^{32} is 33.68 pm in the ground vibration state. The molecule center of mass lies in the distance 24.5 pm from the Carbon atom.

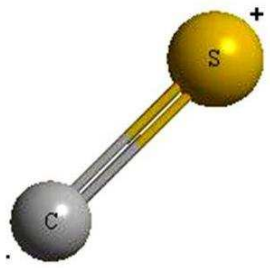

Figure 30: Model of the $CS^{\cdot+}$ cation radical

The $CS^{\cdot+}$ cation radical belongs among linear molecules with values of one inertia momentum that is negligible during rotation of the molecule around its axis ($I_a < < I_b = I_c$).

The permanent dipole moment calculated from initial quantum chemistry calculation is 0.509 Debey.[94]

2.2.2. Reaction Mechanisms

Many scientists studied reaction mechanisms of $CS^{\cdot+}$ origination.[95][96] Several schemes of this radical origin in the interstellar space were proposed.

The cation radical $CS^{\cdot+}$ can originate in clouds with low and medium density, according to the following scheme [96]:

$$SH+C^{+} \rightarrow CS^{\cdot+}+H \qquad (70)$$

This radical can be created in molecular clouds of low and medium density by the following exothermic reactions:

$$C_2+S^{+} \rightarrow CS^{\cdot+}+C \qquad (71)$$

$$CH+S^{+} \rightarrow CS^{\cdot+}+H \qquad (72)$$

$$CH^{+}+S \rightarrow CS^{\cdot+}+H \qquad (73)$$

In dense interstellar clouds, where the cosmic ray radiation is prevalent, $CS^{\cdot+}$ can be synthesized by exothermic charge-transfer reaction of interstellar CS with H^{+}:

$$CS+He^{+} \rightarrow CS^{\cdot+}+He \qquad (74)$$

Then it can be created by reaction of ions with molecules that contain sulfur in dense clouds:

$$C^{+}+OCS^{+} \rightarrow CS^{\cdot+}+CO \qquad (75)$$

$$C^{+}+SN \rightarrow CS^{\cdot+}+N \qquad (76)$$

At the edges of dense clouds, where carbon exists mainly in the ionized form[96], it can be created by the following reaction:

$$C^{+} \text{ a } S \rightarrow CS^{\cdot+} \qquad (77)$$

The radical can also react with H_2, the main collision partner in the Universe, during creation of HCS^{+} and H.[97] On the contrary it can be destroyed by radiationless dissociative electron recombination:

$$CS^{\cdot+}+e^{-} \rightarrow C+S \qquad (78)$$

Drdla et al[79] also suggested that $CS^{\cdot+}$ can create CS in diffuse clouds.

It is likely that $CS^{\cdot+}$ can occur in comets. [84] [97]

Extensive creation and destruction reactions of the $CS^{\cdot+}$ cation, including speed constants and reaction types are located in the UMIST database[98] (www.udfa.net).

Similar reaction mechanisms as $CS^{\cdot+}$ have been displayed by the CO^+ ion found in the Universe in various photo-dissociative regions:

$$CS^{\cdot+} + H_2 \rightarrow HCS^+ \quad (79)$$

$$CO^+ + H_2 \rightarrow HCO^+ \quad (80)$$

$CS^{\cdot+}$, as well as CO^+, can be present in environments, where its creation is fast and hydrogen is in the H II ionized form.

2.2.3. Previous Studies Related to this Work

In 1971 the carbon monosulfide (CS) was recognized in the interstellar space.[99] In 1976 the Coxon et all first measured the $CS^{\cdot+}$ $A^2\Pi_i - X^2\Sigma^+$ system in a laboratory.[100] $CS^{\cdot+}$ was produced by reaction of metastable He with CS_2. Rotational analysis of observed $CS^{\cdot+}$ electronic spectra revealed that some vibrational transitions of the $A^2\Pi_i$ state, especially of $\nu' = 1$, 5, and 6 levels, are strongly perturbed by high vibrational levels of the $X^2\Sigma^+$ state.

Rotationally resolved emission spectrum was recorded in 1978 and the depertubation analysis of the (2.0), (3.0), (4.0), and (5.0) bands was performed. [101] $CS^{\cdot+}$ ion was created from CS_2 by low-pressure hot cathode discharge. Later was this system re-evaluated using Fourier transform emission spectroscopy between 5800 and 14000 cm^{-1}.[95] Production was again with metastable He and CS_2.

In 1981 were proposed mechanisms of creation of $CS^{\cdot+}$.[96] Sulfur compounds like HCS^+ were observed in the interstellar space in the same year.[102]

There were unsuccessful attempts to identify the electron spectrum of $CS^{\cdot+}$ in the interstellar medium in 1986.[103] One year later the sulfur compounds C_2S[104] and C_3S[105][106] were observed in the interstellar medium. In 1993 were observed sulfur compounds like C_5S[106] there. In 1994 Cossart et al has also recorded the $B^2\Sigma^+$-$X^2\Sigma^+$ system in the UV area from 230 to 330 nm.[107]

The absorption near-infrared spectrum band (1, 0) of $CS^{\cdot+}$ was measured in 2000 using velocity modulation laser spectroscopy.[108] The $CS^{\cdot+}$ cation was produced by

application of a.c. discharge to the flowing mixture of CS_2 and helium. This was followed by another measure of the (5,0) band, a new measure of the (6,0) band, a new analysis and a new set of equilibrium constants for both the X and A states.[109] The band (7.1) was measured a year later.[110]

2.2.4. Partial Results and Discussion

The dissertation consists of the experimental part (research, optimization of experimental arrangement, selection of suitable precursor, prediction of spectrum and measurements), the analysis of a part of measured data, and the determination of molecule constants.

Spectrum Prediction

- In order to find the approximate area of electromagnetic spectrum, where we should seek the radical lines, we first performed a spectral prediction using the constants obtained from the previous work by Liu et al in the near infrared.[109] We have substituted the constants B_0, D_0, γ_0 from Liu's measurements [109] to the equation for calculation of rotational energy, and thus obtained approximate frequency values, where lines of this cation for searched transitions could lay.

$$J+1 \leftarrow J = 2B_0(J+1) - 4D_0(J+1)3 \pm \gamma_0 \qquad (81)$$

- These predictions were necessary, since there were no experimentally obtained microwave spectra, and no knowledge, as to where these radical lines could be. The prediction was necessary also due to low signal to noise ratio, and due to critical conditions of creation of the $CS^{\cdot+}$ cation.

Experimental Work

The measurement system consisted of a tunable microwave source, an absorption cell with flow through regime, and a detector. We obtained the microwave radiation using two BWO oscillators (Thomson C.S.F and Istok company Russia) that emitted radiation from 414 to 622 GHz.

Two-meter, double jacket, Pyrex cell with the inner diameter of 5 cm was inserted into a copper solenoid that was used to create the magnetic field for identification of the radical. The precursor was the CS_2 liquid (vapor pressure: 296 Torr at 20 °C) that was placed in a flowing positive column discharge in the mixture with Argon. Restricted flow of liquid oxygen was flowing through the cell jacket to cool the plasma. Temperature was increased or lowered in order to obtain optimum lines by reducing amount of liquid Nitrogen; however, the used experimental arrangement did not enable precise temperature control. $CS^{\cdot+}$ lines were not observed at the room temperature. If the cell was cooled more than necessary, the lines became smaller and disappeared.

Helium cooled InSb bolometer (Q.M.C. Instruments) was used a detector. Based on experience from the previous measurement [108], we applied the electric discharge of the size 140-200 mA. The optimum discharge current was 200 mA, and the partial pressures of the Ar and CS_2 mixture (measured at the room temperature) that gave the best signal to noise ratio, were 6 and 2 mTorr. We increased sensitivity using the 42 kHz frequency modulation, with the following lock-in detection in 2f modulation frequency, therefore resulting line shapes had a form of second derivation.

The measurement error was estimated to be less than 50 kHz.

The experiment arrangement is shown in Figure 31.

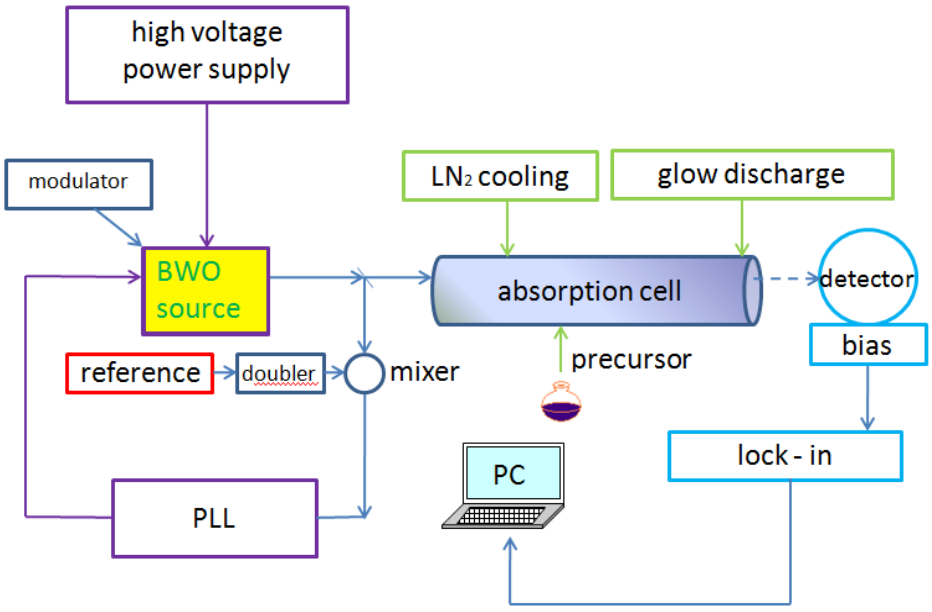

Figure 31: The microwave experiment arrangement

Since this was the very first microwave laboratory experiment we encountered many problems:

- Since we assumed a short cation lifetime, we had to select such conditions of its production that would let us create enough of it for detection in the cell. These conditions differed from the conditions in previous experiments of electronic and vibration spectroscopy. For example, the total pressure in the cell should be lower, in order to prevent excessive expansion of lines in the submillimeter-wave area, and differentiate components of fine splitting. Electronic and vibration spectroscopy often uses helium as a carrying gas to create ions in its discharges. From the previous experimental work performed at the PhLAM laboratories was clear that Argon is more suitable as a carrying gas for creation of ions.[111] The CS_2 precursor is a liquid with melting temperature of -111°C at the atmospheric pressure. For this reason we could not use the cell cooling to the liquid Nitrogen temperature (-196 °C) that would freeze the sample [112] to increase a signal of ion created from gas, which is a normal procedure.
- The dipole moment, on whose intensity the absorption spectrum line intensity depends, calculated using the *ab initio* calculations in the ground vibration state is low (0.509 Debye [93]).For this reason we had to be careful during spectrum investigation in order not to overlook sought lines.
- In addition the magnetically-enlarged negative glow discharges, used to enhance positive ion concentration [113], cannot be used for $CS^{\cdot+}$ since it is an open-shell.

Progress of Measurement

- Based on the spectrum prediction made using results from previous work. [109], it was first sought two strongest lines of fine structure (J=91/2← 81/2 a J = 81/2 ← 71/2) of the transition N = 9 ← 8. We identified both transitions (around 466 GHz) near the predicted area.
- The frequency interval 597.7 MHz between transitions exactly corresponds to the fine splitting constant γ_0 (597.696 ±0.420).
- Then we measured two strongest transition lines N= 8← 7 around 414 GHz that we added to iteration and performed new, more exact, transition predictions (±400 kilohertz) from 518 – 622 GHz.
- According to this, five new lines were identified within ±200 kHz of prediction ranges.

- Altogether we measured 9 transitions in the area of 414 – 622 GHz corresponding to N from 7 to 11.

One of the measured rotation transition is shown in Figure 32.

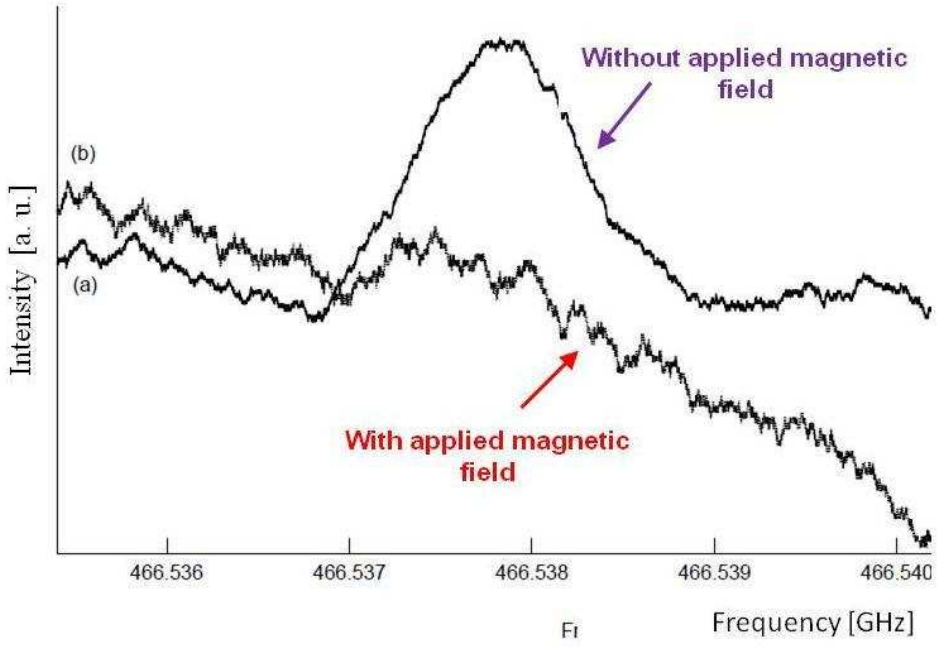

Figure 32: Recording of the N, J =9, 9 1/2←8, 8 1/2 rotational transition of $CS^{\cdot+}$ in the ground electronic state $X^2\Sigma^+$[73]

Due to weak signal to noise ratio each line was measured three times and experimental uncertainty was derived from the capability to reproduce measurement.

The uncertainty also corresponds to similar measurements with comparable signal to noise ratio.

We are certain that we found the sought cation radical $CS^{\cdot+}$ for several reasons:

- Observed lines do not correspond to any frequencies of molecules that could originate, according to our judgment, in the cell (CS, C_2S, C_3S, SO, and SO_2).
- The first two lines were found exactly in predicted locations, and no other lines were found in surroundings of 20MGhz. All pairs of fine splitting lines with the same J had correct fine splitting and similar intensities.
- All nine newly measured lines corresponded to infrared results that give similar constants for this cation.
- The cell was equipped by inductor with multiple windings to generate axial

magnetic field (typically 100 Gauss) in the discharged plasma in order to differentiate paramagnetic and non-paramagnetic absorption lines.

- All lines judged to belong to the $CS^{\cdot+}$ were paramagnetic.

Evaluation of Measured Data, Analysis, Determination of Molecule Constants

Each rotational level of $CS^{\cdot+}$ (beyond N= 0) is divided to two sublevels (N+1/2 and N-1/2), caused by the presence of an unpaired electron. Three lines correspond to each rotational level. Two of them correspond to transitions: $\Delta J=\Delta N=1$, and one transition line $\Delta J=0$ (weaker by two orders in our frequency range).

The analysis was carried out by using the ground state combination differences from the submillimeter-wave spectrum together with the infrared transitions from previous measurement [109], and enabled exact determination of rotational and fine splitting constants of this cation.

The CALPGM fitting program was used for analysis.[69]

The standard deviation was 50 kilohertz.

The exact values of constants are as follows:

Rotational constant	B_0 = 25908.8650 (41) MHz
Centrifugal-stretch constant	D_0 = 41.344 (18) kHz
Rotational–vibration interactive constant	g_0 = 597.629 (41) MHz
Standard deviation:	50kHz

Table 14: Molecular constants of the ground $X^2\Sigma^+$ state of $CS^{\cdot+}$

Constants [MHz]	Horani & Vervloet[95]	Liu et al.[109]	Our work[73]
B_0	25908.99(34)	25908.57(22)	25908.8560(41)
$103\times D_0$	41.07(30)	40.94(17)	41.344(18)
γ_0	596.89(90)	597.70(42)	597.629(41)

The values in parentheses apply to the last digit and denotes uncertainty 1 σ.

Values of the molecule constant B_0 and the centrifugal constant D_0, obtained from analysis, are similar to values from previous measurements, although, concerning the measurement error, this can be an accident.

Value of the spin-rotational constant γ_0 is not too different from the value determined by Liu et al. (2002) (see Table 13).

Fit was done using submillimeter transitions only as well, and the molecule constants were almost identical.

2.2.5. Partial Conclusion

Historically for the first time the rotational spectrum of $CS^{\cdot+}$ cation was measured in the frequency range 414 to 622 GHz. Complete analysis using the data measured in the past as well as new data enabled exact determination of rotational constants as well as the fine structure constants.

Exact predictions of this radical spectrum all the way to the THz area can be made from the results obtained thanks to our measurement and consequent analysis for a series of earth millimeter and submillimeter telescopes, as well as in the high resolved range HIFI instruments (Heterodyne Instrument for remote-infrared area) of the Herschel space laboratory that was brought to space in 2009, and will monitor remote cool space objects, especially dust and nebulae, from which stars and planets are born, for the next three years.

Its search will also be enabled due to finish of building of the international interferometer ALMA (Atacama Large Millimeter Array) that will be represented by the most sensitive network of 50 radio telescopes in the world in the Atacama desert in 2012. This device will serve for search of extrasolar planets, during studies of star and galaxy origins, and for detection of rotational and vibration spectra of interstellar gas molecules.

2.3. Study of Decomposition of Toxic Species Acetonitrile (CH_3CN) and Cyanogen Bromide (BrCN)

This part of my dissertation dissertation is focused to the study of decomposition of the toxic species Acetonitrile (CH_3CN) and Cyanogen Bromide (BrCN), kinetics and mechanics of creation of their decomposition products in extreme conditions simulated in the discharge plasma environment. First I would like to introduce these two investigated species.

Acetonitrile (see Figure 33) belongs to toxins for human organism that damage the central nervous system.[2][114] It irritates mucous membranes during inhalation. Long-term inhalation leads to metabolically produced cyanide poisoning.

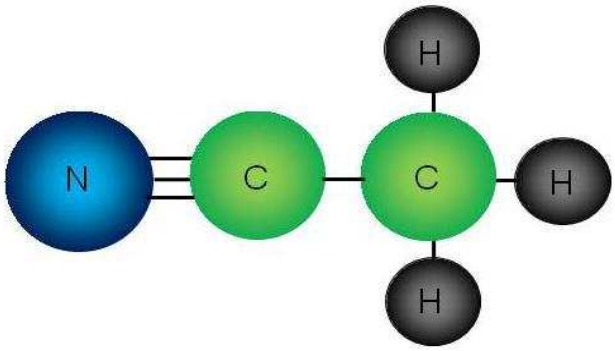

Figure 33: Acetonitrile molecule

It gets into atmosphere primarily during the process of coal gasification [115], due to processes in rubber industry, from automobile exhalations [116], during burning of biomass[117][118], and from waste waters[119] [2].

The average concentration of CH_3CN in troposphere is 150 $pmol.mol^{-1}$.[120] In troposphere acetonitrile reacts with the hydroxyl radical ($\cdot OH$)[120][121], and thus lowers its concentration in the atmosphere, as well as the concentration of oxidation reaction products related to this radical (CO, CH_4). This also causes decrease in ozone destruction caused by $\cdot OH$. Since the acetonitrile lifetime in the atmosphere is 1.5 year[2], its concentration is a characteristic indicator of biomass combustion. The amount of atmospheric acetonitrile is significantly lowered by sorption in seas and oceans. [122][123][2]

Cyanogen Bromide (see Figure 34) belongs to especially dangerous poisons according to the Czech Government Directive no. 10/1999 Coll.

It creates colorless to white crystals with pervasive smell that decompose in wet environment.

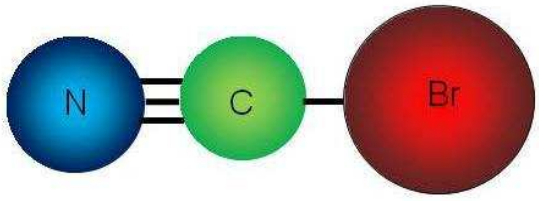

Figure 34: The cyanogen bromide molecule

Cyanogen bromide is very useful in organic chemistry, where it is used as an agent for syndissertation of cyanamides[124] , for modification of biopolymers, proteins and peptids, during chemical syntheses, and for extraction of gold from ores. It found its use also in agriculture in liquidating of pests, and it was made infamous as a fighting agent belonging to the blood agent groups.[125] It is an unstable species that is easily absorbed through skin or digestive tract. It strongly irritates breathing passages, eye conjunctives and the digestive tract. In the amounts larger than 433 mg per m^3 causes death in several minutes. As poison it is thirteen times more effective than chlorine and even more poisonous than cyanogen chloride.

Acetonitrile and cyanogen bromide play an important role in astrochemistry also, where they are a likely source of hydrogen cyanide (HCN) and its unstable linear isomer HNC, which is the reason why these two species were selected for study as possible precursors of **HCN and HNC**.

We can encounter small amounts of hydrogen cyanide in almonds in the form of amygdaline and in raw coal gas. Species that contain the monovalent radical $CN^{\cdot}$ are created from organic species that contain Nitrogen (wool, skin, and keratin) by annealing without access of air.[126]

Cyanide compounds (CN, HCN, and HNC) belong among especially dangerous poisons for a human organism.

HCN has a strong suffocating effect; $CN^{\cdot}$ is quickly absorbed by lungs during inhalation, by stomach mucus if swallowed, and also by unbroken skin.

Both isomers occur in the Universe. HNC is frequently observed in cold, dense molecular clouds [127], cool carbon stars [128], comets or planetary atmospheres [129]. Occurrence in the Universe differs significantly, in cool clouds (temperature around 10 °K) the ratio of HNC/HCN is about 1.55[130], in warmer areas [131] (200 °K) it is only 0.013, however. Currently many authors assume that HCN and HNC originate by dissociation recombination of molecular ions $HCNH^+$ and H_2NC^+. [132][133][134]

2.3.1. Previous Studies Related to this Work

HNC was for the first time observed in the argon matrix in the infrared area of spectrum (600 – 4000 cm^{-1}) in 1963[135] and in the Universe it was for the first time documented through radio astronomy in the center of our galaxy in the Sagittarius star system (molecular cloud Sgr B2) by Snyder and Bhule in 1971[136]. Since it is not possible to differentiate it from its isomer HCN, spectroscopy became the only applicable method for detection of this molecule beyond the collision induced dissociative ionization measurement [137].

It is assumed that in the Universe HCN and HNC isomers occur by the way of ion chemistry, since due to ionization radiation molecules in the Universe are ionized. The simplest ions that form in the discharge with hydrogen content are H_2^+ and H_3^+, from which H_3^+ is a key example of cosmic chemistry that with the $CN^·$ radical reacts and creates $HCNH^+$. By collision of $HCNH^+$ with an electron dissociative recombination occurs and isomers HNC and HCN are produced.

Both isomers originate also by the reaction of the C^+ ion with ammonia; however the originating isomer H_2NC^+ changes to $HCNH^+$ by radiation absorption. HNC is created by a consequent collision with an electron. Reaction of the proton XH^+ (H_3^+, CH^+, NH^+, H_3O^+) donor with HCN or HNC leads back to origination of the $HCNH^+$ ion.[138] Schematic of the creation of HCN and HNC is shown in Figure 35.

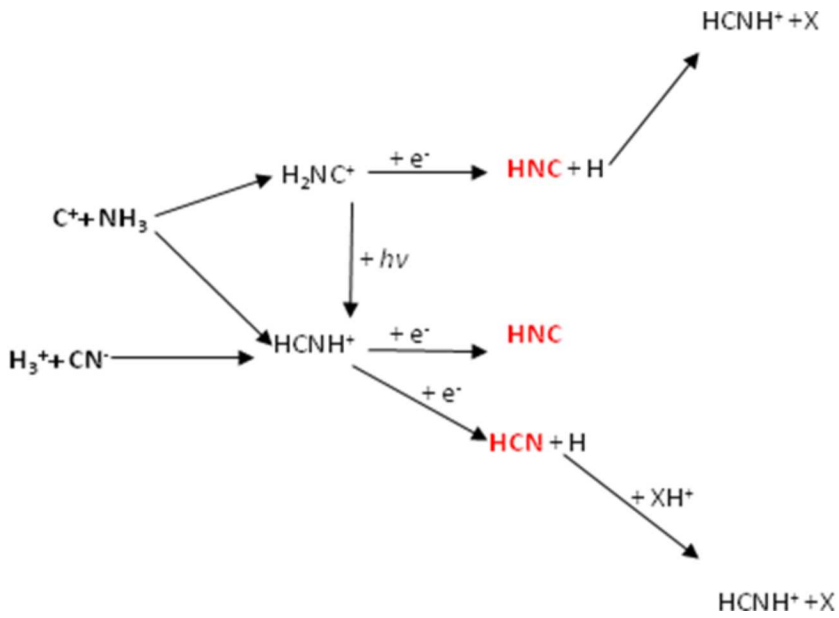

Figure 35: Schematic of the creation of HCN and HNC

Beyond reaction

$$H_2NC^+ + e^- \rightarrow HNC + H \qquad (82)$$

HNC is created in the Universe by the following radical reaction [139]:

$$C + NH_2 \rightarrow HNC + H \qquad (83)$$

Then by conversion of HCN to HNC by suprathermal Hydrogen atoms [140], which plays role in cometary comae.

The equilibrium is then, according to their investigation [141], at 300 K moved in the favor of hydrogen cyanide. By observation of the Hale-Bopp[142][143]comet was found that after approaching the Sun the ratio of HNC/HCN increased from 0.02 to 0.2 maybe due to photochemical reactions.

2.3.2. Experimental Set-Up

Emission spectra of these two species were measured by the Fourier transform infrared spectroscopy using the time resolved spectrometer Bruker IFS 120 HR, with spectral resolution 0.05 cm^{-1}.

This technique enabled us to study processes inside discharge plasma and dynamics of cation and destruction of excited atoms, radicals, and ions.

The basic FTIR experiment arrangement is shown in Figure 36.

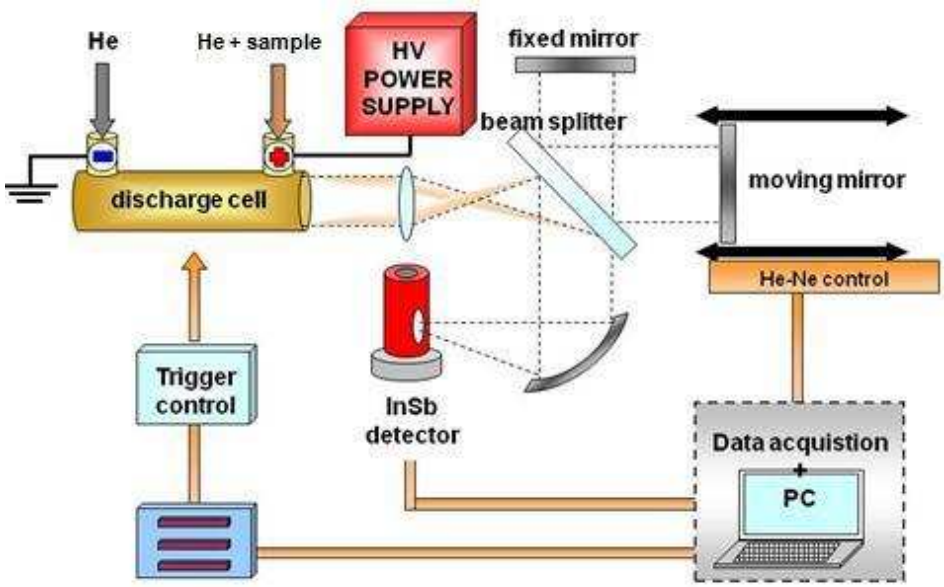

Figure 36: FTIR experiment arrangement [144]

In the used emission arrangement the radiation source was a discharge cell with a sample. Rays from the radiation source fall on a beam splitter and are reflected to a movable or fixed mirror. The passing through and reflected rays interfere with each other. In the absorption arrangement there is a cell with a measured sample between the detector and interferometer. Additional electronic components are used for acquisition of data during time differentiated measurement.

The positive column discharge tube, covered with a glass outer jacket, was 25 cm long with an inner diameter of 12 mm. The a.c. discharge was maintained by a high voltage transistor switch HTS 81 (Behlke electronic GmbH, Frankfurt, Germany) applied between the stainless steel anode and the grounded cathode. The He/precursor plasma was cooled by water in the outer jacket of the cell. The voltage drop across the discharge was 1200 V, with a pulse width of 15 μs and 0.6 A peak-to-peak current.

In both cases the spectral areas 1800–4000 cm^{-1} and 2000 – 6000 cm^{-1} were measured with Ge (germanium) interference optical filters and CaF_2 lenses at a unapodized resolution of 0.05 cm^{-1}. 50 scans were averaged to obtain a reasonable signal-to-noise ratio. The initial pressure of precursor was 0.5 mbar and the He pressure was changed in the range 2 – 4 mbar.

Obtained interferograms were transformed to spectra by the OPUS program Fourier transform: The output of measurement was a matrix of time shifted spectra that was processed by a suitable table processor.

Selected ion flow tube mass spectometry

We found out the exact amounts of stable product concentrations created during decomposition of acetonitrile and cyanogen bromide using the selected ion flow tube mass spectrometry, SIFT-MS. Absolute quantification is achieved on the basis of well defined reaction time, during which chemical ionization takes place in Helium carrier gas flowing through a flow tube into which the reagent ions are injected and the sample is introduced at a known flow rate.

2.3.3. Partial Results and Discussion

When we were investigating behavior of acetonitrile and cyanogen bromide in the Helium matrix without added Hydrogen only, we identified only the $CN^{\cdot}$ radical lines and impurities in the form of HCN and HBr, etc. in the spectrum (see Figure 37). These impurities were caused by air leaking into the cell, in spite of a maximum effort to seal the whole system (initial pressure was 0.5 mbar).

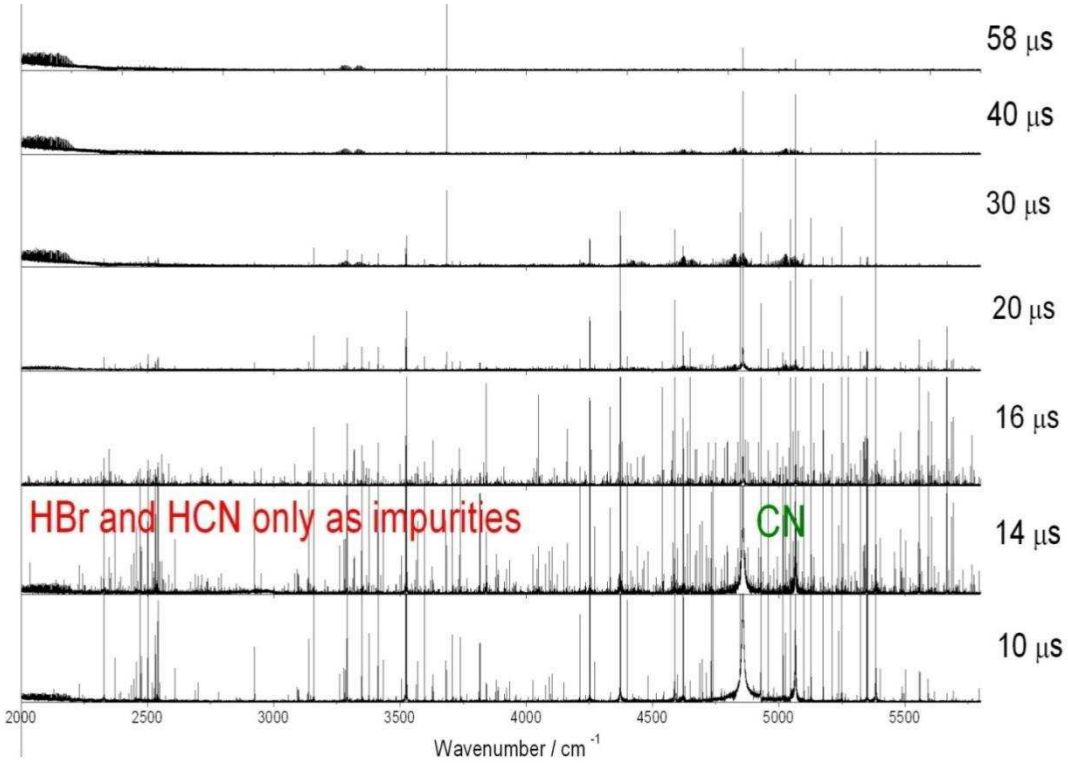

Figure 37: Time resolved BrCN spectra without added hydrogen (kinetics of species originating during and after application of electric discharge)

The change occurred with added molecular Hydrogen that significantly influenced creation of hydrogen cyanide (HCN) and its isomer (HNC) (see Figure 38 and 39).

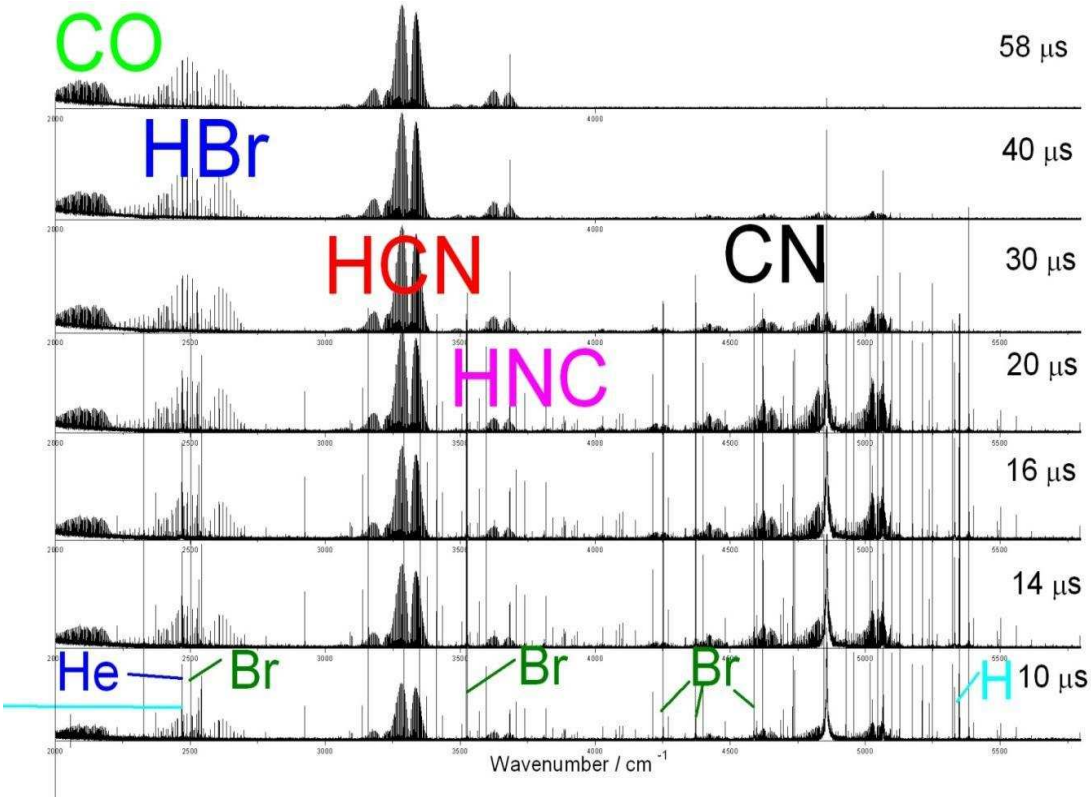

Figure 38: The time resolved BrCN spectra with added Hydrogen (kinetics of species originating during and after application of electric discharge)

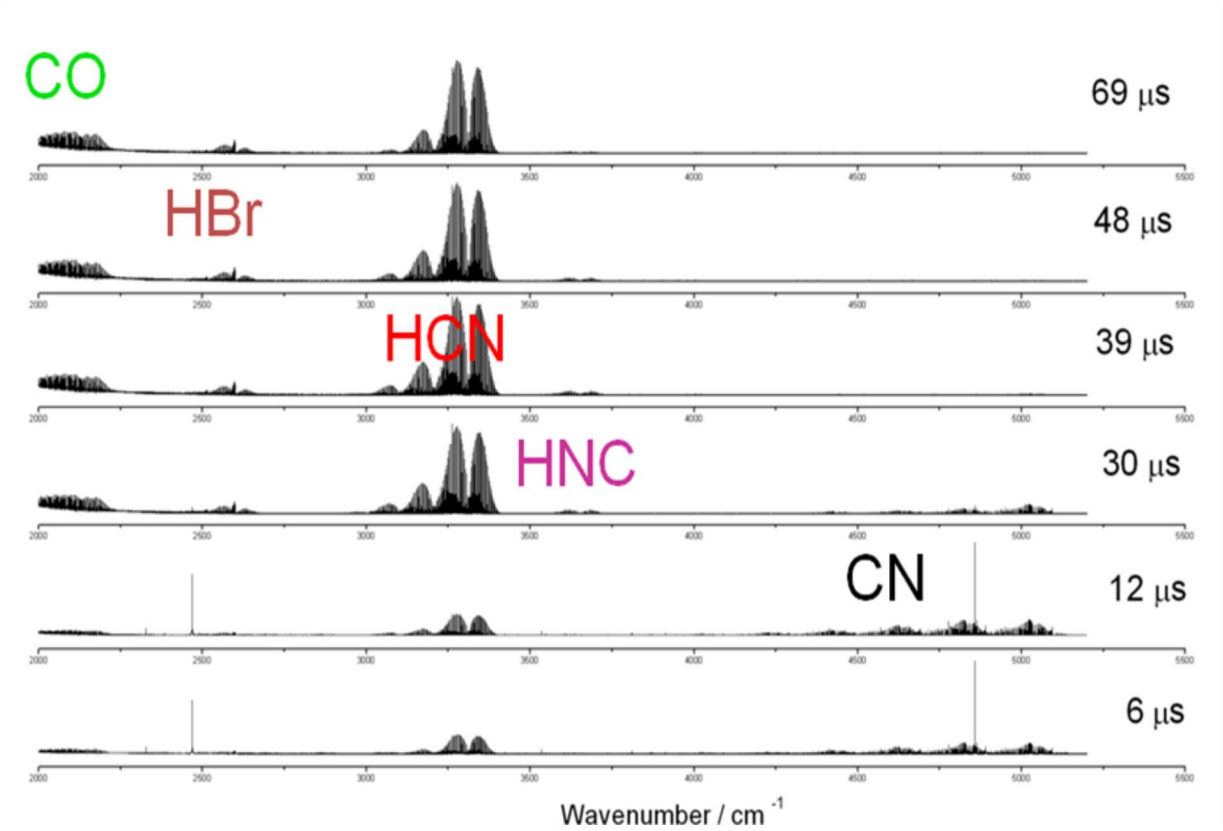

Figure 39: The time resolved CH_3CN spectra with added Hydrogen (kinetics of species originating during and after application of electric discharge)

The Figures 40 and 41 show the overview of the emission spectra of H_2/BrCN/He and H_2/CH_3CN/He discharge.

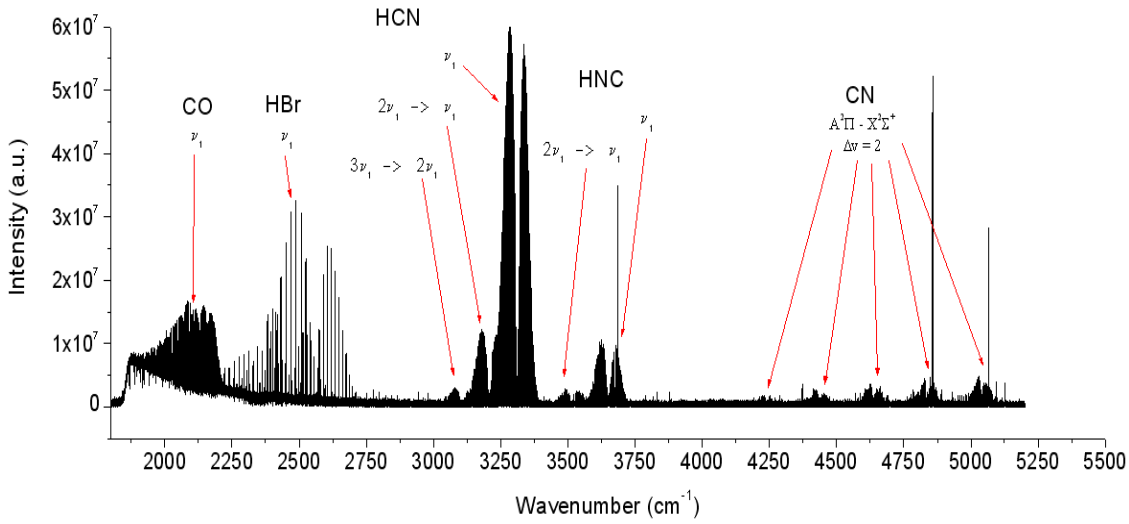

Figure 40: Emission spectrum of H_2/BrCN/He discharge [144]

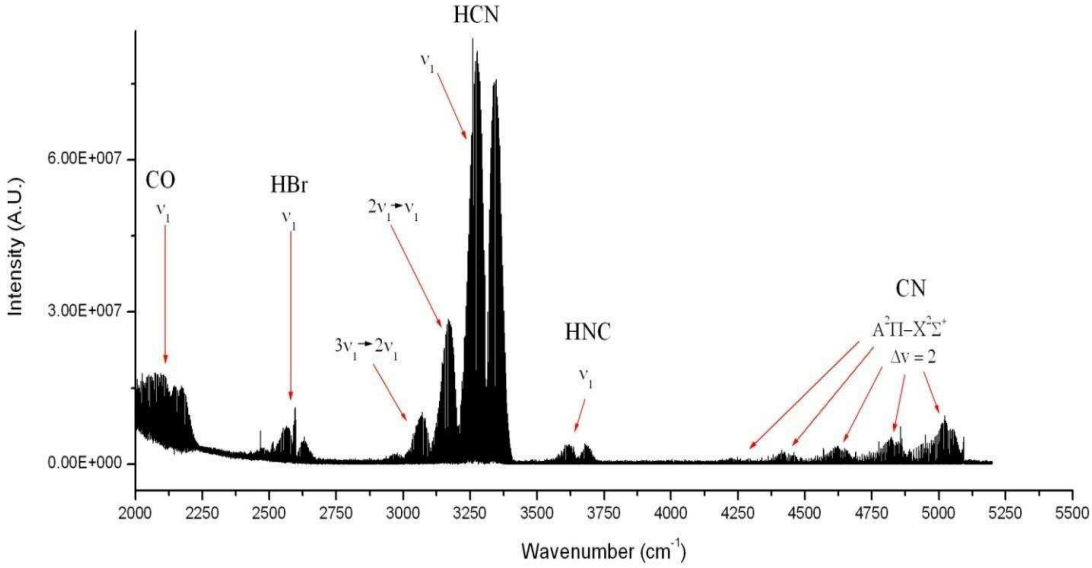

Figure 41: Emission spectrum of H_2/CH_3CN/He

The products of decomposition processes CH_3CN and BrCN are shown in Figure 42.

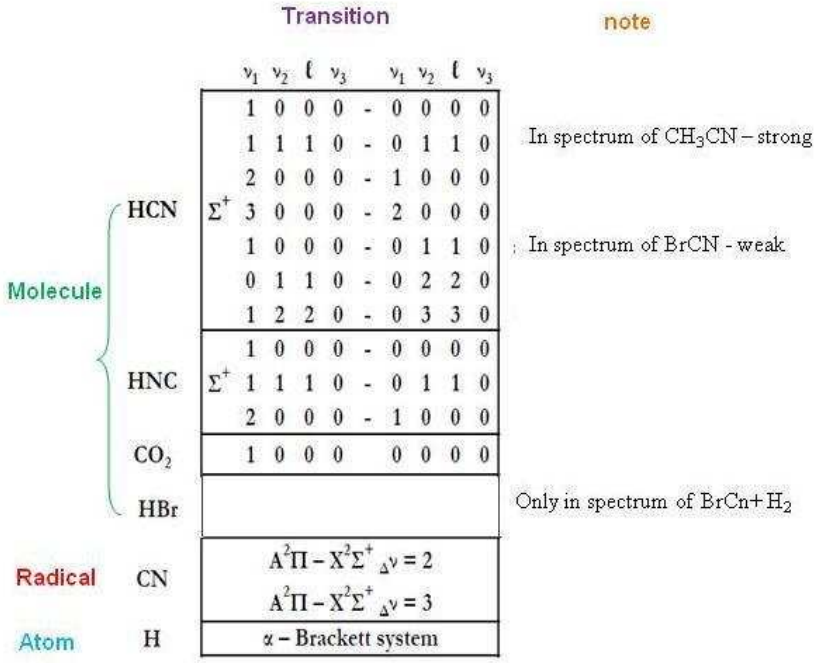

Figure 42: Products of decomposition processes CH_3CN and BrCN [144]

Below (Figure 43, 44) is shown dynamics of creation and destruction of individual samples. It is apparent that atom lines originated from molecules by application of electric discharge are destroyed and recreate molecules after the discharge and that cyanide compounds are created continuously even after the discharge is over.

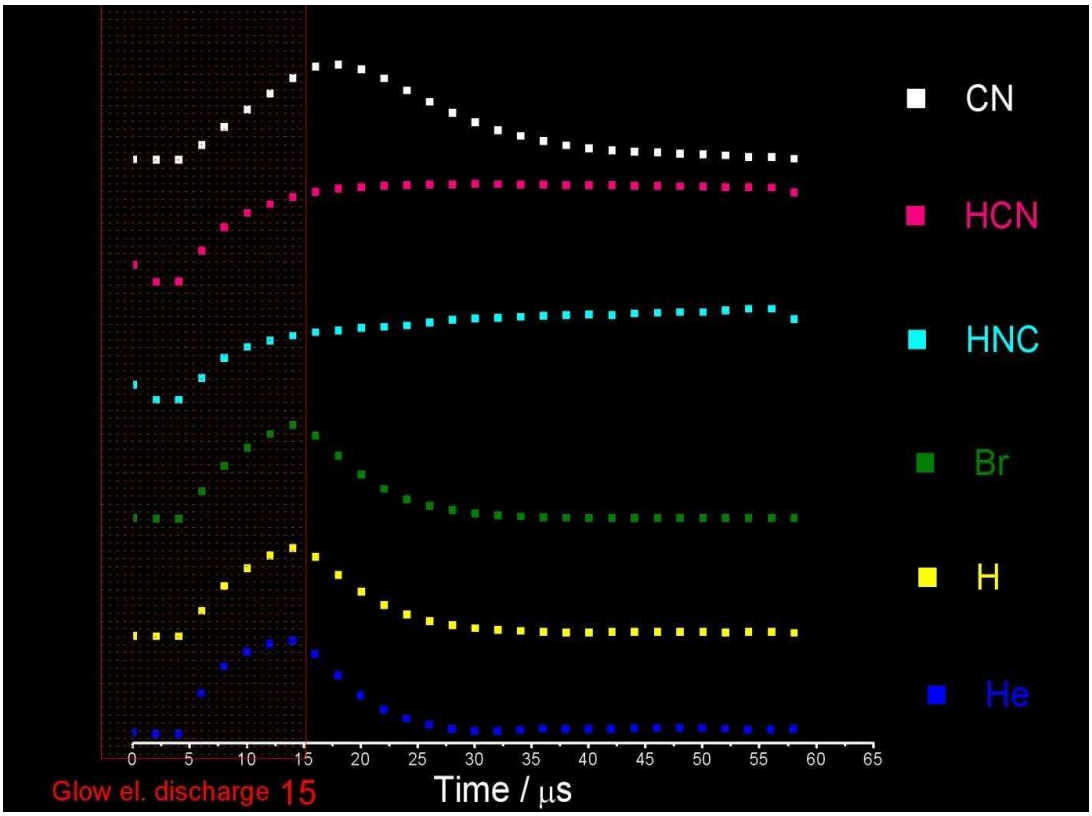

Figure 43: Dynamics of creation and destruction of individual samples in the CH_3CN spectrum

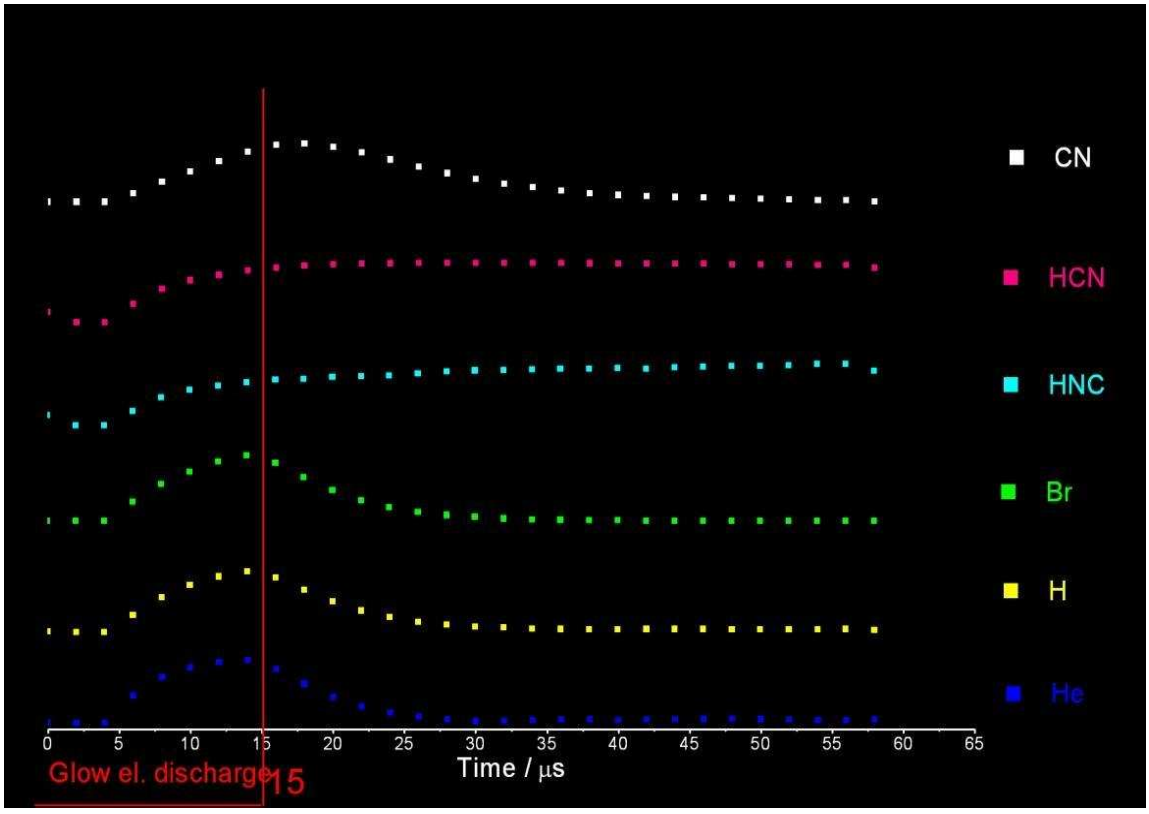

Figure 44: Dynamics of creation and destruction of individual samples in the BrCN spectrum

The Figures 45, 46, 47 show decays of the P, Q, and R branches of the $CN^{\cdot}$ hot band for transition $A^2\pi - X^2\Sigma^+$ identified in the CH_3CN spectrum. As can be seen the lifetime of this radical is about 10 μs.

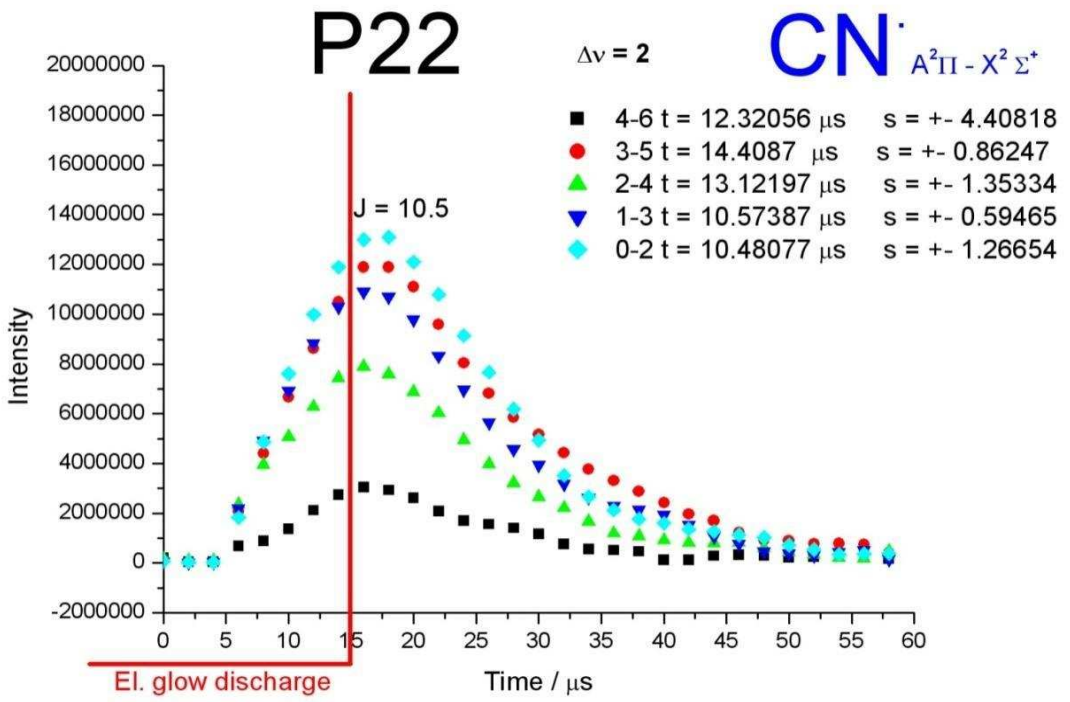

Figure 45: Decays of $CN^{\cdot}$ (P branch) in spectrum $CH_3CN/H_2/He$

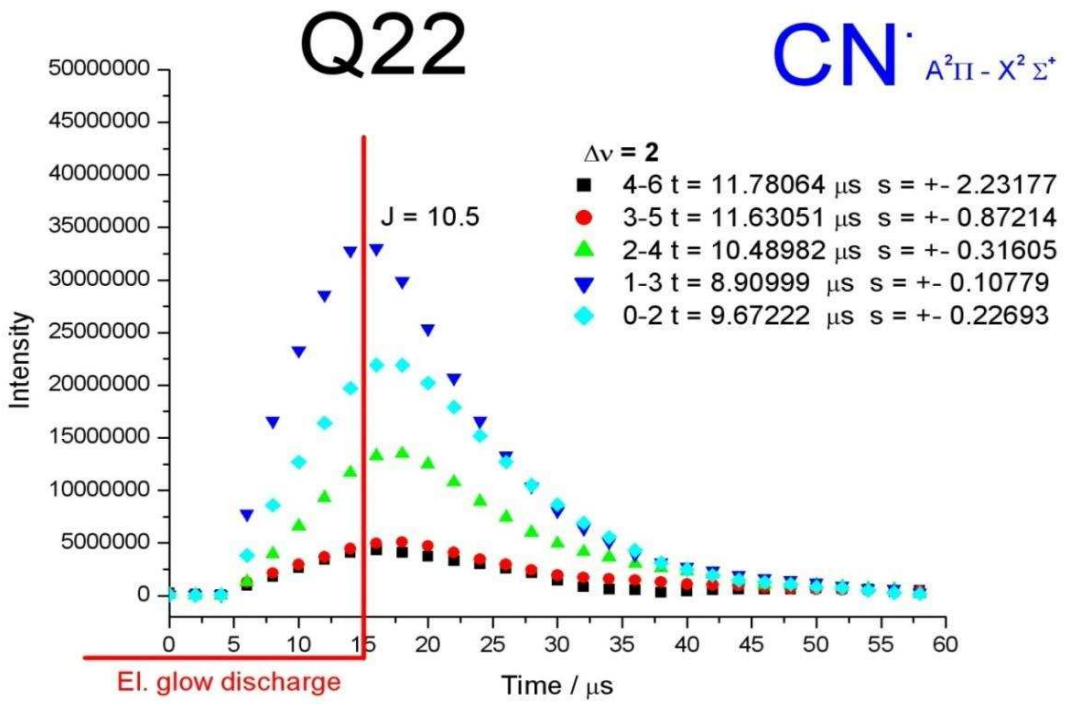

Figure 46: Decays of CN· (Q branch)) in spectrum $CH_3CN/H_2/He$

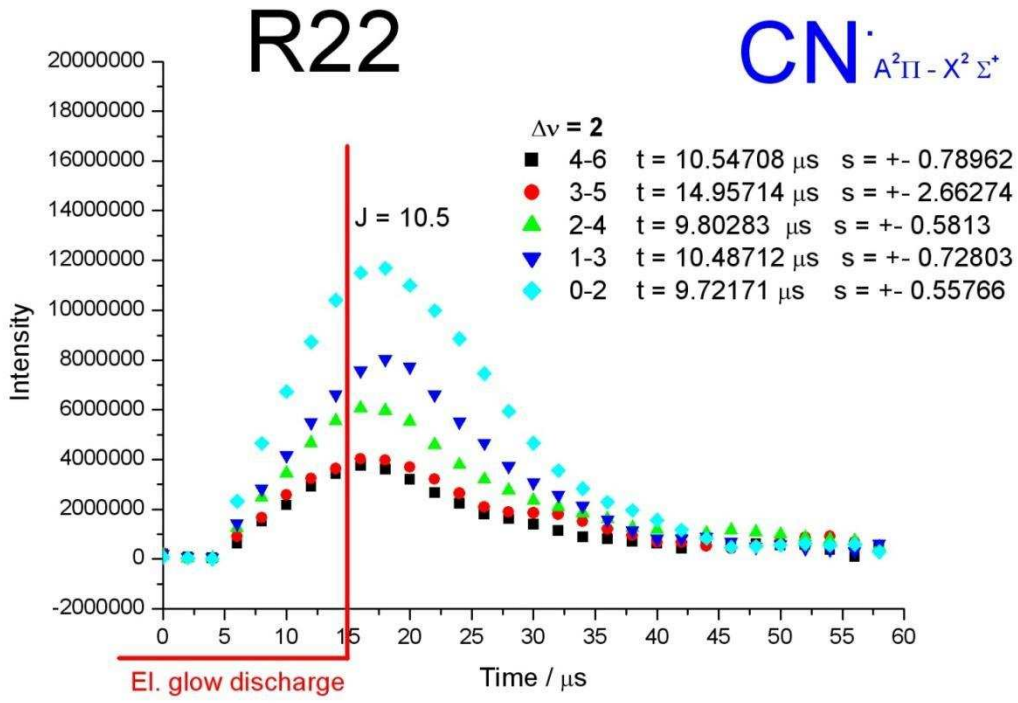

Figure 47: Decays of CN·(R branch) in spectrum $CH_3CN /H_2/He$

We did not observe any ions in glow discharge emission spectra. Even molecular hydrogen that is the precursor of H_3^+ was not detected in the observed systems.

Probably if we put only He and H_2 into the cuvette, this very stable ion H_3^+ would be created. However, we also added BrCN and CH_3CN that prevented the occurrence of this ion to the cuvette.

Based on the absence of emission lines of the H_3^+ ion and its precursor - molecular hydrogen H_2 in our spectra we assume that in the positive column of a glow discharge the isomers HCN and HNC are produced by radical chemistry.

It is most likely that in discharge in the mixture **BrCN/H_2** takes place dissociation of hydrogen to the $H^{\cdot}$ radical, and consequently reaction of hydrogen with the halogenated molecule occurs:

$$H + BrCN \rightarrow HNC + Br \quad (84)$$

$$H + BrCN \rightarrow HNC + Br \quad (85)$$

$$H + BrCN \rightarrow HBr + CN^{\cdot} \quad (86)$$

Then dissociation of the BrCN precursor also occurs in the discharge according to the following equations:

$$BrCN + e^- \rightarrow CN^{\cdot} + Br + e^- \quad (87)$$

$$BrCN + He^* \rightarrow CN^{\cdot} + Br + He \quad (88)$$

In the discharge then occurs reaction of the $CN^{\cdot}$ radical with hydrogen

$$H + CN^{\cdot} \rightarrow HCN \quad (89)$$

$$H + CN^{\cdot} \rightarrow HNC \quad (90)$$

$$H_2 + 2CN^{\cdot} \rightarrow 2HCN \ [145] \quad (91)$$

Repeated decomposition of hydrogen cyanide to the CN radical [146] is a very small reaction:

$$H + HCN \rightarrow H_2 + CN^{\cdot} \quad (92)$$

The created $CN^{\cdot}$ radical can react with the precursor molecule according to the equation.[147]

$$CN^{\cdot} + BrCN \rightarrow (CN)_2 + Br \quad (93)$$

However, $(CN)_2$ was not detected in the discharge, so it must be a slow reaction that can be neglected in comparison with the $H+CN^{\cdot}$ reaction and fast dissociation of BrCN.

We assume that the balance between HCN and HNC is given by a collision with the Hydrogen radical when HCN originates from HNC and vice versa.

Acetonitrile is most likely dissociated in the discharge just like BrCN by collision with a fast electron or excited He during origination of the $CN^{\cdot}$ radical:

$$CH_3CN + He^* \rightarrow CN^{\cdot} + \text{other products} + He \qquad (94)$$

$$CH_3CN + e^- \rightarrow CN^{\cdot} + \text{other products} + e \qquad (95)$$

It is assumed that this reaction consists of the partial dissociation reactions:

$$CH_3CN = CH_2CN + H \qquad (96)$$

while the last step is splitting to atomic Carbon and the CN radical

$$CCN = C + CN^{\cdot} \qquad (97)$$

whereas this reaction is very fast, and only the $CH^{\cdot}$ radical is present in detectable concentration.

The CH or C-CN radicals were not detected at the discharge emission spectra in acetonitrile. We assume that decomposition of these radicals is very fast and that they are present in discharges in small concentrations, smaller than C-CN.

Creation of $CN^{\cdot}$ can be assumed also according to the equation:

$$CH_3CN + H = CH_4 + CN^{\cdot} \qquad (98)$$

Speed of this reaction is very small, however, and that is why it can be neglected.

The reaction mechanism of the HCN and HNC isomers creation is, similarly like in the case of discharge in BrCN, collision of the $CN^{\cdot}$ radical or the HNC and HCN reaction products with hydrogen.

2.3.4. Partial Conclusion

The results bring information about behavior of investigated species under extreme conditions, about lifetime of atoms and molecules that originate from a parent substance.

Priceless is also the work methodology that we tested and applied, and later on used during another performed experiment of fluorized substances within electrical charge, where we studied kinetics of the reaction and behavior of molecules in plasma. These experiments were not included in my dissertation.

The $CN^{\cdot}$ radical, HCN hydrogen cyanide and its isomer HNC were identified in all measured spectra. The discharge molecular dynamics was analyzed based on timing of creation and destruction of individual products. As opposed to the Universe the HCN and HNC isomers are created from radicals, not ions. Rotation - vibration bands of HCN and HNC have been observed in the ground and several excited states. Strongest HNC emission was observed in BrCN + H_2 / He discharge. All transitions of the $CN^{\cdot}$ radical have approximately the same lifetime on the order of tenth of μs.

In case of HCN 2000-1000 transition is stronger than 1110 – 0110. Only in the BrCN discharge intensities are close together. In case of HNC 1110 – 0110 transition is stronger than 2000 – 1000. Explanation is some kinetic mechanism producing excited HCN 2000 – 1000 state in cases of hydrogen separation from some parent molecule.[144]

2.4. Ammonia Studies

In this part of my dissertation I deal with the spectroscopic detection of ammonia. I took part in the international study about effect of trace amounts of ammonia on the environment within the project COST 729. I have studied ecological impact of ammonia in surroundings of its point source at the prestigious Centre for Ecology & Hydrology (CEH), Natural Environment Research Council in Edinburgh, specifically I analyzed data obtained from the measurement from an aerodynamic tunnel and investigated influence of conifers on the amount of emitted ammonia. I also participated in building of a measurement apparatus that used the method of laser optoacoustic detection, and thus gained precious experience that I later used in proposal of an experiment in the J. Heyrovsky's Physical Chemistry Institute, where the optoacoustic cell was designed and built, with consequently built laser optoacoustic detection arrangement with the cell inside of an optic resonator for measuring of trace amount of ammonia, and suitable for measurements of other gaseous species.

2.4.1. Ammonia

Under normal conditions ammonia is a colorless gas approximately by half lighter than air, with sharp acrid smell. It is easily liquefied and it is soluble in water. It creates NH_4^+ ammonia ions in solution.

Ammonia can react with oxidizing species. It reacts with acids creating ammonia salts, for example, with Sulfuric acid it creates ammonium sulfate.
With water it creates caustic lye, and with air explosive mixtures.

It is strongly corrosive on metals, especially on copper alloys.

According to the Czech Law no. 440/2008 Coll., about Chemical species and preparations, ammonia is classified as a toxic and caustic species dangerous to the environment. Ammonia is contained in the environment in an ionized form (NH_4^+), but also in the non-ionized one (NH_3). Acute effects on human and mammal health are caused by caustic character of its concentration solution, irritation effects of gaseous ammonia, and extreme cold that occurs in contact with liquid ammonia.

Currently ammonia attracts significant attention, and various international institutions (e.g. Centre for Ecology & Hydrology (CEH), Natural Environment Research Council v Edinburgh) are engaged in ammonia studies. Ammonia is also dealt with within the project for integrated European research NitroEurope that is a part of the sixth framework EU program for research and technological development and that runs from the February of 2006 to 2011. This problematics has been investigated in the Czech Republic since 1996, when the EU Council Directive 96/61/EC, now 2008/1/EC (IPPC) became valid.

2.4.2. Sources of Ammonia

Ammonia originates by microbial decomposition of organic remnants, excrements, and animal urine. The main source of ammonia emission to atmosphere is then agriculture, especially intensive breeding of farm animals, storing of remainder biomass, and its application into soil during fertilization, waste water from agricultural production, and also decomposition of human and animal biological waste (see Figure 48).

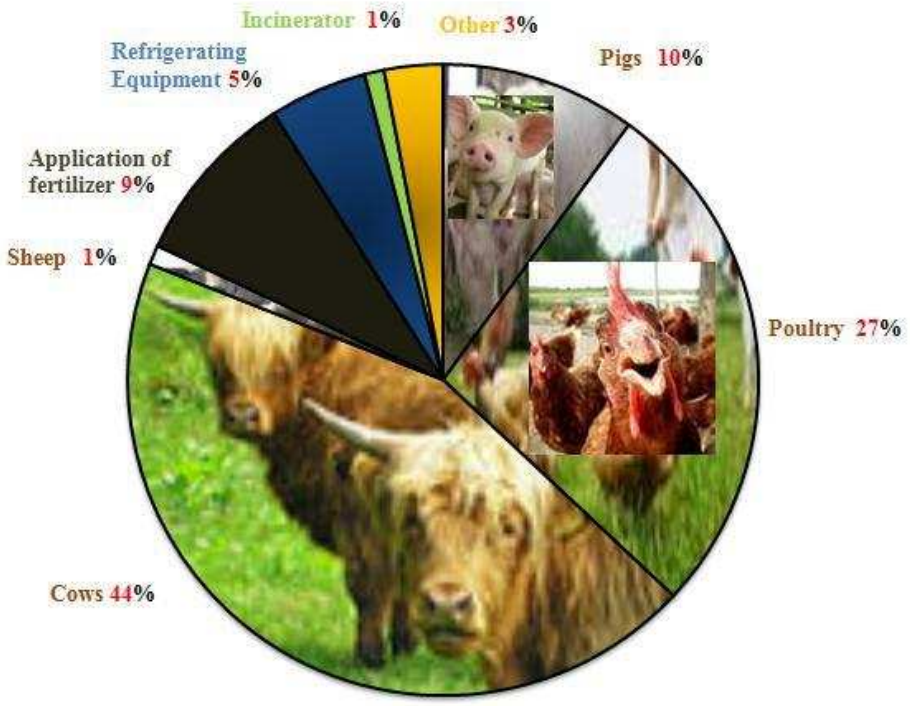

Figure 48: Shares of individual sources on the total ammonia emissions [148]

Ammonia concentration values in stables are influenced primarily by the amount of nitrogen in excrements, whose amount depends on the amount of Nitrogen species in feed, pH and moisture of bedding, stable microclimate with possibility of physical fixation of ammonia, chemical fixation of ammonia, species of bred animals, animal density, ventilation system and modification of inner microclimatic parameters.

Other sources that have a smaller share in total ammonia emissions are a production of nitric acid, fertilizers, and explosives, and some other industries (pharmaceutical industry, petrochemical industry), sewage waste waters, waste water from thermal processing of coal and galvanization, industrial A/C, production of ice, usage of fertilizers that contain ammonia sulfite $(NH_4)_2SO_4$ and NH_4NO_3 ammonium nitrate.[149] The system of release of ammonium sulfite and ammonium nitrate depends on a fertilizer utilization system. Release is higher when the fertilizer stays on the earth surface than when it is ploughed down to soil. Especially high release occurs when fertilizer is sprayed to irrigate soil with high pH, during higher temperatures and dry conditions, also in soil with low cation capacity like sands. The release is decreased during growing of plants that cannot release ammonia.[150]

Ammonia is further contained in raw food, some paints, lacquers, print colors, glues, and it is added to processed food.[151] In small amount it occurs in cigarette smoke, and it is emitted by human and animal life processes (exhaling, sweating) in minimum amounts.[149]

It is used in food refrigeration equipment in refrigeration plants, breweries, dairies and soft drink plants and winter stadiums in large extent. The last mentioned contain a large amount of ammonia. Waterless ammonia is used in 155 winter stadiums and about 500 to 600 large capacity facilities in the food industry in the Czech Republic.[152]

High concentration can appear in water in higher locations, isolated lakes and in places where waste water is drained.

The world ammonia emissions were calculated at 22 to 35 million tons per year.[153]

Pollution limits, pollution sources and individual pollutants, limits, and fees for them are set by a series of legislative regulations - e.g. the Law no. 309/1991 Coll., 117/1997 Coll., and 389/1992 Coll. The maximum permissible concentration of ammonia in the stable environment is set to 0.0025 % vol.

2.4.3. Ammonia Lifecycle in the Environment and Its Effect on Human Health

Ammonia is a key component in nitrate compound cycles (see Figure 49). By some bacteria (e.g. acidophilic ones that can live in the environment with neutral or low pH) it is transformed to nitrate that is received by plants and becomes a part of proteins and nucleic acids. Most organisms can accept Nitrogen only in its inorganic form (ammonia, nitrites, and nitrates) or is organic form (urea and proteins). Land animals get rid of Nitrogen by excreting urea, from which is ammonia released by consequent activities of microorganisms. After plants die Nitrogen is transformed to ammonia that is changed to nitrates by bacteria and algae. They are later reduced to Nitrogen that returns to the air. Bacteria are mostly responsible for the return release of Nitrogen in the air. Ammonia enriches surface waters with nutrients. Nutrients are necessary for a healthy ecosystem, but excessive amounts of nutrients (especially of Nitrogen and Phosphorus) can lead to euthrophication, i.e. to harmful effects and die-out of fish due to increase in algae and cyanobacteria. Ammonia occurs in water in the form of ammonia ions that can be highly toxic to fish and water plants in large concentrations. In water with sufficient amount of oxygen ammonia it is oxidized to nitrates that are significantly less toxic for aquatic organisms then nitrification bacteria.[151]

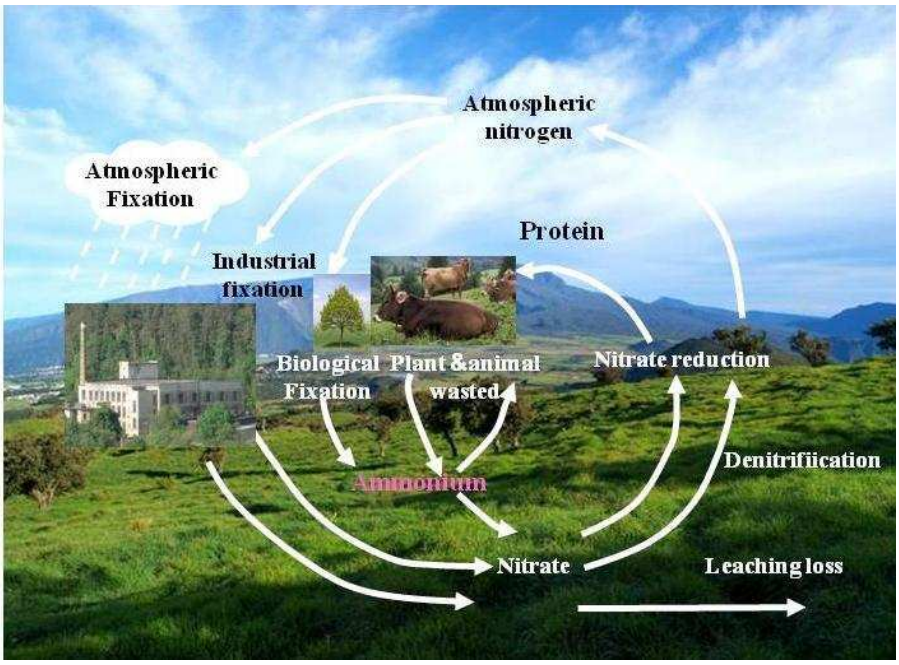

Figure 49: The ammonia and Nitrogen cycles in the environment [150]

Also plants can be affected if they are exposed to higher concentrations of ammonia both in the air, and in water. Ammonia occurs in soils especially in the form of ammonia ion. Since ammonia form of Nitrogen is a key source of Nitrogen for plants, Nitrogen industrial fertilizers are applied, however, they release nitrates into ground water. The ground water can then be unsuitable for use by humans, or if used, there are high costs related to cleaning from and removal of nitrates. Presence of nitrates (directly from fertilizers or due to bacterial oxidation of ammonia) also increases acidity of soils. The soil acidity is also increased by deposition from atmosphere. Ammonia makes relatively stable salts with sulfates and nitrates (originating from acid gases SO_2, SO_3, and NO_x) that are present in atmosphere. These salts are faster released from atmosphere in the form of rain or fallout in comparison with acid gases and ammonia itself, and get into soils this way. Although ammonia itself is an alcalic species, it takes part in acidic depositions. Penetration and consequent increased content of ammonia in atmosphere is also undesirable, since it is one of originators of the photo-chemical smog that belongs to the most important pollution problems of European cities atmosphere.

It is contained in large amounts in atmospheres of large Sun system planets (Jupiter, Saturn, Uranus, and Neptune) and also in the atmosphere of Saturn's moon Titan. It was also found in comets. It is one of molecules that occur in the interstellar space.

2.4.4. Risks Related to Ammonia

Acute effects on human and mammalian health occur due to the caustic character of concentrated ammonia solution, irritating effects of gaseous ammonia, and extreme cold that occurs during contact with liquid ammonia. Ammonia is easily absorbed through upper respiratory tract mucus membranes and digestive tract. Absorbed ammonia quickly spreads around the whole body. A serious acute exposure can lead to death within several minutes or it can cause deterioration of lung function. Short time exposure to ammonia can irritate eyes, and burn skin with the risk of permanent consequences. Ammonia also irritates nasal mucous membranes, mouth, pharynx, also caused cough and difficulty breathing. Exposure to higher concentrations can cause water in lungs (edema), or serious breathing difficulties. [5] Skin contact with liquid ammonia causes cold burns, usually without blisters and carbonification. Contact with

concentrated ammonia solution causes caustic burns on skin, and serious injury to eyes can occur. [151]

In the stable environment inhaling of sub-toxic amount causes primarily meta-toxic effect to the human, animal and plant health, where primarily decreased affectivity of immune system against infectious diseases is the result.

Basic rules of safety management in objects that is necessary to consider the potential sources of ammonia with concentrations significantly exceeding allowed limits - localities inside industrial zones (e.g. cooling units of food plants, chemical refineries, or buildings with technologies that use ammonia as coolant), and also densely populated areas (with winter stadiums) - are set by the European Directive known as SEVESO II (in the Czech Republic implemented by the Law no. 59/2006 Coll., On prevention of serious accidents).

Key factors implemented within related regulations lay either in prevention of emergency situations in side dangerous buildings themselves, and also in an effort to mitigate possible accidents consequences related to human health and life, property, and environment (environmental aspects) in the surroundings of these objects. Risk analysis and evaluation that includes modeling of accident consequences represents one of the most important steps in the process of development and implementation of Safety Management Systems – SMS. Beyond regulations stemming out of the SEVESO II directive the above mentioned principles are contained also in the Law no. 76/2002 Coll., as amended, "About integrated prevention" (i.e., in the IPPC directive) in context of industrial risks. This procedure can be understood as a connection and logical unification of environmental aspects related to undesirable consequences of accidents (acute risks) and medium to long-term negative effects (chronic risks) from industrial activities. Reference documents (BREFs) were published for implementation of main principles of the IPPC Directive that include the appropriate Best Available Techniques - BAT; in case of ammonia this is, beyond others, the Large Volume Inorganic Chemicals – Ammonia, Acids and Fertilizers BREF document approved on December 7, 2006.

Ammonia emission effects are geographically significant both on local, and on global scales. Aspects of over the border effects of NH_3 emissions are therefore monitored within the UNECE Convention on Long Range Transboundary Pollution. Protection of lives and environment in the context of industrial accidents related to a

possible ammonia leak is then dealt with within the Convention on the Transboundary Effects of Industrial Accidents (1992). From the point of view of long-term effects on environment is ammonia evaluated as a eutrotrophical acidifying harmful species as well. Since 2010 its emission limits fall under the National Emissions Ceilings Directive (NECD) that sets legally obligatory admissible emission for ammonia, and also NO_x, SO_2, and volatile organic compounds - VOC) on national levels.

2.4.5. Partial Results and Discussion

During my doctoral studies I participated in three independent studies related to ammonia that will be described in the following chapter.

1. Influence of Conifers on the Amount of Ammonia Emitted from a Point Source

At CEH (Natural Environment Research Council - Billett Section laboratories, Mark Sutton Ammonia group) Institute in Edinburgh, Great Britain I have analyzed data obtained from the experiment performed by dr. Christine Braban et all. in the aerodynamic tunnel the Atmospheric Flow Laboratory at the former Silsoe Research Institute (SRI).

This facility reproduced realistic turbulent wind conditions of up to 5 m/s. Evergreens of up to 2 m in height with up to 1m shrubs/plants upstream was used to create a windbreak design for the recapture of a controlled ammonia release in the wind tunnel at different distance/height combinations (simulated by ground level and elevated sources in the wind tunnel) from the source. In addition, a control experiment without a windbreak was undertaken to assess the experimental recapture efficiency. During one run the trees was misted with dilute acid to provide “perfect” sinks and measure the maximum achievable ammonia uptake Growth lights was installed in the wind tunnel to ensure light conditions (and stomatal conductances) representative of outside conditions (see Figure 50).

The experiments consisted of a simultaneous controlled release of ammonia gas and a tracer (methane) made either from a ground level or an elevated (1m) line source at the start of the working section of the wind tunnel.

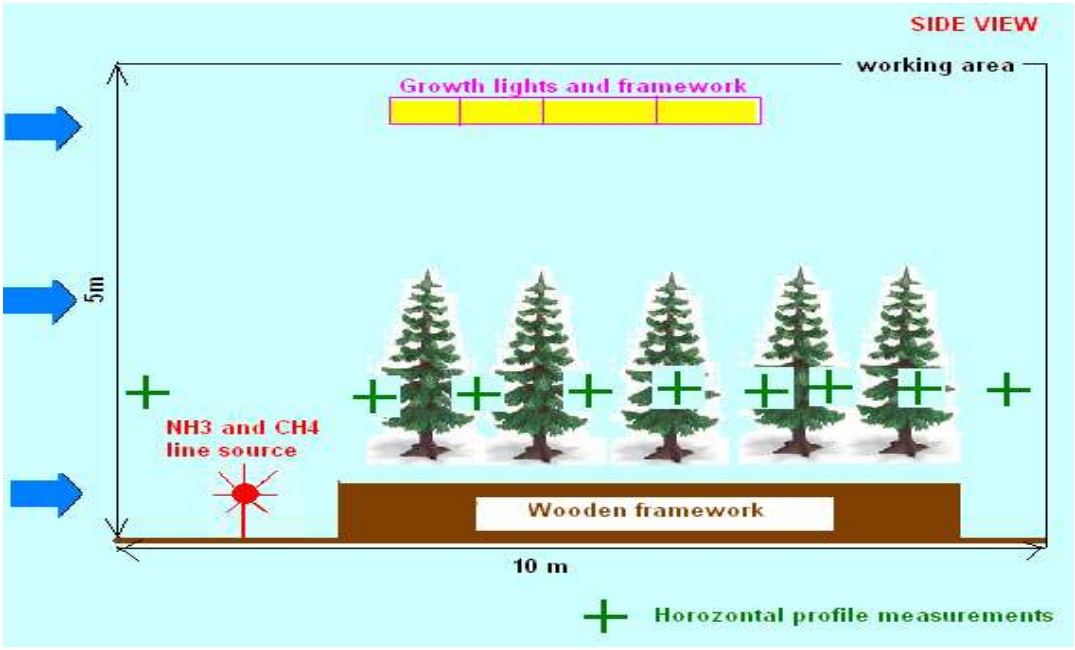

Figure 50: The wind tunnel schematic

Figure 51 shows horizontal profile of the measured area.

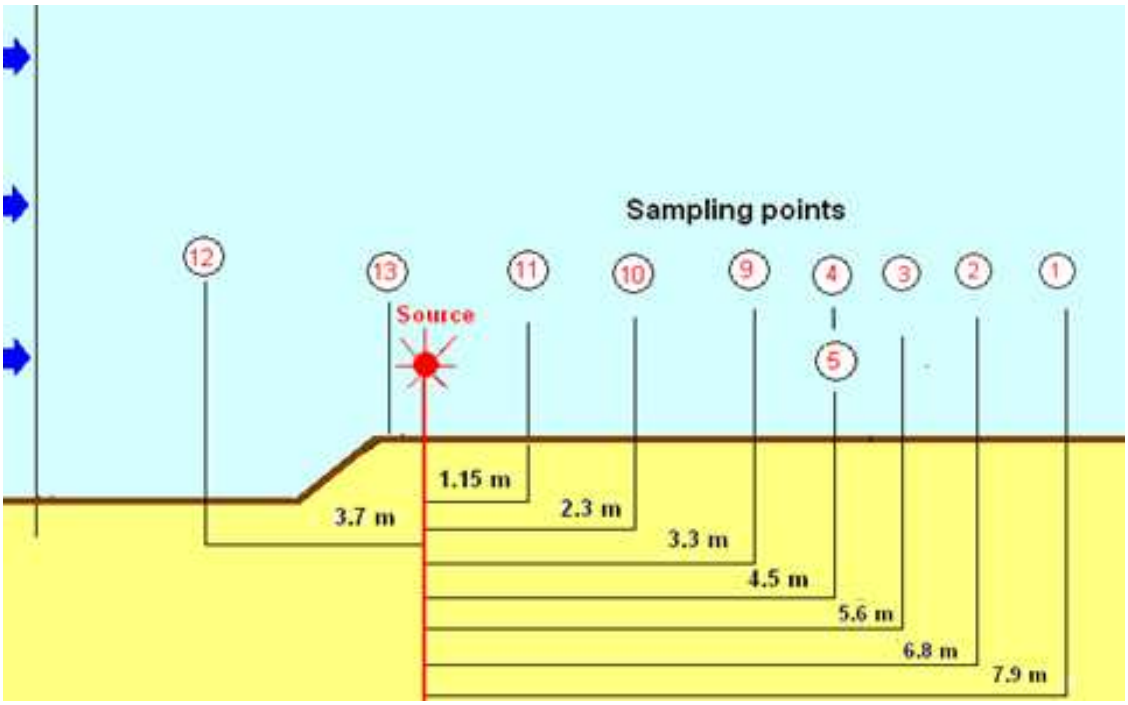

Figure 51: Horizontal profile of the measured area

The methane tracer and ammonia concentrations were monitored using a tunable diode laser absorption spectrometer (TDL-AS; CEH). While the decrease in was monitored using a TDL-AS also measured using a photo-acoustic NH_3 detector (CEH).

My work was based on comparison of remaining (not absorbed or dispersed) concentration of ammonia and the methane. The analysis of the 35 independent measurements in 10 sampling points was done.

One of the measurement graphs is shown in Figure 52 for illustration.

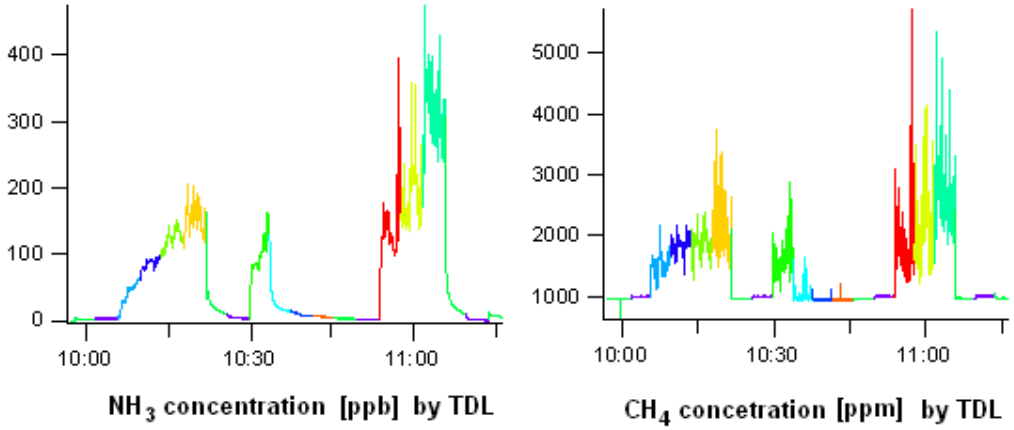

Figure 52: One of the measurement graphs

Full horizontal profile analysis of all the measurements was done. Except for a few exceptions the results showed a net uptake of ammonia by the vegetation.

From 280 compared points only in 15 cases was the absorption of the methane bigger then ammonia, which is likely to be due to either turbulent effects or instrument issues. I have to mention that it was really the pilot study which brings new ideas and plans to continue on this subject. One of the graphs showing the difference between remain concentration of NH_3 and CH_4 is shown in Figure 53.

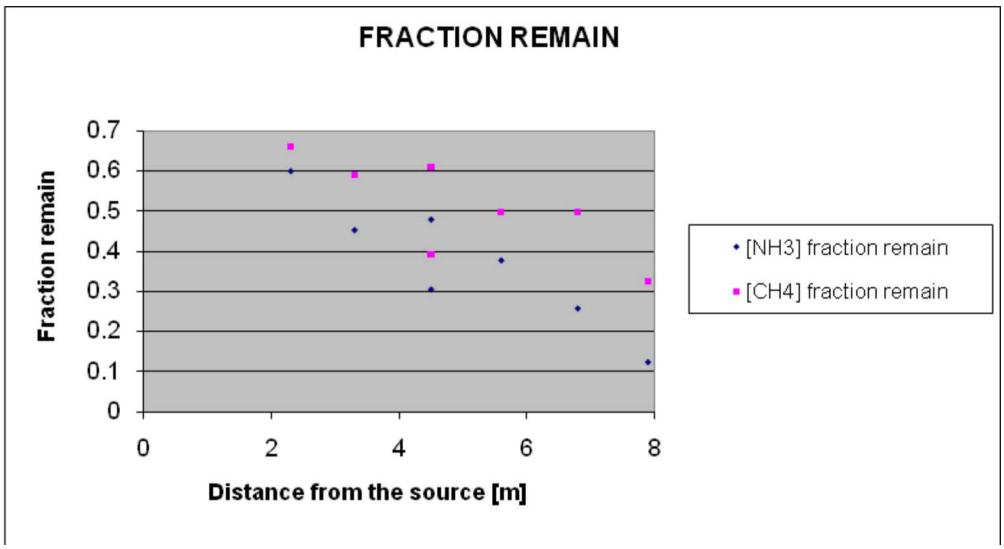

Figure 53: One of the investigated graphs (remain concentration of NH_3 and CH_4)

The absorption capacity would potentially be bigger, if the broadleaved trees were used.

2. Construction of experimental setup for trace measurement of ammonia

Another part of my scientific work consists of participation on construction of experimental setup for trace measurement of ammonia.

In this place I would like to show how simple it is to create an experimental arrangement that allows you to measure both trace amounts of ammonia (in our case), and relative humidity (see Figure 54). For the measurement we used the Nitrolux-100 (Pranalytica Inc.), detection instrument, an ambient NH_3 analyzer that uses resonant optoacoustic spectroscopy and a line-tunable carbon dioxide (CO_2) laser to provide continuous or on-demand measurements.

At the beginning of measurement we set a constant flow of carrier gas that was constantly controlled by a float flow-meter (rotameter) and regulated by a sensitive valve. The gas mixture of N_2 and NH_3 went through the system of interconnected standard plastic tubes. Part of the gas went to a vessel sealed by a photo-foil, in which relative humidity was measured, and a part to the optoacoustic analyzer.

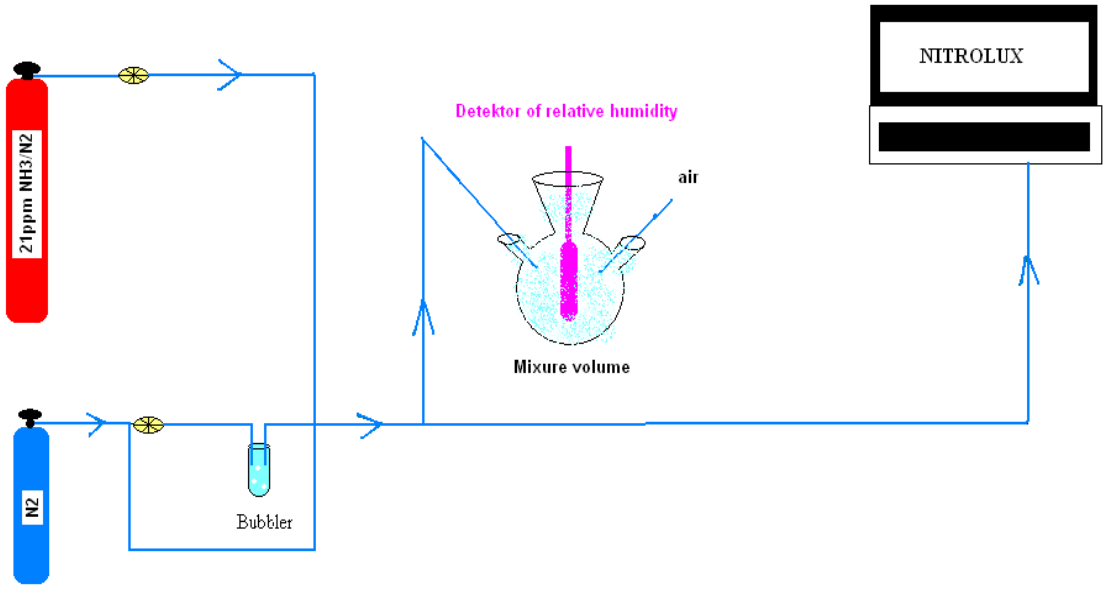

Figure 54: Experimental setup for measurement of trace amount of ammonia

The analyzer enables to detect up to trace amounts of gas. Its disadvantage is a high acquisition price.

Technical parameters of Nitrolux-100 (Pranalytica Inc.):

Range:	0 – 300 ppb
Operating temperatures:	10 – 30 ^{o}C
Operating RH	0 – 95 %
Sample flow:	~ 1200 – 1600 sccm
Dimensions:	19” x 8” x 24“
Weight:	32 kg

Its disadvantage is a high acquisition price.

I used the experience obtained during construction of this simple arrangement for later experimental work in the Czech Republic.

3. Design and Construction of a Optoacoustic cell for Measurements of Trace Amounts of Ammonia

I have participated in design and construction of an optoacoustic cell and experimental arrangement of the laser optoacoustic detection (PAS) with a cell inside of a resonator at the J. Heyrovský Institute Physical Chemistry of ASCR.

PAS is highly sensitive that enables discovery of even trace amounts of species, therefore it is a very efficient tool for concentration studies for monitoring of gaseous pollutants (NH_3, NO, NO_2, CH_3OH, CH_3CH_2OH, $CH_3CH{=}CH_2$, C_6H_6, $CH_2{=}CH_2$), monitoring of greenhouse gases and gases produced in breeding farm animals, consequently also for monitoring of ammonia creation. It even appears as the most reliable method for determination of ammonia trace amounts.[154]

An optoacoustic (OA) cell - a space, in which interaction between particles of flowing through gas and laser radiation occurs - was made of steel with low coefficient of heat expansion and good chemical properties.[156] During construction we were inspired by the previous study performed by Angeli et al.[155] The total length of the cell was 42 mm that corresponded to one quarter of λ_{ac} acoustic wave, and the inner diameter of 50 mm (Fig. 56). It is an open cell without windows, which is an advantage, since the window material does not affect photoacoustic signal. [155] However, we had to minimize acoustic losses of an open cell. For this reason the cell was provided by two

attenuating spaces (filters) at the entrance and exit that are 168 mm long and serve for elimination of parasitic acoustic signals that originate thanks to the absorption of excitation radiation by cell windows. Their size is one quarter and one half of an acoustic wave. This arrangement allows creation of well separated first azimuthal resonance in 2 kHz.[156]

Figures 55 and 56 shows outer and inner filter casting of the optoacoustic cell.

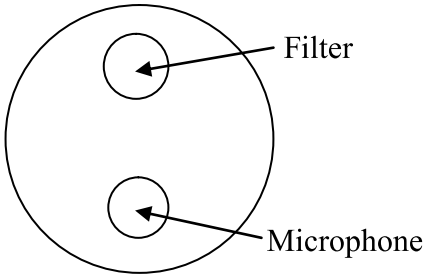

Figure 55: Outer and inner filter casing

Radii: Outer and inner filter casing

r of microphone = approx. 12 mm

r of cell = 50 mm

r of outer casing = 12 mm

r of inner casing = 4 mm

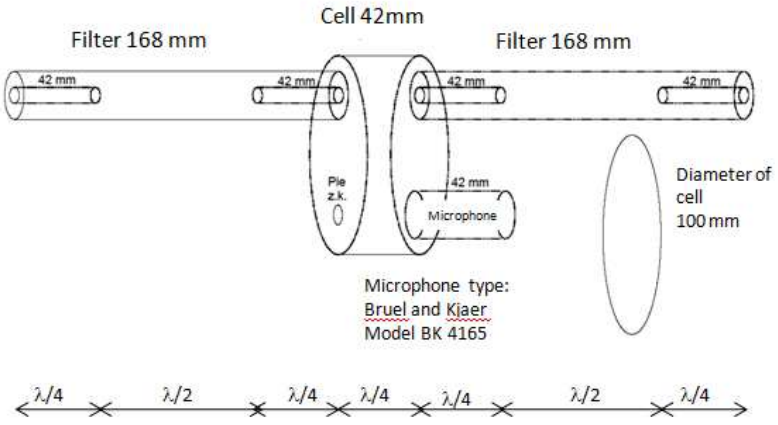

Figure 56: Cell design

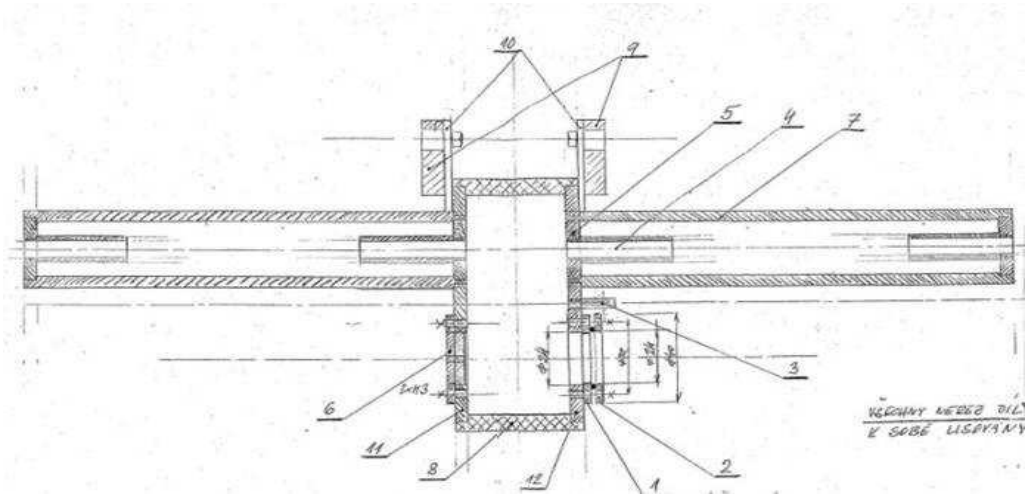

Figure 57: Drawing of the optoacoustic cell

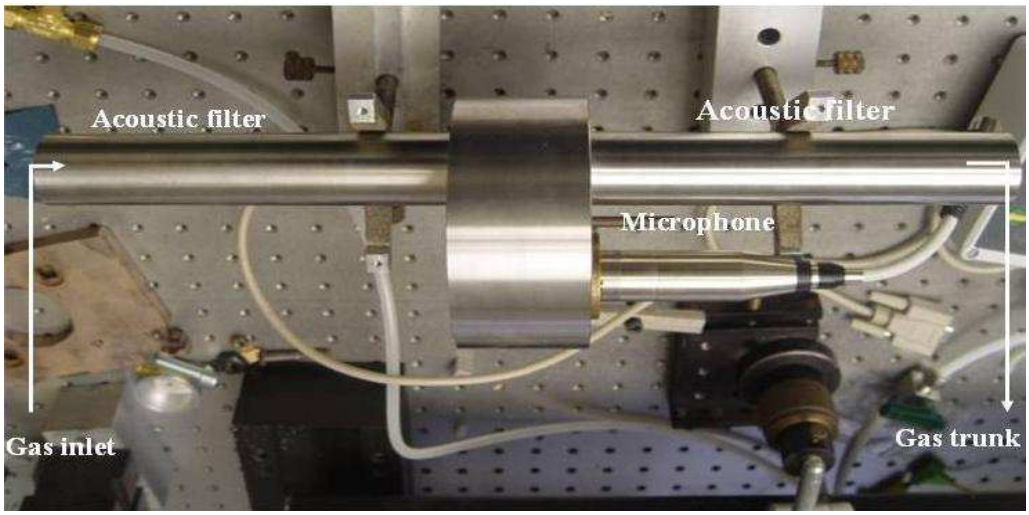

Figure 58: Assembled optoacoustic cell

For experimental arrangement a gas CO_2 laser, whose active environment consists of the mixture of CO_2, N_2, and He in the defined ratio approx. 1:2:8 (ratio of partial pressures), was used as a radiation source. It is a laser with optical resonator, in which the OA cell and rotating shutter (chopper) providing modulation of radiation is placed. OA signal is recorded by a sensitive microphone that is firmly seated in the cell's body.

From the practical standpoint the optical path was set using the He-Ne laser, whose red color beam is visible to human eye as opposed to CO_2 laser.

We were using the microphone Bruel and Kjaer BK 4165 with sensitivity of approx. 50 mV/Pa inserted into a cell body as a detector of pressure changes.

The experimental arrangement is shown in Figure 59.

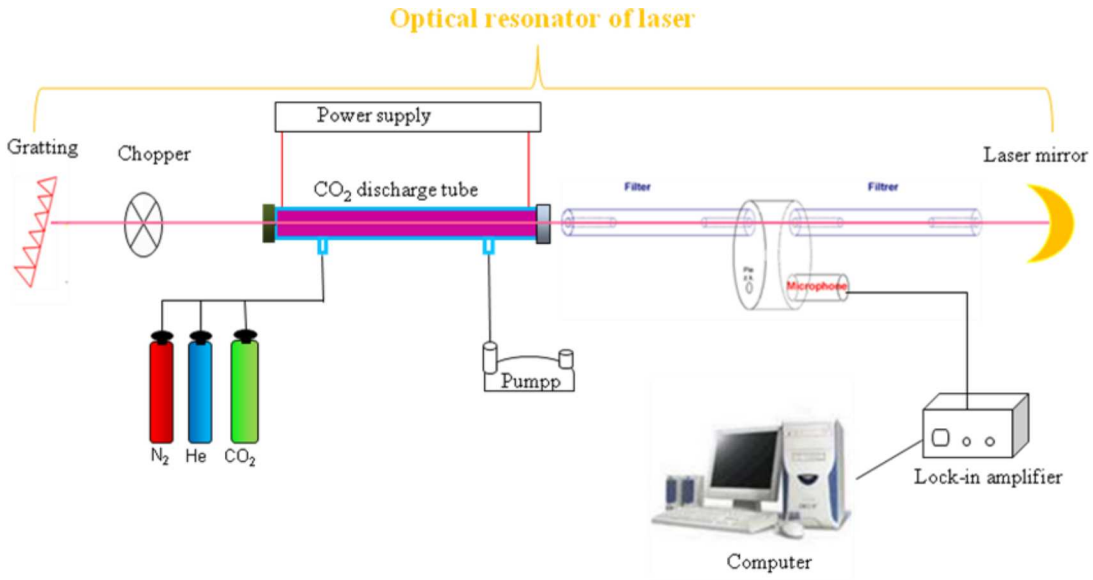

Figure 59: Optoacoustic experimental arrangement

2.4.6. Partial Conclusion

Within my dissertation I have also studied ammonia. An experimental arrangement using the laser optoacoustic detection method to measure trace amounts of ammonia was set up. I analyzed the data obtained from the experiment in aerodynamic tunnel. It is apparent from results that trees play important role in the process of decreasing of concentration of ammonia emitted to the air.

My work also consisted of designing and constructing of an optoacoustic cell, an experimental arrangement of the laser optoacoustic detection with the cell inside a resonator that would be suitable for measurement of trace amounts of ammonia. Until now there was testing, optimization, and methodical improvement of diagnostic techniques using a supercharged CO_2 laser with active mixture from CO_2, N_2 and He. This method can be used both in laboratory conditions (experiment in simulated wind tunnel atmosphere, where we can map dispersion and distribution of ammonia in surroundings of an emission source), and in various distances from the pollution source (modeling of ammonia spread into surrounding countryside – so called pollution gradient).

The future plan is to use this experimental setup in the experiment in the wind tunnel, into which we would place a model of selected stable, including nearby surroundings, water courses and small Greenleaf trees, and monitor flowing of ammonia

in this model and the influence of emitted ammonia concentration by trees inserted into atmosphere.

Based on obtained results we would like to be able to formulate measures to mitigate impact of emitted ammonia to the health of animals, people and plants, quality of animal agricultural production, and quality of the environment near pollution sources.

3. Conclusion of Dissertation

In my dissertation work I have studied chemical species that are significant due to their existence and influence they have on human health, environment, atmospheric chemistry, and astrochemistry by various spectroscopic methods. This way I tried very sensitive methods and experimental equipment that made possible even kinetic measurement of ions.

The work consists of a theoretical part with basic principles of spectroscopy and quantum physics outlined, and from a part describing my own work that I performed during my doctorate studies.

The theoretical part is written in a form that would serve as a basic material for studies of students, who would like to become familiar with principles of spectroscopy, and perform spectroscopic experiments.

Description of the work is divided into four thematic parts that describe four independently performed experiments. Partial conclusions discuss obtained results in detail. I would like to summarize these results here.

Analyses of the ν_4 asymmetrical and ν_2 symmetrical bands in the infrared spectrum of $FCO_2^{\cdot}$ radical that belongs to significant intermediate products of degradation processes of halogen hydrocarbons during reactions in the atmosphere, combustion, and combustion processes was performed for the very first time during my dissertation work. The detailed analysis led to determination of rotational constants, centrifugal distortion constants, and fine fissure constants of both bands.

Historically for the first time a spectroscopically unequivocal identification of the $CS^{\cdot+}$ molecule radicals was performed in high spectral resolution, i.e., on rotational level in the frequency range 414 to 622 GHz. This complete analysis allowed to exactly determine values of rotational constant and fine splitting constants that will help in predictions of line positions of this cation up to the THz area, and thus will help in its search in the Universe.

Further we have designed and performed experiments including measuring of spectra of cyanide species BrCN and CH_3CN, these molecules were studied in the low temperature plasma environment. From results of time resolved spectroscopic studies is apparent that many highly toxic species and also reactive samples originate from

acetonitrile and cyanogen bromide in the low temperature plasma conditions. The results bring us information about behavior of these species under extreme conditions, about lifetime of atoms and molecules, and radicals that originate from parent substance. Since acetonitrile is produced during burning of biomass and also, for example, from automobile exhalations, kinetic studies of the products of thermic decomposition of species performed in relatively well defined environment of the positive discharge column are useful both from the point of view of deeper understanding of elementary physical and chemical processes taking place in the Universe, and also within the framework of fire safety practice.

Finally I studied the ecological impact of ammonia near its point source and impact of trees on the amount of ammonia in the air. I also designed and build an optoacoustic cell for the experimental arrangement of the laser optoacoustic detection method. We plan to use this experimental arrangement, very sensitive to measurement of even trace amounts of ammonia and other gaseous pollutants, during experimental work in an aerodynamic tunnel during modeling of ammonia spread from a model of a selected stable. Since the research of technologies and principles that lower ammonia emissions during breeding of farm animals is currently one of the basic directions of sustainable and ecological agricultural production, then this topic is very important.

Some species investigated during my doctorate studies were not measured or analyzed in the given area of electromagnetic spectrum yet. The work thus brings significant scientific knowledge important for further research and understanding of reaction mechanisms that the measured species participate in atmosphere, interstellar space, or in plasma.

During my doctorate studies I cooperated with the following prestigious international institutions:

- J. Heyrovsky Institute of Physical Chemistry by the Academy of Sciences of the Czech Republic

- Laboratoire de Physique des Lasers, Atomes et Molécules, PhLAM), Université Lille 1 in France

- Berchische Universität in Wuppertal

-Centre for Ecology & Hydrology (CEH), Natural Environment Research Council in Edinburgh

The work thus significantly contributes to development of science and research at the Faculty of Safety Engineering.

Also its contribution in the field of expanding cooperation both with Czech, and international institutions is considerable.

4. Závěr disertační práce

Ve své disertační práci jsem studovala chemické látky, významné svou existencí a působením na lidské zdraví, životní prostředí, atmosférickou chemii a astrochemii různými spektroskopickými metodami. Vyzkoušela jsem si takto velice citlivé metody a experimentální vybavení, které umožňovalo i kinetické měření iontů.

Práce se skládá z části teoretické, v niž jsou nastíněny základní principy spektroskopie a kvantové fyziky, a z části v niž je popsaná má vlastní práce, které jsem se během svého doktorského studia věnovala.

Teoretická část je psaná takovou formou, aby sloužila jako podklad ke studiu studentům Vysoké škole báňské, kteří by se rádi seznámili s principy spektroskopie a chtěli se zabývat spektroskopickým experimentem.

Popis vlastní práce je rozdělen do čtyř tematických celků, které popisují čtyři nezávislé, uskutečněné experimenty. V dílčích závěrech jsou podrobně diskutovány získané výsledky. Na tomto místě bych chtěla tyto výsledky shrnout.

V rámci mé disertační práce byla vůbec poprvé provedena analýza asymetrického vibračního pásu ν_4 a symetrického pásu ν_2 infračerveného spektra $FCO_2^{\cdot}$ radikálu, který patří mezi významné meziprodukty degradačních procesů halogenových uhlovodíků při reakcích v atmosféře, při hoření a spalovacích procesech. Detailní analýza vedla k určení rotačních konstant, centrifugálně distorzních konstant a konstant jemného štěpení pro oba sledované pásy.

Historicky poprvé byla uskutečněna také první spektroskopicky jednoznačná identifikaci molekulového radikálů $CS^{\cdot+}$ s vysokým spektrálním rozlišení, tj. na rotační úrovni ve frekvenčním rozsahu 414 až 622 GHz. Celková analýza umožnila přesné určení hodnot rotační konstanty, konstanty jemného štěpení, které poslouží k predikování poloh linii tohoto kationtu až do THz oblasti a napomůže tak v jeho hledání ve vesmíru.

Dále byly navrženy a uskutečněny experimenty zahrnující měření spekter kyanových látek BrCN a CH_3CN a bylo studování chování těchto molekul v prostředí nízkoteplotního plazmatu. Z výsledků provedených časově rozlišených spektroskopických studií je zřejmé, že z acetonitrilu a bromkyanu vzniká v podmínkách nízkoteplotní plazmy řada vysoce toxických látek a také reaktivních specií. Výsledky

přinášejí informace o chování látek za extrémních podmínek, době života atomů a molekul a radikálu vznikajících z mateřské substance. Jelikož acetonitrilu je produkován při spalování biomasy a dále například z automobilových exhalací, jsou kinetické studie produktů tepelného rozkladu látek provedené v relativně dobře definovaném prostředí pozitivního výbojového sloupce užitečné nejen z pohledu hlubšího pochopení elementárních fyzikálně-chemických procesů probíhajících ve vesmíru, ale též v rámci požárně-bezpečnostní praxe.

Nakonec byl studován ekologický impakt amoniaku v okolí jeho bodového zdroje a vliv stromů na množství amoniaku v ovzduší. Byla také navržena a sestavena optoakustická kyveta experimentální sestavy metody laser optoakustické detekce. Toto experimentální uspořádání, velice citlivé k měření i stopových množství amoniaku a dalších plynných polutantů, plánujeme využít při experimentální práci v aerodynamickém tunelu při modelování šíření amoniaku z modelu vybrané stáje. Jelikož je výzkum technologií a principů snižujících emise amoniaku při chovu hospodářských zvířat v současné době jedním ze základních směrů udržitelné a ekologické agrární produkce, je toto téma velmi aktuální.

Některé látky, zkoumané v rámci mého doktorského studia, nebyly ještě dosud v dané oblasti elektromagnetického spektra proměřeny či analyzovány. Práce tak přináší významné vědecké poznatky důležité pro další výzkum a porozumění reakčních mechanismů, jichž se změřené látky účastní ať už v atmosféře, v mezihvězdném prostoru nebo či v plazmatu.

Během svého doktorského studia jsem spolupracovala s prestižními mezinárodními institucemi

- Ústav fyzikální chemie J. Herovského, akademie věd České republiky

- Laboratoire de Physique des Lasers, Atomes et Molécules, PhLAM), University Lile 1 ve Francii

- Berchische Univeresität ve Wuppertal

-Centre for Ecology & Hydrology (CEH), Natural Environment Research Counil v Edinburghu

Práce tak velmi přispívá k rozvoji vědy a výzkumu na Fakultě bezpečnostního inženýrství.

Nezanedbatelný je tedy také přínos na poli prohlubující se spolupráce s jak českými, tak zahraničními institucemi.

5. Résumé

Le sujet de ma thèse abordait l´étude des matières chimiques, importantes par leur existence et leur impact sur la santé humaine, l´environnement, la chimie atmosphérique et l´astrochimie en utilisant les différentes méthodes spectroscopiques. De cette façon, j´ai essayé des méthodes très sensibles ainsi que l´équipement experimental qui m´a permis d´utiliser également les mesures cinétiques d´ions.

Ma thèse comprend la partie théorique, abordant les principes fondamentaux de la spectroscopie et de la physique de quantum, et la partie décrivant mon propre travail, auquel je me suis dédiée lors de mes études de doctorat**.**

En ce qui concerne la partie théorique, sa forme permet son utilisation en tant que la base pour les étudiants de la Haute école des études minières, susceptibles de connaître les principes de la spectroscopie et intéressés par des expériences spectroscopiques.

La description de mon travail est divisée en quatre sujets thématiques décrivant quatre expériences indépendantes réalisées. Les conclusions partielles discutent de façon détaillée les résultats obtenus. Je voudrais présenter la synthèse de ces résultats.

Dans le cadre de ma thèse a été effectuée pour la première fois l´analyse de la bande de vibrations asymetrique ν_2 et de la bande symétrique du spectre infrarouge du radical $FCO_2^{\cdot}$, un des produits intermédiaires importants des process de dégradation des carbures d´halogène pendant la réaction dans l´atmosphère, la combustion et les process de combustion. Le résultat de l´analyse détaillée a permis de déterminer des constantes de rotation, des constantes de distorsion de centrifuge ainsi que des constantes de la fine scission pour les deux bandes analysées.

Historiquement pour la première fois a été également effectuée l´identification spectroscopiquement univoque de l´ion des radicaux de molécule $CS^{\cdot+}$, à différenciation spectrale très élevée, cela veut dire au niveau de rotation de la gamme de fréquence de 414 à 622 GHz. L´analyse globale a permis de faire une détermination précise des valeurs de la constante de rotation, de la constante de la scission fine, permettant de déterminer les positions des lignes de ce cation jusqu´à la zone THz ce qui permettra sa recherche dans l´univers.

Ensuite ont été proposées et effectuées des expériences incluant les mesures des spectres des matières de cyane BrCN et CH_3CN et le comportement de ces molécules

dans le milieu du plasma à basse température a été soumis aux études. Grâce aux résultats des études spectroscopiques différenciées, nous pouvons voir qu´à partir de l´acétonitrille et le cyanure de brome, dans les conditions du plasma à basse température apparaît toute une série des matières à toxicité élevée ainsi que des espèces réactives. Les résultats nous présentent des informations sur le comportement des matières dans des conditions extrêmes, des informations sur la durée de vie des atomes et des molécules ainsi sur le radical naîssant de la substance- mère. Comme l´acétonitrille est le produit de la combustion de la biomasse et des exhalations d´automobiles, les études cinétiques des produits de la décomposition thermique des matières, effectuées dans le milieu de la colonne de décharge positive, relativement bien défini, sont utiles non seulement parce qu´elles permettent mieux comprendre des process physico- chimiques élémentaires de l´univers, mais aussi utiles sur le plan de la pratique dans le domaine de la sécurité anti- incendie.

Finalement, j´ai étudié l´impact écologique de l´ammoniaque sur l´environnement près de sa source ponctuelle ainsi que l´impact des arbres sur la quantité de l´ammmoniaque dans l´atmosphère. Une cuve opto-acoustique du jeu expérimental de la méthode laser de la détection opto-acoustique a été conçue. Cette disposition expérimentale, très sensible pour mesurer les oligo- quantités de l´ammoniaque et d´autres matières polluantes gazeuses, pourrait être également utilisée pendant le travail expérimental dans le tunnel aérodynamique lors du modelage de l´expansion de l´ammoniaque du modèle de l´étable choisie. Comme la recherche dans le domaine des technologies et des principes, diminuant les émissions de l´ammoniaque lors de l´élevage du bétail, est aujourd´hui une des tendances principales de la production soutenable et de l´agriculture écologique, il s´agit d´un sujet très actuel.

Certaines matières, analysées dans le cadre de ma thèse, n´ont pas été encore mesurées ou analysées dans le domaine donné du spectre électromagnétique. Ma thèse apporte des connaissances scientifiques très rélévantes à utiliser dans la recherche et permet de mieux comprendre des mécanismes de réaction, à laquelle interviennent les matières mesurées soit dans l´atmosphère, dans l´univers ou dans le plasma.

Lors de l´élaboration de ma thèse, j´ai collaboré avec des établissements internationaux très prestigieux, à savoir:

- Institut de la chimie de physique J. Herovský, Académie des sciences de la République Tchèque

- Laboratoire de Physique des Lasers, Atomes et Molécules, PhLAM), Université Lille 1, France

- Berchische Univeresität, Wuppertal, Allemagne

-Centre for Ecology & Hydrology (CEH), Natural Environment Research Counil, Edinburgh

De cette façon, ma thèse contribue au développement de la science et la recherche à la Faculté de l´engeneering de sécurité.

La contribution dans le domaine de la collaboration avec les établissements tchèques et étrangers est aussi très importante.

6. References

[1] HOLOUBEK, I. *Troposférická chemie*. Brno: Masarykova Univerzita, 2005.159 p. ISBN 80-210-3656-7.

[2] KANIA, *P. Rotačně-hyperjemná spektroskopie atmosféricky významných specií*. Praha, 2006. 125 p. Dissertation. VŠCHT.

[3] FIŠER, J.; ZEMÁNEK, F. *Struktura látek: atomy, molekuly, krystaly*. Praha: Karolinum, 1994. 255 p.

[4] *Http://climate.psu.edu/* [online]. 2010 [cit. 2010-07-12]. [4] Training Manual for FROST. WWW: <http://climate.psu.edu/data/frost/frosttraining.php>.

[5] Jan Marek. *Humoristické listy*. 1889, XXXI, 27, p. 247.

[6] *McGraw Hill Encyclopedia of Science and Technology*. New York: McGraw-Hill Professional, 2007. 15600 p. ISBN 978-0071441438.

[7] JAMMER, M. *The Conceptual Development Of Quantum Mechanics (International series in pure and applied physics).* New York: McGraw-Hill, 1966. 399 p.

[8] HEILBRON, J. L. *Dilemmas of an Upright Man: Max Planck and the Fortunes of German Science* . Harvard University Press, 2000. 272 p. ISBN 978-0674004399.

[9] SODOMKA, L.; SODOMKOVÁ, M. *Nobelovy ceny za fyziku:1901-1997*. Praha: SET OUT, 1997. 157 p. ISBN 80-902058-5-2.

[10] FEYNMAN, R. P.; LEIGHTON, R. B. ; SANDS, M. *The Feynman Lectures on Physics: Commemorative Issue Vol 3*. Reading: Addison Wesley, 1971. 400 p. ISBN 978-0201021189.

[11] FEYNMAN, R. P. *Six Easy Pieces: Essentials of Physics Explained by Its Most Brilliant Teacher*. New York: Perseus Books, 1994. 176 p. ISBN 978-0201409550.

[12] R. NĚMCOVÁ, I.; ČERMÁKOVÁ, L.; RYCHLOVSKÝ, P. *Spektroskopické analytické metody I*. Praha: Karolinum, 1997. 166 p. ISBN80-7184-365-2.

[13] HALLIDAY D., RESNICK R., WALKER J. Fundamentals of Physics. Willey & Sons, 2004. 1136p. ISBN 978-0471216438.

[14] BEISER, A. *Perspectives of Modern Physics*. New York : McGraw-Hill, 1969. 624 p. ISBN 978-0070850477.

[15] *Http://astronuklfyzika.cz/* [online]. 2010 [cit. 2010-07-12]. http://astronuklfyzika.cz/JadRadFyzika.htm. WWW: <http://astronuklfyzika.cz/JadRadFyzika.htm>.

[16] HERZBERG, G. *The Spectra and Structure of Simple Free Radicals*. New York: Dover Publication Inc., 1971. 226 p. ISBN 0-486-49539-6.

[17] *Http://aldebaran.feld.cvut.cz/* [online]. 2010 [cit. 2010-07-12]. Http://aldebaran.feld.cvut.cz/vyuka/ekologie_a_Volné radikály, excitované částice a elektricky nabité částice v atmosféře. WWW: http://aldebaran.feld.cvut.cz/vyuka/ekologie_a_ekotechnika/prednasky/Iondopl.doc.

[18] KEWLEY R., WINNEWISSER M., SASTRY K. V. L. N., GORDY W. *J. Chem. Phys.* 39, 2856 (1963).

[19] WINNEWISSER M., SASTRY K. V. L. N., COOK R. L., GORDY W. *J. Chem. Phys.* 41, 1687 (1964).

[20] CHEN, F. F. *Úvod do fyziky plazmatu*. Praha: Academia, 1984.

[21] HRUBÝ, V. *Studium interakce plazma-pevná látka pomocí hybridního modelování*. Praha, 2009. 83 s. Diploma thesis. Universita Karlova.

[22] BERNATH P. F. *Annu. Rev. Phys. Chem.* 41, 91–122 (1990).

[23] DAVIES P. B., MARTIN P. A. *Chem. Phys. Letters* 87, 6434 (1987).

[24] CIVIŠ S. , ZELINGER Z., TANAKA K. T. *J. Mol. Spectrosc.* 187:1, 82–88 (1998).

[25] GUDEMAN C. S., BEGEMANN M. H. B, PFAFF J. SAYKALLY R. J., *Phys. Rev. Lett.* 50, 727 (1983).

[26] ZELINGER Z., BERSCH A., PETRI M., URBAN W. CIVIŠ S., *J. Mol. Spectrosc.* 171, 579–582 (1995).

[27] ZELINGER Z., CIVIŠ S., KUBÁT P., ENGST P. *Infrared Physics and Technology* 36: 1, 537–543 (1995).

[28] MOORE, W. J. *Fyzikální chemie*. Praha: Státní nakladatelství technické literatury, 1979. 976 p.

[29] GORDY W., COOK R. L. *Microwave Molecular Spectra*. New York: John Wiley & Sons, 1970. 944 p. ISBN-13 978-047108681.

[30] KROTO H. W. *Molecular Rotation Spectra*. New York: Dover Publications, 1992. 352 p. ISBN 978-0486495408.

[31] TOWNES C. H., SCHAWLOW A. L. *Microwave Spectroscopy*. New York: Dover Publications, 1975. 698 p. ISBN 978-0486617985.

[32] SUGDEN T. M., KENNEY C. N. *Microwave Spectroscopy of Gases*, London: D.Van Nostrand Company, 1965. 349 p. ISBN 978-0442080785.

[33] GORDY W., SMITH W. V.: TRAMBARULO R. F. *Microwave Spectroscopy*, New York: Dover Publications, 1953.

[34] WATSON J. K. G. *Vibrational Spectra and Structure: A series of advances 6*. Amsterdam: Elsevier Science, 1977. 396 p. ISBN 978-0444413802.

[35] KOLESNÍKOVÁ L., *Hyperjemná struktura v radikálech a ve standardních molekulách*. Praha, 2007. 84p Diploma thesis. VŠCHT.

[36] BERNATH P. F. *Spectra of Atoms and Molecules*. Oxford: Oxford University Press, 1995. 454 p. 978-0195177596.

[37] HORÁK M.; PAPOUŠEK D. *Infračervená spektra a struktura molekul*. Praha: Academia, 1976. 840 p.

[38] CLEETON C. E., WILLIAMS N. H., *Physical Review*, *4,* 234-237, (1934).

[39] LOVE, W. Magnetrons (Chapter 2) in *Handbook of Microwave Technology - Volume 2*, San Diego: Academic Press, 1995, p. 679 ISBN: 978-0123746979.

[40] WILSON, J. D. Traveling Wave Thermionic Devices in *Handbook of Microwave Technology - Volume 2*, San Diego: Academic Press, 1995, p. pp. 57-95. 978-0123746979.

[41] FERUS M., KAWAGUCHI K., JUHA L., CIVIŠ S. *J. Chem. Phys.* submitted (2010).

[42] KAWAGUCHI K., HAMA Y., NISHIDA S.*J. Mol. Spect.* 232, 1 (2005).

[43] FERUS M., CIVIŠ S. *Čs. čas. fyz.* 58:3 (2008).

[44] BELL, A.G. *Am. J. Sci*., 20, 305 – 324 (1880).

[45] ZELINGER, Z. *Chemické listy*. 80, 673-680(1985).

[46] HERECOVÁ, L., et al. Optoakustická detekce plynů a možnosti jejího využití při monitorování slévárenských technologií. In. *Sborník vědeckých prací Vysoké školy báňské - Technické univerzity Ostrava : Řada hutnická*. Ostrava: VŠB-TU Ostrava, 2007. p. 81-93. ISBN 9788024815480. ISSN 1210-0471.

[47] NEVRLÝ, V., et al. Laserová optoakustická detekce plynů v bezpečnostním inženýrství. In *Sborník přednášek*. Ostrava : VŠB-TU Ostrava, 2007.

[48] ENGST, P., HORÁK, M. *Aplikace laserů*. Praha: SNTL, 1989. 208 p.

[49] STŘIŽÍK M., *Infračervená spektroskopie s optoakustickou detekcí jako selektivní metoda monitorování znečištění ovzduší*. Praha 1995. Diploma thesis. Universita Karlova.

[50] ARGÜELLO G.A.,GROTHE H., KRONBERG M., WILLNER H., MACK, H.G. *J. Phys. Chem.* 99, 17525 (1995).

[51] ZELINGER Z. *Infračervená a mikrovlnná spektroskopie reaktivních molekul významných v procesech hoření a atmosférické chemie.* Ostrava, 2009. 119p. Habilitation:VŠB-TU Ostrava.

[52] BREIDUNG, J., THIEL, W. *J. Phys. Chem. A*, 110:4, 1575–1585.(2006) DOI: 10.1021/jp053883v

[53] ZELINGER Z., DRÉAN P., WALTERS A., MORENO J. R. A., BOGEY M., PERNICE H., VON AHSEN S., WILLNER H., BREIDUNG J., THIEL W., BURGER H. *J. Chem. Phys.* 118:3, 1214–1220 (2003).

[54] HOLLAS J. M. *High resolution spectroscopy*. Chichester : John Willey & Sons, 1998. 743 p. ISBN 978-0471974215.

[55] ALLEN H. C. Jr., CROSS P. C. *Molecular Vib – Rotors*. Willey & Sons, 1963. 324 p.

[56] AHSEN S., WILLNER H., ARGÜELLO G. A.: *J. Fluorine Chem.* 125, 1057 – 1070 (2004).

[57] MARICQ M. M., SZENTE J. J., DIBBLE T. S., FRANCISCO J. S. *J. Phys. Chem.* 98, 12294 – 12309 (1994).

[58] WALLINGTON T. J., ELLERMANN T., NIELSEN O. J., SEHESTED J. *J. Chem. Phys.* 98, 2346 – 2356 (1994).

[59] FRANCISCO J.S., GOLDSTEIN A.N. *Chem. Phys.* 173, 73(1988).

[60] FRANCISCO J. S., OSTAFIN A. *Mol. Phys.* 68, 255 (1989).

[61] ZELINGER Z., BAILLEUX S., BABÁNKOVÁ D., ŠIMEČKOVÁ M., STŘÍTECKÁ L., KOLESNÍKOVÁ L., MUSIL P., KANIA P., URBAN Š, BECKERS H., WILLNER H. *J. Mol. Spect.*, 243, 218–221(2007).

[62] KOLESNIKOVA L, VARGA J, BECKERS H, ET AL. *J. Chem. Phys.* 128**,** 22 **(**2008**).**

[63] ZARE R. N. *Angular Momentum*, New York: John Wiley & Sons, 1988. 368 p. ISBN 978-0471858928.

[64] BROWN J. M., SEAR T. J. *J. Mol. Spectrosc.* 75, 111–133 (1979).

[65] VAN VLECK J. H. *Rev. Mod. Phys.* 23, 213–227(1951).

[66] RAYNES W. T. *J. Chem. Phys.* 41 (1964).

[67] PERRIN A., FLAUD J.M., CAMY-PEYRET C.,.VASSEROT A.M, GUELACHVILI G., GOLDMAN A., MURCRAY F.J., BLATHERWICK R.D. *J. Mol. Spectrosc.* 154, 391(1992).

[68] PERRIN A., STŘIŽÍK M., BECKERS H., WILLNER H., ZELINGER Z., PRACNA P., NEVRLÝ V., GRIGOROVÁ E. *Molecular Physics*, 108:6, 723–731(2010).

[69] PICKETT H. M. *J. Mol. Spectrosc.*, 148, 371 (1991).
See also: http://spec.jpl.nasa.gov/ftp/pub/calpgm/

[70] PEARSON R. G. *Symmetry Rules for Chemical Reactions*, New York: John Wiley & Sons, 1976, 560 p, ISBN 978-0471014959.

[71] DAVIDSON E. R., BORDEN W. T. *J. Phys. Chem*. 87, 4783–4790 (1983).

[72] *Http://blog.deepskycolors.com/* [online]. 2009 [cit. 2010-07-12]. Nebulas. WWW: <http://blog.deepskycolors.com/archive/2009/09/19/orions-Deep-Field--Belt-and-sword.html>.

[73] BAILLEUX S., WALTERS A., GRIGOROVA E., MARGULES L. *ApJ*. 679:1, 920–924, (2008).

[74] HUBER, K. P., HERZBERG, G. 1979, *Molecular Spectra and Molecular Structure IV: Constantsof Diatomic Molecules*, New York: Van Nostrand, 1979, 716p. ISBN 978-0442233945.

[75] HAUSCHILDT H., GUSTEN R., PHILLIPS T. G., SCHILKE P., SERABYN E., WALKER C. K., *First Detection of CS/10-9/ in Galactic Star Forming Cores*, *A&A*, 273, L23 (1993).

[76] WALKER, C. K., LADA, C. J., YOUNG, E. T., MALONEY, P. R., WILKING, B. A. *ApJ*, 309 L47 (1986).

[77] HAYASHI M., SUZUKI S., OMODAKA T., & HASEGAWA T., *ApJ*, 288, 170 (1985).

[78] HASEGAWA T., et al. *ApJ*, 283, 117 (1984).

[79] DRDLA K., KNAPP G. R., VAN DISHOECK E. F. *ApJ*, 345, 815 (1989)

[80] LINDQVIST M., NYMAN L. A., OLOFSSON H., WINNBERG A. *A&A*, 205, L15(1988).

[81] VAN DISHOECK E. F., JANSEN D. J., PHILLIPS T. G. *A&A*, 279, 541 (1993).

[82] BREGMAN J. D., GOEBEL J. H., STRECKER D. W. *ApJ*, 223, L45 (1978).

[83] JACKSON W. M., HALPERN J. B., FELDMAN P. D., RAHE J. *A&A*, 107, 385 (1982).

[84] SMITH A. M., STECHER T. P., CASSWELL L. *ApJ*, 242, 402 (1980).

[85] LATTER W. B., WALKER C. K., MALONEY P. R. *ApJ*, 419, L97(1993).

[86] STÖRZER H., STUTZKI J., STERNBERG A. *A&A*, 296, L9 (1995).

[87] FUENTE A., RODRÍGUEZ-FRANCO A., GARCÍA-BURILLO S., MARTÍN-PINTADO J., BLACK J. H. *A&A,* 406, 899 (2003).

[88] FUENTE A., MARTÍN-PINTADO J. *ApJ*, 447, L07(1997).

[89] RIZZO J. R, FUENTE A., RODRÍGUEZ-FRANCO A., GARCÍA-BURILLO S. *ApJ*, 597, L153(2003).

[90] SAVAGE C., ZIURYS L. M., *ApJ*, 616, 966 (2004).

[91] FUENTE A., GARCÍA-BURILLO S., GERIN M., RIZZO J. R., USERO A., TEYSSIER D., ROUEFF E., LE BOURLOT J. *ApJ*, 641, L105(2006).

[92] FUENTE A., BLACK J. H., MARTÍN-PINTADO J., RODRÍGUEZ-FRANCO A., GARCÍA-BURILLO S., PLANESAS P., LINDHOLM J. *ApJ*, 545, L113(2000).

[93] SPAANS M., MEIJERINK R. *ApJ*, 664, L23 (2007).

[94] BLÖCKER J. H., REINSCH E. A., ROSMUS P., WERNER H. J., & KNOWLES P. *J., Chem. Phys.*147, 99 (1990).

[95] HORANI M., VERVLOET M. *A&A*, 256, 683 (1992).

[96] QUARTA M. L., SINGH P. D. *A&A*, 98, 384 (1981).

[97] LEACH S. *A&A*, 187, 195(1987).

[98] WOODALL J., AGÚNDEZ M., MARKWICK-KEMPER A. J., MILLAR T. J. *A&A,* 466, 1197(2007). www.udfa.net

[99] PENZIAS A. A., SOLOMON P. M., WILSON R. W., JEFFERTS K. H. *ApJ*, 168, L53(1971).

[100] COXON J. A., MARCOUX P. J., SETSER D. W. *Chem. Phys.*, 17, 403 (1976).

[101] GAUYACQ D., HORANI M. *Can. J. Phys.*, 56, 587 (1978).

[102] THADDEUS P., GUELIN M., LINKE R. A. *ApJ*, 246, L41(1981).

[103] FERLET R., ROUEFF E., CZARNY J., FELENBOK P. *A&A*, 168, 259(1986).

[104] SAITO S., KAWAGUCHI K., YAMAMOTO S., OHISHI M., SUZUKI H., KAIFU N. *ApJ*, 317, L115 (1987).

[105] YAMAMOTO S., SAITO S., KAWAGUCHI K., KAIFU N., SUZUKI H., OHISHI M. *ApJ*, 317,L119 (1987).

[106] BELL M. B., AVERY L. W., FELDMAN P. A. *ApJ*, 417, L37(1993).

[107] COSSART D. *J. Mol. Spectrosc.,* 167, 11 (1994).

[108] LIU Y., LIU H., GAO H., DUAN C., HAMILTON P. A., DAVIES P. B. *Chem. Phys. Lett.,* 317, 181(2000).

[109] LIU Y., DUAN C., LIU J., WU L., XU C., CHEN Y., HAMILTON P. A., DAVIES, P. B. *J.Chem. Phys.,* 116, 9768 (2002).

[110] DUAN C., WU L., CHEN Y., LIU Y. *J. Mol. Spectrosc.,* 217, 146 (2003).

[111] CIVIŠ S., WALTERS A., TRETYAKOV M. Y., BAILLEUX S., BOGEY M. *J. Chem. Phys.*, 108, 8369 (1998).

[112] DIXON T. A., WOODS, R. C. *Phys. Rev. Lett*., 34, 61 (1975).

[113] DE LUCIA F. C., HERBST E., PLUMMER G. M., BLAKE G. A. *J. Chem. Phys.*, 78, 2312 (1983).

[114] NAZAROFF W. W., SINGER B. C., *Journal of Exposure Analysis and Environmental Epidemiology* 14, S71-S77(2004).

[115] MOHR D. H., KING C. J., *Environ.Sci.Technol.* 19, 929-935(1985).

[116] HOLZINGER R., JORDAN A., HANSEL A., LINDINGER W., *Journal of Atmospheric Chemistry,* 38, 187-193(2001).

[117] LOBERT J. M., SCHARFFE D. H., HAO W. M., CRUTZEN P. J., *Nature (London, United Kingdom) 346* 552-554 (1990).

[118] HOLZINGER R., WARNEKE C., HANSEL A., JORDAN A., LINDINGER W., SCHARFFE D. H., SCHADE G., CRUTZEN P. J., *Geophys.Res.Lett. 26* 1161-1164 (1999).

[119] HAWTHORNE S. B., SIEVERS R. E., *Environ.Sci.Technol. 18* 483-490 (1984).

[120] SCHNEIDER J., BURGER V., ARNOLD F., *J.Geophys.Res., [Atmos.] 102* 25501-25506 (1997).

[121] BRASSEUR G., ARIJS E., DE RUDDER A., NEVEJANS D., INGELS J., *Geophys.Res.Lett. 10* 725-728 (1983).

[122] JOST C., TRENTMANN J., SPRUNG D., ANDREAE M. O., DEWEY K., *Geophys.Res.Lett. 30* ASC(2003)..

[123] DE GOUW J. A., WARNEKE C., PARRISH D. D., HOLLOWAY J. S., TRAINER M., FEHSENFELD F. C., *J.Geophys.Res., [Atmos.] 108* ACH2-1-ACH2/8, (2003).

[124] KUMAR, V. *Cyanogen Bromide (CNBr)*, *SYNLETT* 10, 1638–1639(2005). 17.

[125] HOSSEINI, S., H. Investigation of sensing effects of polystyrene-graft-polyaniline for cyanide. *Journal of Applied Polymer Science,* vol. 101, no. 6, p. 3920-3926. DOI: 10.1002/app.22874

[126] REMY H., *Lehrbuch der anorganischen Chemie*, *Band I.,* Leipzig: Akademische Verlagsgesellschaft Geest und Portig K. G. 1957, 862p.

[127] GOLDSMITH P. F., LANGER W. D., ELLDER J., IRVINE W., KOLLBERG E. *Astrophys. J*. 249, 524 (1981).

[128] NYMAN L. A., OLOFSSON H., JOHANSSON L. E. B., CARSTROM U. WOLSTENCROFT R. *Astron. Astrophys.* 1:269, 377 (1993).

[129] LELLOUCH E., ROMANI P. N., ROSENQVIST J. *Icarus* 108, 112 (1994).

[130] IRVINE W. M., SCHLOERG F. P. *Astrophys J*. 282, 516 (1984).

[131] SCHILKE P., WALMSLEY M. C., PINEAU DES FORESTS G., ROUELL E., FLOWER D. R., GUILLOTEAU S. *Astron. Astrophys*. 256, 595 (1992).

[132] WATSON W. D. *Rev. Mod. Phys*. 48, 513 (1976).

[133] TURNER B. E., PIROGOV L., MINH Y. C. *Astrophys. J.* 483, 235 (1997).

[134] ALLEN T. L., GODDARD J. D., SHAEFER H. F. *J. Chem. Phys.* 73:7, 3255 (1980).

[135] MILLIGAN D. E., JACOX M. E. *J. Chem. Phys.* 3:39, 712 (1963).

[136] SNYDER L. E., BHUL D. *Bull. Am. Astron. Soc*. 3, 388 (1971).

[137] BURGERS P. C., HOLMES J. L., MOMMERS A. A., TERLOUW J. K. *Chem. Phys. Lett*. 1:102, 1 (1983).

[138] BROWN R. D., BURDEN F. R., CUNO A. *Astrophys. J.* **347**, 855 (1989).

[139] HERBST E., TERZIEVA R., TALBI D. *Mon. Not R. Astron. Soc*. 311, 869 (2000).

[140] RODGERS S. D., CHARNLEY S. B. *Astrophys. J.* 501, L227 (1998).

[141] SUMATHI R., NGUYEN M. T. *J. Phys. Chem.* A 102, 8013 (1998).

[142] KAWAGUCHI K., HIROTA T., YAMAMOTO S., SAKAMOTO A., UKUTA N.: *Astrophys. J.* 520, 895 (1999).

[143] IRVINE W. M., DICKENS J. E., LOVERLL A. J., SCHLOERB P. F., SENAY M., BERGIN E. A., JEWITT D., MATTHEWS E. *Farad. Discuss.* 109, 475 (1998).

[144] FERUS M., KUBELÍK P., CIVIŠ S., GRIGOROVÁ E., ZELINGER Z., KAWAGUCHI K. In *Book of Abstracts of The 21st Colloquium on High Resolution Molecular Spectroscopy*. 2009. ISBN 978-88-904362-0-8.

[145] JACOBS A., WAHL M., WELLER R., WOLFRUM J. *Symp. Int. Combust. Proc.* 22, 449 (1989).

[146] BAULCH D.L., DUXBURY J., GRANT S.J., MONTAGUE D.C. *J. Phys. Chem. Ref. Data* 10, 1 (1981).

[147] HARUHIKO I, KAWAMURA Y. *Journal of Non-Crystaline Solids* 354, 3267 (2008).

[148] BATTYE, R., BATTYE, OVERCASH, C., FUDGE *Development and selection of ammonia emission factors*, Final Rep. prepared for U. S. Environ. Prot. Agency, Off. of Res. and Dev., EPA contract 68-D3-0034, Work Assignment 0-3, USEPA, Research Triangle Park, N. C., 1994.

[149] MÜLLEROVÁ M., BENEŠ P.: Informace o látkách zařazených do Integrovaného registru znečišťování. Vysoká škola chemicko-technologická v Praze, Ústav chemie ochrany prostředí. Zpracováno pro Ministerstvo životního prostředí. Praha, listopad 2005 *Integrovaný registr znečišťování* [online]. 2008 [cit. 2010-04-27]. Látka: Amoniak. Dostupné z WWW: <http://www.irz.cz/latky/amoniak>.

[150] *Environmental protection agency* [online]. 2009 [cit. 2010-04-27]. Ammonia. Dostupné z WWW: http://www.epa.gov/agriculture/ag101/impactammonia.html adapted from Livestock and Poultry Environmental Stewardship Curriculum.

[151] *Inchem* [online]. Ammonia safe and healthy guide. Geneva: World Health Organization for the International, 1990 [cit. 2010-04-27]. Dostupné z WWW: <http://www.inchem.org/documents/hsg/hsg/hsg037.htm>. ISBN 92-4-151037-4.

[152] MIKA O. J., et al. Vojenské zdravotnické listy: *Čpavková havárie v Bělehradě 1998 Případová studie* [online]. 2005 [cit. 2010-04-27]. Fakulta vojenského zdravotnictví UO v Hradci Králové. Dostupné z WWW: <http://www.pmfhk.cz/VZL/VZL%202_2005/4%20Mika-W.pdf>.

[153] MELENOVÁ L. et al. *Chem. Listy*, 97: 7, 562–568 (2003).

[154] NAVAROVÁ H. *Česká bioklimatologická společnost* [online]. [cit. 2010-04-27]. Různé metody zjišťování koncentrace amoniaku ve stájích. Dostupné z WWW: <www.cbks.cz/sbornikRackova03/sections/2/Navarov.pdf>.

[155] ANGELI G. Z., BOZOKI Z., MIKLOS A., LORINCZ A., THONY A., SIGRIST M. *Reviw of scientific instruments*, 62: 3, 810-813(1991)

[156] REPOND P., SIGRIST M. W. *Applied Optics*, 35: 21, 4065-4085(1996).

7. List of Figures

8. List of Tables

9. List of Own Publications

International Journals

Bailleux S., Walters A., **Grigorová E.**, Margulès L.. The Submillimeter-Wave Spectrum of the CS+ Radical Ion. *The Astrophysical Journal*. **679**:1, 920–924, (**2008**).

Zelinger Z., Střižík M., Kubát P., Civiš S., **Grigorová E.**, Janečková R., Zavila O., Nevrlý V., Herecová L., Bailleux S., Horká V., Ferus M., Skřínský J., Kozubková M., Drábková S., Jaňour Z. Dispersion of light and heavy pollutants in urban scale models:CO2 laser photoacoustic studies. *Applied spectroscopy*. **63**:4, 430–436, (**2009**).

Skřínský J., Janečková R., **Grigorová E.**, Střižík M., Kubát P., Herecová L., Nevrlý V., Zelinger Z., Civiš S. Allan variance for optimal signal averaging-monitoring by diode-laser and CO_2 photo-acoustic spectroscopy. *Journal of Molecular Spectroscopy.* **256:1**, 99–101, (**2009**).

Perrin A., Střižík M., Beckers H., Willner H., Zelinger Z., Pracna P., Nevrlý V., **Grigorová E.** First analysis of the high resolution FTIR spectrum of the ν_2 band of the FCO_2 radical at 970.2 cm^{-1}. *Molecular Physics*, 108:6, 723–731, **(2010)**

International Conferences

Zelinger, Z.; **Grigorová, E.**; Janečková, R.; Zavila, O.; Poulain, C.; Suau, A.; Kubát, P.; Střižík, M.; Danihelka, P. Application of spectroscopic methods for physical modelling of a light, heavy and reactive pollutant dispersion. In *Book of Abstracts of the 19th International Conference on High Resolution Molecular Spectroscopy*. Edit. by O. Bludský, P. Pracna and Š. Urban. Praha: ICT Press, **2006**, 188; ISBN 80–7080-612–5.

Skřínský J., Janečková R., **Grigorová E**., Střižík M., Kubát P., Herecová L., Nevrlý V., Zelinger Z., Civiš S. Allan variance for optimal signal averaging - stable and unstable molecules monitoring by diode-laser and co_2 laser photoacoustic spectroscopy.

In *Book of Abstracts of the 20th International Conference on High Molecular Spectroscopy*. O. Bludský, P. Pracna and S. Urban (Eds.). Praha: ICT Press, **2008**. ISBN 978–80-7080–*689-0.*

Střižík M., Perrin A., Beckers H., Nevrlý V., **Grigorová E**., Zelinger Z., Pracna P., Willner H. Analysis of the ν_2 band of the FCO_2 radical: preliminary results. In *Book of Abstracts of the 20th International Conference on High Molecular Spectroscopy. O. Bludský, P. Pracna and S. Urban (Eds.). Praha: ICT Press, **2008.*** ISBN 978–80-7080–689-0.

Bailleux S., **Grigorová E.**, Margulès L., Walters A. The submillimetre-wave laboratory spectrum of the CS^+ radical ion. In *Book of Abstracts of the 20th International Conference on High Molecular Spectroscopy. O. Bludský, P. Pracna and S. Urban (Eds.). Praha: ICT Press, **2008***. ISBN 978–80-7080–689-0.

Bailleux S., **Grigorová E**., Zelinger Z., Beckers H., Willner H. Analysis of the fourier-transform infrared spectrum of the ν_4 band of the fluoroformyloxyl radical, FCO_2, in the X^2B_2 state. In *Book of Abstracts of the 20th International Conference on High Molecular Spectroscopy. O. Bludský, P. Pracna and S. Urban (Eds.). Praha: ICT Press, **2008***. ISBN 978-80-7080-689-0.

Nevrlý V., Bitala P., Střižík M., Zelinger Z., Danihelka P., Kollárik T., **Grigorová E.**, Jánošík L., Jelínková R., Mikoczy A., Filipi B., Dudáček A. Infrared Imaging of Uninhibited Cup-Burner Flame. In Book of Abstract: 4th European Combustion Meeting. Vienna/Austria: Verlag ProcessEng Engineering GmbH, 2009. Infrared Imaging of Uninhibited Cup-Burner Flame. Poster session, PS19. s. 317. ISBN 978–3-902655–06-6. *Book of Abstracts of the ECM 2009 FOURTH EUROPEAN COMBUSTION MEETING, 14* (**2009**). Vienna University of Technology, Vienna, Austria.

Ferus M., Kubelík P., Civiš S., **Grigorová E.**, Zelinger Z., Kawaguchi K. Formation and decay of HCN/HNC in a positive column discharge. *Book of Abstracts of*

The 21st Colloquium on High Resolution Molecular Spectroscopy, Castellammare di Stabia, Italy, **2009**. ISBN 978-88-904362-0-8.

Skřínský J., Janečková R., **Grigorová E.**, Zelinger Z.,Střižík M., Kania P., Bailleux S., Wlodarczak G. Detection of gas-phase stable and unstable species in the context of environmental impacts of increasing industrialization. In 3rd International Conference SECURE SLOVAKIA and EU. 12-13. 11. **2009**, Slovakia..

Other Publications

Grigorová E., Zelinger Z.,Střižík M., Bailleux S., Wlodarczak G., Bitala P., Nevrlý V. Využití mikrovlnné spektroskopie při studiu reaktivních látek; *Sborník vědeckých prací Vysoké školy báňské - Technické univerzity Ostrava* (**2009**), 1:4., 27-32. ISSN: 1801-1764.

10. Copies of Publications Related to PhD work

Dispersion of Light and Heavy Pollutants in Urban Scale Models: CO_2 Laser Photoacoustic Studies

Z. ZELINGER,* M. STŘIŽÍK, P. KUBÁT, S. CIVIŠ, E. GRIGOROVÁ, R. JANEČKOVÁ, O. ZAVILA, V. NEVRLÝ, L. HERECOVÁ, S. BAILLEUX, V. HORKÁ, M. FERUS, J. SKŘÍNSKÝ, M. KOZUBKOVÁ, S. DRÁBKOVÁ, and Z. JAŇOUR

J. Heyrovský Institute of Physical Chemistry, v.v.i., Academy of Sciences of the Czech Republic, Dolejškova 3, CZ-182 23 Prague 8, Czech Republic (Z.Z., P.K., S.C., E.G., R.J., V.H., M.F., J.S.); VŠB–Technical University of Ostrava, Faculty of Safety Engineering, Lumírova 13, CZ-700 30 Ostrava 3–Výškovice, Czech Republic (M.S., E.G., R.J., O.Z., V.N., L.H., J.S.); Laboratoire de Physique des Lasers, Atomes et Molécules, CERLA, UMR CNRS 8523, Université de Lille 1, F-59655 Villeneuve d'Ascq Cedex, France (S.B.); ETH Zurich, Laboratorium für Physikalische Chemie, Wolfgang-Pauli-Str. 10, CH-8093 Zürich, Switzerland (V.H.); VŠB – Technical University of Ostrava, Faculty of Mechanical Engineering, 17.listopadu 15, CZ-708 33 Ostrava – Poruba, Czech Republic (M.K., S.D.); and Institute of Thermomechanics, v.v.i., Academy of Sciences of the Czech Republic, Dolejškova 5, CZ-182 23 Prague 8, Czech Republic (M.S., V.N., Z.J.)

The distribution of pollutants in two urban scale models (point emission source and street canyon with extensive transport) was investigated by means of CO_2 laser photoacoustic spectroscopy in the region of the atmospheric window (9–10 μm). The experimental results of physical modeling are in a good agreement with the numerical calculations performed in the frame of computational fluid dynamic (CFD) modeling. Methanol, ethanol, and ozone (examples of light pollutants), as well as sulfur hexafluoride and 1,2 dichlorethane (examples of heavy pollutants), were selected on the basis of their high resolution spectra acquired by Fourier transform and laser diode spectroscopy.

Index Headings: **Air pollution; CO_2 laser photoacoustic spectroscopy; PAS; Laser diode spectroscopy; Fourier transform spectroscopy; Wind tunnel; Physical modeling; Computational fluid dynamics; CFD modeling.**

INTRODUCTION

Laser spectroscopic techniques are powerful tools for the investigation of air pollution.[1] Selective, sensitive, and nondestructive laser-based analytical methods have been steadily more employed to monitor trace amounts of gases present in the atmosphere.[2–5] Elevated concentration levels of both primary and secondary atmospheric pollutants mainly occur in the lower parts of the troposphere, the region where relevant physical-chemical processes are also directly influenced by the presence of earth's surface. This part of the troposphere is known as the atmospheric boundary layer.[6] Currently, information on phenomena related to the dispersion of air pollution[7,8] within the atmospheric boundary layer can be assessed only by two basic approaches.

Monitoring the motion of pollutants in a realistic atmosphere is mostly complicated and expensive, often providing incomplete results limited only to particular places. Mathematical models employing numerical calculations or methods based on physical modeling[9–11] are usually applied to overcome such lack of measurements in the realistic atmosphere. To validate the numerical models,[12–15] wind tunnel experiments are also strongly recommended. Due to their selectivity, sensitivity, and ability for on-line detection, infrared laser spectroscopic techniques are good candidates for analytical tools for physical modeling of processes taking place in the atmospheric boundary layer. One of the useful tasks supporting physical modeling is to investigate the dispersion of inert atmospheric tracers. Such tracers can be used to establish flow fields in the simulated boundary layer. The tracers to select must follow physical properties appropriate for the measurements in the wind tunnel (e.g., density of pollutants), and they should be detected by a suitable fast detection technique.[16] Simulating pollutant behavior differing by masses[17] and the chemical behavior of these pollutants[18–21] represent crucial tasks in the field of the physical modeling of air pollution dispersion.[22] In this paper, we focus mainly on studying the behavior of pollutants of different masses. In addition, we also marginally deal with the chemical behavior of the model atmospheric pollutants, with ozone serving as a model of a reactive pollutant. In view of the current approaches applied in the field of physical simulations of the atmospheric boundary layer processes, our contribution represents the first modeling study of simultaneous dispersion of light and heavy pollutants.

Monitoring trace concentration levels of atmospheric pollutants is readily carried out by absorption spectroscopy within the atmospheric window where the absorption of both H_2O and CO_2 molecules is negligible.[23] Pollutants such as ethanol, methanol, sulfur hexafluoride, 1,2-dichloroethane, and ozone that have their absorption bands within the atmospheric window (round 9–10 μm) can be monitored at their rotation-vibration bands. The molecular masses of these model pollutants span the range of two and a half orders of magnitude. To determine the reactivity of the selected model pollutants is not easy; however, ozone is a well known oxidant the reactivity of which is at least one order of magnitude higher compared to that of other model pollutants. Their absorption lines overlap fairly well with the emission spectrum of the CO_2 laser. Employing the Fourier transform infrared (FT-IR) spectrometer and a laser diode system, we have recorded the infrared absorption spectra of the above-mentioned model pollutants to find the most convenient absorption lines (analytically) before applying them to physical modeling using the CO_2 laser photoacoustic spectrometry (PAS) method. The concept of PAS detection was demonstrated to be a sensitive and suitable method for measurement of concentration profiles of pollutants in wind tunnels[4,24] (CO_2 laser as a single radiation source, time resolution 1 s). When combined with the CO_2 laser it allows measurements to be performed within a linear dynamic range up to six orders of magnitude wide.[25]

In this paper we present results of spectroscopic measurements of light (ethanol, methanol, and ozone) and heavy (sulfur hexafluoride and 1,2-dichlorethane) pollutants. This study was

Received 7 August 2008; accepted 7 January 2009.
* Author to whom correspondence should be sent. E-mail: zelinger@jh-inst.cas.cz.

0003-7028/09/6304-0430$2.00/0

aimed at the development of a step-by-step methodology employing spectroscopic techniques in physical modeling. The methodology is well-demonstrated on the two urban scale systems—a point emission source and a street canyon. Furthermore, the comprehensive study is extended by comparing the data with the results of computational fluid dynamics (CFD) modeling in the case of the point emission source.

EXPERIMENTAL

The following model pollutants were used: methanol (company: Lach-Ner s.r.o, Czech Republic; purity: p.a. 99.5%), ethanol (company: Lach-Ner, s.r.o.; purity: 99.8%), SF_6 (company: Messer; purity: 99.9%), 1,2-dichlorethane (company: LACHEMA Czech Republic; purity: p.a.), and ozone (home-made production based on the use of Hg lamp ozonolyzer; concentration of ozone was calculated from absorption coefficient[26]).

The high-resolution Fourier transform infrared spectrometer Bruker IFS 120FT-IR makes use of a cell with a 20 cm path length and the resolution is 0.0035 cm^{-1}. The spectrometer is equipped with a Globar light source and a HgCdTe detector provided with the KBr beam splitter. Experimental details of the FT spectrometer used are shown in Ref. 27. An extensive description of the diode laser spectrometer employed was presented previously.[28,29] The diode laser (Laser Components GmbH) was placed in a laser head cooled by the He cryostat. The laser was temperature and current controlled using Laser Photonics units, model L5731, at a temperature of 30–70 K and a current of 30–500 mA. A lens focuses the laser beam into a (Czerny–Turner) monochromator to separate single laser modes from the spectrum. The radiation leaving the monochromator was directed either into a reference cell, a Ge etalon (0.04 cm^{-1}), or into an absorption cell loaded with the gas being studied. The absorption spectrum was recorded with a photoconductor HgCdTe detector operated at liquid nitrogen temperature. The signal from the detector was fed into a digital oscilloscope (Le Croy 9361). The spectra were measured using the current (saw-tooth) modulation of the laser.

Spectroscopic experiments aimed at the application of CO_2 laser photoacoustic spectrometry to physical modeling were performed within a low speed, straight open wind tunnel (constant 1.5 m × 1.5 m cross-section, length of 20.5 m, a working section 2 m long). The 30 kW ventilator with a thyristor speed regulator was used to simulate the atmospheric boundary layer with a reference speed ranging from 1 to 12 $m \cdot s^{-1}$. Details of the whole experiment are described in our previous works.[24,30,31] The boundary layer quantities on the inlet of the working section corresponded to those of the neutrally stratified rural atmospheric boundary layer. Atmospheric samples contaminated with the model pollutant were continuously taken at individual, precisely defined places (either the urban scale street canyon model or the model of a point emission source). A movable teflon tube connected through the photoacoustic cell with a pump was used for continuous sampling of the atmosphere at defined places. Samples of the atmosphere were taken with the probe with a rate ranging from 3 to 4 $cm^3\ s^{-1}$, which are negligible volumes considering the dynamics of the given wind tunnel. The photoacoustic cell was a thermally stabilized brass tube with a length of 38 cm and diameter of 8 mm. Detection was performed on longitudinal acoustical resonance (modulation frequency 1.2 kHz, the phase is set on the maximum of the photoacoustic signal).

A set of silicone and/or polyethylene tubes sealed on both ends with steel balls and filled with the investigated model pollutant served as well-defined permeation standards to calibrate the equipment as well as for the analysis itself.[32] We also extended our dispersion studies using an auxiliary model pollutant, ethane, to allow better comparison, interpretation, and understanding of processes. In physical modeling ethane is often used as a reference gaseous pollutant due to its density (similar to that of air). Concentration levels of ethane were measured by a customary flame ionization detector (Rosemount Analytical NGA 2000-TFID). The emission of the model pollutants was assured by the permeation method[33,34] or by the method of gas mixing and gas flow controlling with a mass flow controller and/or by the combination of both these methods.

NUMERICAL METHODS

Numerical models have begun to play an important and often dominant role in environmental assessment. When studying the dispersion of atmospheric pollutants emitted into the atmospheric boundary layer by the ground emission sources (located especially in urban, rural, or industrial areas), a turbulent model,[6,35,36] based on the solution of three-dimensional, time-dependent conservation equations (ideal gas law, continuity equation, Navier–Stokes equation, convection-diffusion equation, energy equation written for static enthalpy), is usually preferred over a model representing an application of the statistical theory of turbulent diffusion (commonly used Gaussian plume model). In particular the micro- and small-scale dynamical modeling employs the so-called Reynolds Average Method (RAM models) based on time-averaged quantities of turbulent flow and on Reynolds averaging the Navier–Stokes equations.[36,37] The standard k-ε (kinetic turbulent energy – dissipation) model, a member of the RAM model family, currently represents the most promising tool when investigating turbulent effects on the pollutant dispersion within the atmospheric boundary layer. Employing the k-ε model,[37] besides the above-mentioned conservation equations it is necessary to introduce transport equations for the turbulent kinetic energy and the dissipation rate. The transport equation for the kinetic turbulent energy is

$$\frac{\partial}{\partial t}(\rho k) + \frac{\partial}{\partial x_j}(\rho \bar{u}_j k) = \frac{\partial}{\partial x_j}\frac{\mu_t}{\sigma_k}\frac{\partial k}{\partial x_j} + \underbrace{\mu_t\left(\frac{\partial \bar{u}_k}{\partial x_j} + \frac{\partial \bar{u}_j}{\partial x_k}\right)\frac{\partial \bar{u}_k}{\partial x_j}}_{\text{P-shear production}} \underbrace{-g_j\frac{\mu_t}{\rho\sigma_k}\frac{\partial \rho}{\partial x_j}}_{\text{G-production due to buoyancy}} - \rho\varepsilon \quad (1)$$

and the transport equation for the dissipation rate ε is

$$\frac{\partial}{\partial t}(\rho\varepsilon) + \frac{\partial}{\partial x_j}(\rho \bar{u}_j \varepsilon) = \frac{\partial}{\partial x_j}\frac{\mu_t}{\sigma_\varepsilon}\frac{\partial \varepsilon}{\partial x_j} + C_{1\varepsilon}\frac{\varepsilon}{k}[P + (1 - C_{3\varepsilon})G] - C_{2\varepsilon}\rho\frac{\varepsilon^2}{k} \quad (2)$$

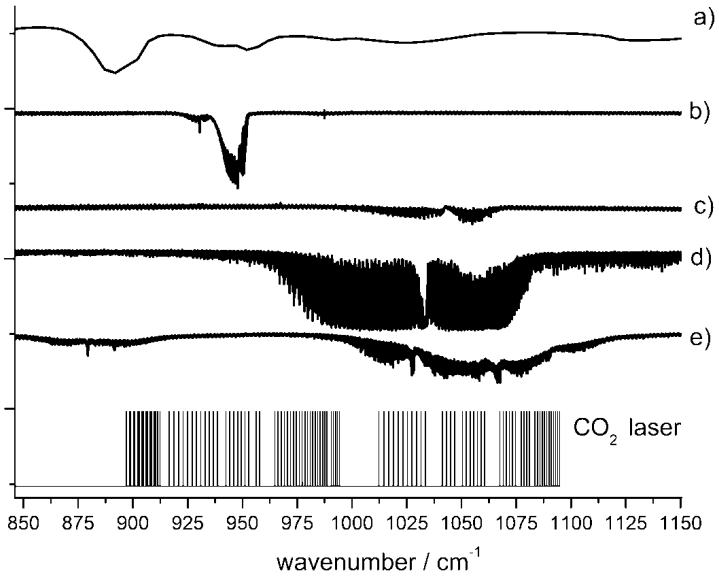

FIG. 1. Absorption spectra in the 850 to 1150 cm^{-1} range of (*a*) dichlorethane, 10 Torr, 0.1 cm^{-1}, 50 scans; (*b*) sulfur hexafluoride, 0.4 Torr, 0.01 cm^{-1}, 100 scans; (*c*) ozone, 20 Torr, 0.01 cm^{-1}, 100 scans; (*d*) methanol, 8.9 Torr, 0.01 cm^{-1}, 50 scans; and (*e*) ethanol 5 Torr, 0.01 cm^{-1}, 50 scans measured by the FT-IR spectrometer. The emission lines of the CO_2 laser are also shown.

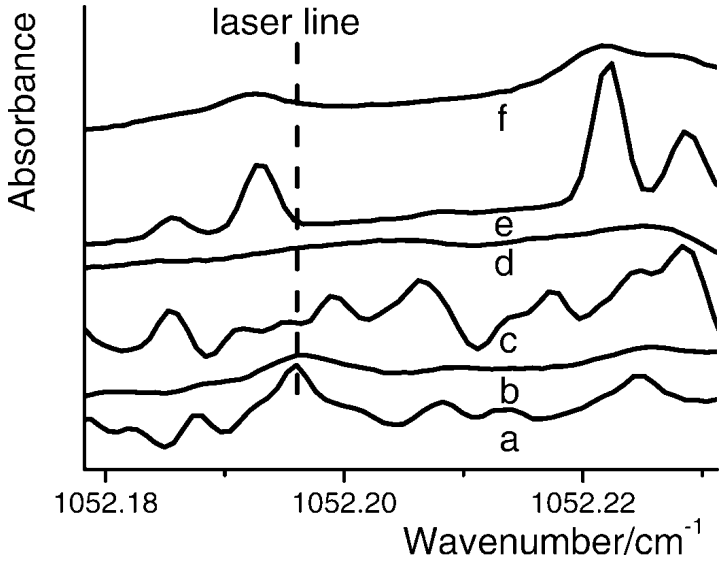

FIG. 2. High resolution absorption spectra of gaseous pollutants recorded by the diode laser spectrometer at different pressures: (*a*) ethanol (231 kPa), (*b*) mixture of ethanol (231 kPa) and air (total pressure 1760 kPa), (*c*) SF_6 (24.9 kPa), (*d*) mixture of SF_6 (24.9 kPa) and air (total pressure 403.8 kPa), (*e*) ozone (5.7 kPa), and (*f*) mixture of ozone (5.7 kPa) and air (total pressure 412 kPa). The spectra are offset; the dashed line denotes the 9P(14) emission line of the CO_2 laser (1052.1956 cm^{-1}).

P and *G* occurring in Eqs. 1 and 2 written for *k* and ε denote the shear and buoyancy production of turbulent kinetic energy (TKE), and $C_{1\varepsilon}$, $C_{2\varepsilon}$, and $C_{3\varepsilon}$ are empirical constants. The ratio *G*/*P* is closely related to the stability of the atmospheric boundary layer. In the convective boundary layer, the positive buoyancy contributes to the production of TKE. On the contrary, TKE is consumed under statically stable conditions. If the buoyancy term is around zero, then the boundary layer is said to be neutral. While the constants $C_{1\varepsilon}$ and $C_{2\varepsilon}$ are defined (e.g., by Launder and Spalding[38]), the value of $C_{3\varepsilon}$ depends on the buoyancy term *G*, which can be either positive or negative, and thus has to be adapted following the modeled atmospheric stratification. σ_k, and σ_ε in the equations denote the turbulent Prandtl number [-] for *k* and ε.

The standard k-ε model was developed and integrated in the customary FLUENT™ 6.2 computational fluid dynamics environment.[37] The investigated model of the point source was studied by mathematical modeling, by applying the finite-volume method. For the FLUENT™ 6.2 k-ε dynamic turbulent model used, the physical conditions (i.e., the definition of emission source and meteorological conditions) corresponded to those of the experiment performed within the simulated atmospheric boundary layer in the wind tunnel. The measuring section of the aerodynamic tunnel has a cubic shape with dimensions of 2 m (length), 1.5 m (height), and 1.5 (width). The Gambit™ 2.1.6. preprocessor was employed to prepare a three-dimensional (3D) computational grid consisting of 337 500 cells. The geometry of the aerodynamic tunnel was meshed in three basic steps. In the first step, all edges were meshed constantly. Considering the investigated problem, the mesh on edges were compressed into the middle section of the geometry moderately (with respect to the position of the pollutant source). In the second step all surfaces were meshed. Two-dimensional cells were created using the predefined scheme QUAD (elements: Quad; type: Map). Finally the volume was meshed as well. Three-dimensional cells were created using the predefined scheme HEX (elements: Hex; type: Map). The final mesh was tested using the internal Gambit™ 2.1.6. procedure and was shown to be of the best quality.

RESULTS AND DISCUSSION

Spectroscopic Measurements. Absorption spectra of model pollutants were studied by FT-IR and diode laser infrared spectroscopy covering a spectral region round 10 μm that accommodates the emission bands of the CO_2 laser. High resolution absorption spectra of molecules measured by the Bruker IFS 120 FT-IR spectrometer (maximum resolution 0.0035 cm^{-1}), with emission lines of the CO_2 laser, are depicted in Fig. 1. From Fig. 1 it is evident that all mentioned molecules are likely candidates for monitoring in the region of the CO_2 laser. High resolution absorption spectra of gaseous ethanol, ozone (models of "small" pollutant), sulfur hexafluoride (example of a heavy pollutant), and their mixtures with air at different pressures are shown in Fig. 2. The widths of individual spectral lines of pure pollutants (Figs. 2a, 2c, and 2e) are influenced by pressure broadening so that the Doppler width of the lines becomes distinguishable only at pressures below 0.5 kPa. The pressure broadening caused by cumulative increments of air in the mixture leads to a large distortion of the line shapes resulting in decreased absorption coefficients (Figs. 2b, 2d, and 2f).

Several emission lines belonging to the 9P branch emission band of the CO_2 laser could interfere with the absorption lines of model pollutants. The information about line shapes is available from quantitative databases containing the vapor-phase infrared spectra[39] and from molecular absorption databases.[40] For instance, the 9P(14) emission CO_2 laser line coincides with the absorption lines of ozone (Fig. 2e) and hence seems to be an optimal candidate for ozone monitoring.[26,41,42,43] The frequency of this laser emission line, however, does not match those of absorption lines of sulfur hexafluoride[44,45] and ethanol at low pressure (Figs. 2a and 2c). Although the CO_2 laser line sometimes overlaps only with the wings of absorption bands broadened under higher pressure

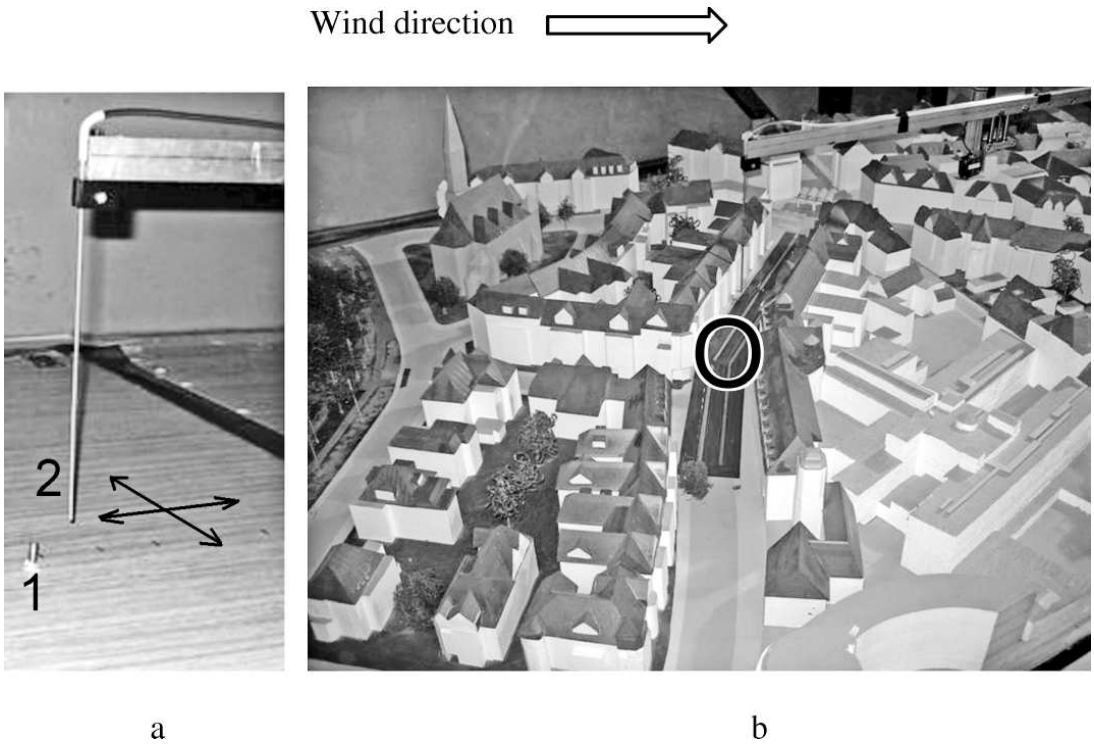

FIG. 3. (**a**) Model of the chimney (1) and the moveable sampling probe (2); (**b**) Urban scale model of the Podbielski street (a part of the Hannover agglomeration at a scale of 1:200), the investigated section is circled.

(Figs. 2b and 2d), the results obtained demonstrate clearly that the sensitivity and the broad linear dynamic range of the CO_2 laser photoacoustic technique used here is sufficient for applying this method for monitoring low concentration levels of the model gaseous pollutants in question.

Monitoring the atmosphere surrounding the models placed in the wind tunnel was ensured by using the CO_2 laser photoacoustic gas analyzer tuned to the CO_2 laser emission lines that were preselected on the basis of the Fourier transform infrared and diode laser infrared spectroscopic study described.

Point Emission Source. The model chimney used as a point emission source was 20 mm high and its inner diameter was 6 mm. The model was placed within the working section of the wind tunnel (Fig. 3a). A spatially adjustable sampling probe introduced into the wind tunnel was employed to continuously sample the atmosphere at precisely defined places. Each point was measured five times by 200 s scans. We estimate the level of reproducibility to be 10–15% for the whole experiment.

Figure 4a compares the experimental data of measurements carried out at individual sampling points with the numerical calculations for a light pollutant (methanol). The highest concentration was found near the point emission source; furthermore, the concentration depends strongly on the vertical position of the sampling sites. There is a balance between the

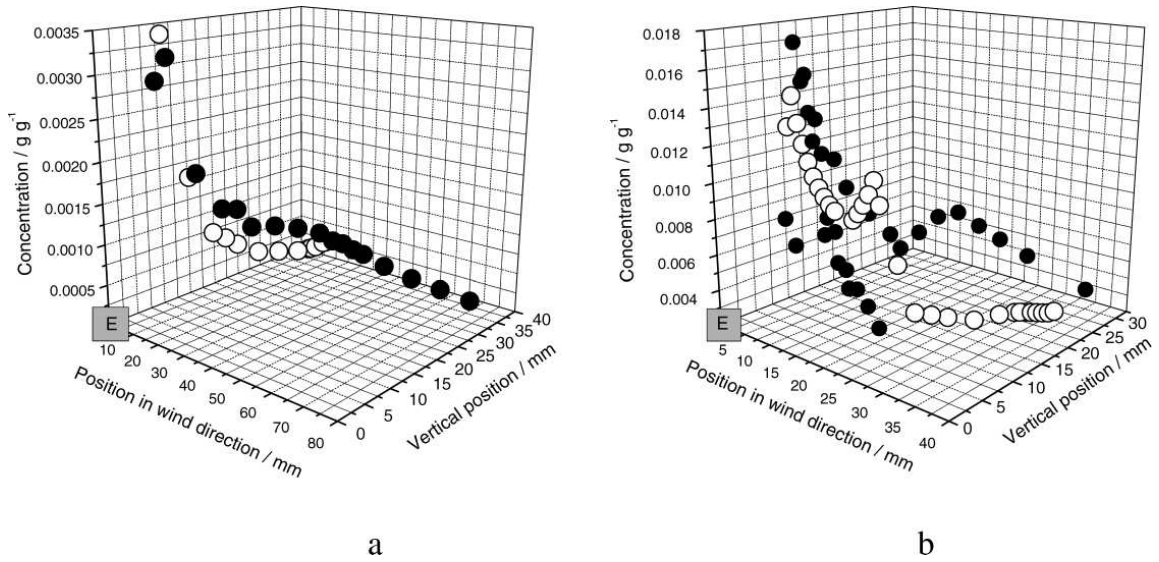

FIG. 4. Comparison of the measured (●) and calculated (○) concentrations in a 3D view for (**a**) methanol (light pollutant) and (**b**) 1,2-dichlorethane (heavy pollutant). Sampling sites are in the direction of the wind (along the axis of the wind tunnel); the vertical position is measured relative to the bottom of the wind tunnel; the position (0, 0) denotes the location of the emission source E.

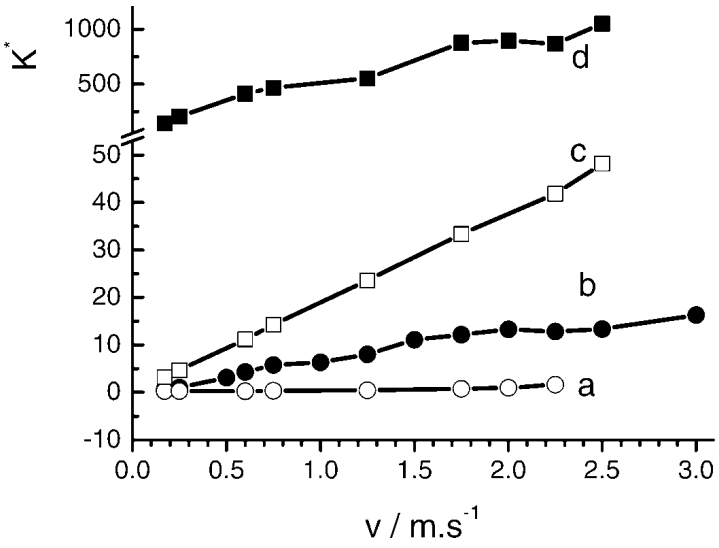

FIG. 5. Urban scale model: the dependencies of the dimensionless mean concentration K^* (calculated from Eq. 3) on the reference wind speed in the wind tunnel for (*a*) ethanol, (*b*) ethane, (*c*) ozone, and (*d*) sulfur hexafluoride.

observed and the calculated concentrations: the concentration level tends to zero as the vertical position increases.

The sampling sites were chosen to follow the main stream of a plume generated by the point emission source. For the heavy pollutant (1,2-dichlorethane) the scheme of sampling points was changed due to entirely different physical behavior of the latter gas. The results of experimental measurements and numerical modeling corresponding to those sampling points are depicted in the Fig. 4b. Studies on the pollutant dispersion[46] show a similar outcome in the case of a heavy pollutant. Heavy pollutants in particular are expected to disperse in the atmosphere similar to the larger-sized particles; however, they are greatly affected by gravity and thus have a shorter residence time in the atmosphere.[47]

In both cases the agreement between experiment and calculation is very good. Two main differences between the light and the heavy pollutant were observed: (1) for the heavy pollutant the zero concentration level was achieved at a shorter distance in the wind direction (approximately half of the magnitude) as compared to the light pollutant, and (2) the higher concentration levels were also found at sampling sites at small vertical positions up to a relatively higher position in the wind direction.

Urban Street Canyon. The other, much more complex, urban scale model was that of a street canyon: a model of the Podbielski street, a part of Hannover agglomeration, at a scale of 1:200 (Fig. 3b).

Vehicles slowly moving in the street in both directions were simulated by two line sources emitting continuously studied pollutant. The mentioned line source is a line consisting of 3750 parallel needle nozzles (2 cm long, inner diameter of 0.1 mm). The small diameter of the needle nozzles causes large hydrodynamic resistance.

To allow an inter-comparison of all results collected for light and heavy model pollutants, absolute concentration values (depending on emission fluxes) were converted into dimensionless ones, also reflecting the geometry of the model used. Measured concentration, C [g·cm^{-3}] was converted into dimensionless concentration, K, using the height H [cm] of buildings, the transverse length L [cm] of the street, the reference wind speed U [cm·s^{-1}] outside the street canyon, and the concentration flux of the pollutant line source Q [g·s^{-1}],

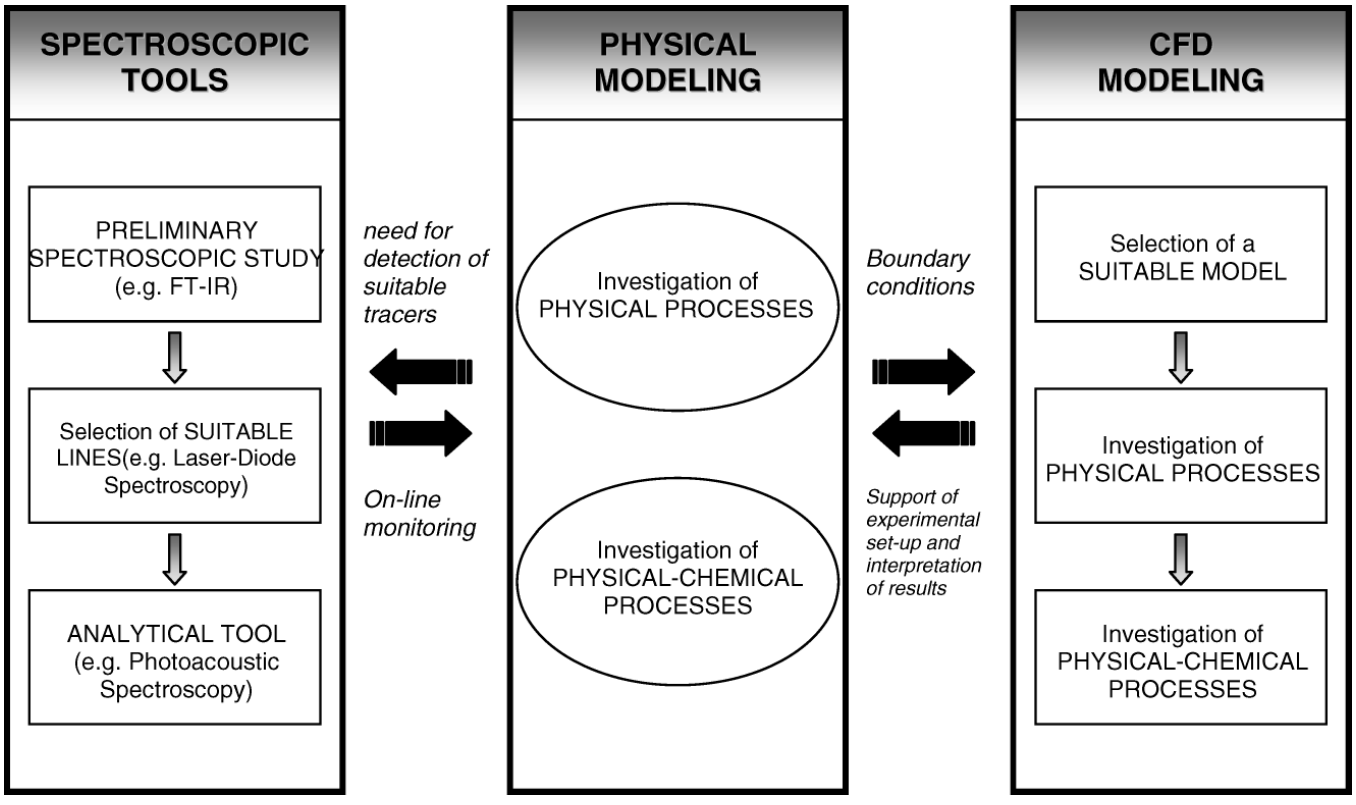

FIG. 6. Methodology combining spectroscopic methods and modeling facilities allows investigation of the dispersion of air pollutant within the atmospheric boundary layer.

according to the formula

$$K = \frac{CHUL}{Q} \quad (3)$$

The difference between the light (ethanol, ethane, and ozone) and heavy (sulfur hexafluoride) pollutants can be observed in Fig. 5. As seen in Eq. 3 the dimensionless concentration K is proportional to the reference wind speed. However, the slope of this dependence is apparently larger for the heavy pollutants than it is for light and reactive pollutants. Therefore, one prefers mass dependence rather than reactivity dependence. Data of independent dispersion studies[16,17] agree with our results in the case of heavy pollutants.

The results for ozone (which are of importance for atmospheric processes) are similar to those obtained for other light pollutants (see Fig. 5). Ozone itself is not of such reactivity in the absence of reactant; it belongs to a group of moderately long living species with temporal scale ranging from a few days to one year.[48] Such similarity for all relatively stable chemical species is important for epidemiological studies, in particular when assessing exposure of population to the air pollution.[49] Differences in ozone behavior for urban air pollution within the formation of photochemical pollutants are discussed elsewhere.[18,19]

CONCLUSION

The selected molecular models of gaseous atmospheric pollutants were studied by methods based on absorption spectroscopy. These methods were used to extend the techniques employed so far to model processes taking place in the atmospheric boundary layer. They enable the investigation of simultaneous dispersion of model atmospheric pollutants differing by their masses, as was well demonstrated in our study dealing with model light (methanol, ethanol), heavy (sulfur hexafluoride, 1,2-dichlorethane), and reactive (ozone) pollutants.

Consequently, CO_2 laser photoacoustic spectroscopy was applied as the main analytical tool in physical modeling the dispersion of pollutants within urban scale models. The main difference was found between the light and heavy pollutants. The drawbacks of the present system are its relatively large complexity.

Combining the spectroscopic approaches and modeling facilities (Fig. 6) for investigation of pollutant dispersion offers great possibilities for further development. On one hand it makes physical modeling easier, while being more comprehensive on the other hand (as it enables investigation of chemical reactions in a simulated atmospheric boundary layer).

ACKNOWLEDGMENTS

The authors gratefully acknowledge the financial support from the Ministry of Education, Youth and Sports of the Czech Republic provided via grants OC111, OC186 (within the frame of the EU COST 729 Action) and the Research program LC06071. A part of the research was also supported by the Czech Science Foundation (grant no. 202/06/0216) and by the Ministry of the Environment of the Czech Republic (VaV project no. SPII 1a10 45/07). The experiments were carried out within the frame of the European Community Research Infrastructure Action under the FP6 Structuring the European Research Area Programme, EUSAAR Contract N RII3-CT-2006-026140.

1. M. W. Sigrist, "Air Monitoring, Optical Spectroscopic Methods", in *Encyclopedia of Environmental Analysis and Remediation*, R. A. Meyers, Ed. (Wiley, New York, 1998), p. 84.
2. A. Wiacek, J. R. Taylor, K. Strong, R. Saari, T. E. Kerzenmacher, N. B. Jones, and D. W. T. Griffith, J. Atmos. Ocean. Technol. **24,** 432 (2007).
3. N. Glatthor, T. von Clarmann, H. Fischer, B. Funke, S. Gil-Lopez, U. Grabowski, M. Hopfner, S. Kellmann, A. Linden, M. Lopez-Puertas, G. M. Tsidu, M. Milz, T. Steck, G. P. Stiller, and D. Y. Wang, Atmos. Chem. Phys. **6,** 2767 (2006).
4. Z. Zelinger, M. Střižík, P. Kubát, Z. Jaňour, P. Berger, A. Černý, and P. Engst, Opt. Lasers Eng. **42,** 403 (2004).
5. Z. Zelinger, B. Barret, P. Kubát, P. Ricaud, J.-L. Attie, E. LeFlochmoen, J. Urban, D. Mutargh, and M. Střižík, Mol. Phys. **104,** 2815 (2006).
6. R. B. Stull, *An Introduction to Boundary Layer Meteorology* (Kluwer Academic Publishers, Dordrecht, 1994).
7. M. Schatzmann, B. Leitl, and J. Liedtke, Environ. Monitor. Assess. **65,** 249 (2000).
8. S. Vardoulakis, B. E. A. Fischer, K. Percleous, and N. Gonzalez-Flesca, Atmos. Environ. **37,** 155 (2003).
9. A. P. G. Sagrado, J. van Beeck, P. Rambaud, and D. Olivari, J. Wind Eng. Indust. Aerodynam. **90,** 321 (2002).
10. Z. Zelinger, M. Střižík, P. Kubát, K. Lang, K. Bezpalcová, and Z. Jaňour, Intern. J. Environ. Anal. Chem. **86,** 889 (2006).
11. S. Civiš, Z. Zelinger, M. Střižík, and Z. Jaňour, "Simulation of Air Pollution in a Wind Tunnel", in *Spectroscopy from Space*, J. Demaison, Ed. (Kluwer Academic, Dordrecht, 2001), p. 275.
12. S. Di Sabatino, R. Buccolieri, B. Pulvirenti, and R. Britter, Atmos. Environ. **41,** 8316 (2007).
13. F. I. Khan and S. A. Abbasi, J. Hazardous Mater. **80,** 15 (2000).
14. M. T. Boehm and D. E. Pylor, Atmos. Environ. **39,** 4841 (2005).
15. J. Pospíšil, J. Katolicky, and M. Jicha, Sci. Total Environ. **334,** 185Sp. Iss. SI (2004).
16. J. E. Cermak, A. G. Davenport, E. J. Plate, and D. X. Virgas, Eds., *Wind Climate in Cities*, NATO ASI Series E: Applied Science (Kluwer Academic Publisher, Dordrecht, 1995), vol. 277.
17. G. Ooms and H. Tennekes, Eds., *Atmospheric Dispersion of Heavy Gates and Small Particles*, International Union of Theoretical and Applied Mechanics, Symposium, Delft, The Netherlands (Springer-Verlag, Berlin, 1984).
18. S. Sillman, Atmos. Environ. **33,** 1821 (1999).
19. M. E. Jenkin and K. C. Clemitshaw, Atmos. Environ. **34,** 2499 (2000).
20. P. Tulet, V. Crassier, and R. Rosset, Environ. Model. Software **15,** 693 (2000).
21. Z. Zelinger, P. Kubát, M. Střižík, P. Danihelka, K. Bezpalcová, Z. Jaňour, S. Drábková, M. Kozubková, P. Berger, A. Černý, and P. Engst, "Urban air pollution and its photochemistry studied by laser spectroscopic methods", in *Remote Sensing of the Atmosphere for Environmental Security*, A. Perrin, N. Ben Sari-Zizi, and J. Demaison, Eds., NATO Security Through Science Series – C: Environmental Security (Springer, Dordrecht, 2006), p. 301.
22. S. Civiš, M. Střižík, Z. Jaňour, J. Holpuch, and Z. Zelinger, J. AOAC Int. **85,** 243 (2002).
23. M. W. Sigrist, "Air Monitoring by Laser Photoacoustic Spectroscopy", in *Air Monitoring by Spectroscopic Techniques*, M. W. Sigrist, Ed., Chemical Analysis Series (Wiley, New York, 1994), vol. 127, p. 163.
24. Z. Zelinger, S. Civiš, and Z. Jaňour, Analyst (Cambridge, U.K.) **124,** 1205 (1999).
25. M. W. Sigrist, "Air Monitoring by Laser Photoacoustic Spectroscopy", in *Air Monitoring by Spectroscopic Techniques*, M. W. Sigrist, Ed., Chemical Analysis Series (Wiley, New York, 1994), vol. 127, p. 163.
26. J. Codnia and M. L. Azcarate, Opt. Lasers Eng. **39,** 619 (2003).
27. S. Civiš, T. Šedivcová-Uhlíková, P. Kubelík, and K. Kawaguchi, J. Mol. Spectrosc. **250,** 20 (2008).
28. Z. Zelinger, S. Civiš, P. Kubát, and P. Engst, Infrared Phys. Technol. **36,** 537 (1995).
29. Z. Zelinger, P. Kubát, and J. Wild, Chem. Phys. Lett. **368,** 532 (2003).
30. Z. Zelinger, I. Jančík, and P. Engst, Appl. Opt. **31,** 6974 (1992).
31. Z. Zelinger, M. Střižík, P. Kubát, and S. Civiš, Anal. Chim. Acta **422,** 179 (2000).
32. Z. Zelinger, P. Engst, Z. Papoušková, and M. Jakoubková, "Trace Analysis of Freons by Optoacoustic CO_2 Laser Detection", in *Photoacoustic and Photothermal Phenomena*, P. Hess and J. Pelzl, Eds., Springer Ser. Opt. Sci. (Springer-Verlag, Berlin, Heidelberg, 1988), vol. 58, p. 131.
33. Z. Zelinger, Z. Papoušková, M. Jakoubková, and P. Engst, Coll. Czech. Chem. Commun. **53,** 749 (1988).
34. V. Steiner, P. Engst, Z. Zelinger, and M. Horák, Coll. Czech. Chem. Commun. **54,** 2667 (1989).
35. F. T. M. Nieuwstadt, J. G. M. Eggels, R. J. A. Janssen, and M. B. J. M. Pourquié, "Direct and Large-Eddy Simulations of Turbulence in Fluids",

in *Future Generation Computer System* (Elsevier Science Publishers B. V., New York, 1994), vol. 10, Issues 2–3, pp. 189–205.
36. S. Drábková and P. Platoš, "Numerical Simulation as a Tool for the Solution and Understanding of Practical Air Pollution Probléme", in Proc. of the Conference on Modelling Fluid Flow (CMFF'03) (Budapest, Budapest University of Technology and Economics, 2003), pp. 501–506.
37. Fluent Inc., Fluent 6.2, available from http://sp1.vsb.cz/DOC/Fluent_6.1/html/ug/main_pre.htm.
38. B. E. Launder and D. B. Spalding, *Mathematical Models of Turbulence* (Academic Press, London, 1979).
39. S. W. Sharpe, T. J. Johnson, R. L. Sams, P. M. Chu, G. C. Rhoderick, and P. A. Johnson, Appl. Spectrosc. **58,** 1452 (2004).
40. L. S. Rothman, R. R. Gamache, R. H. Tipping, C. P. Rinsland, M. A. H. Smith, D. C. Benner, V. M. Devi, J. M. Flaud, C. Camypeyret, A. Perrin, A. Goldman, S. T. Massie, L. R. Brown, and R. A. Toth, J. Quant. Spectrosc. Radiat. Trans. **48,** 469 (1992).
41. S. Lundqvist, J. Margolis, and J. Reid, Appl. Opt. **21,** 3109 (1982).
42. J. M. Hoell, C. N. Harward, C. H. Bair, and B. S. Williams, Opt. Eng. **21,** 548 (1982).
43. J.-M. Flaud, C. Camy-Peyret, C. P. Rinsland, M. A. H. Smith, and V. M. Devi, *Atlas of Ozone Spectral Parameters from Microwave to Medium Infrared* (Academic Press, Inc., Boston, 1990).
44. H. Stafast, W. E. Schmid, and K. L. Kompa, Opt. Commun. **21,** 121 (1977).
45. R. R. Gamache, N. Lacome, G. Pierre, and T. Gabard, J. Mol. Struct. **599,** 279 (2001).
46. J. A. Havens and T. O. Spicer, "Gravity Spreading and Air Entrainment by Heavy Gas Instantaneously Released in a Calm Atmosphere", in *Atmospheric Dispersion of Heavy Gases and Small Particles*, G. Ooms and H. Tennekes, Eds. (Springer-Verlag, Berlin, 1984).
47. L. Y. Chan and W. S. Kwok, Atmos. Environ. **34,** 4403 (2000).
48. J. H. Seinfeld and S. N. Pandis, *Atmospheric Chemistry and Physics, From Air Pollution to Climate Change* (John Wiley and Sons, New York, 1998).
49. S. Kingham, D. Briggs, P. Elliott, P. Fischer, and E. Lebret, Atmos. Environ. **34,** 905 (2000).

Molecular Physics
Vol. 108, No. 6, 20 March 2010, 723–731

Taylor & Francis
Taylor & Francis Group

INVITED ARTICLE

First analysis of the high resolution FTIR spectrum of the ν_2 band of the FCO_2 radical at 970.2 cm^{-1}

A. Perrin[a]*, M. Střižík[b], H. Beckers[c], H. Willner[c], Z. Zelinger[d], P. Pracna[d], V. Nevrlý[b] and E. Grigorová[bd]

[a]*Laboratoire Interuniversitaire des Systèmes Atmosphériques (LISA, UMR 7583 CNRS and Universities Paris Est and Paris 7-Diderot), Université Paris XII, 61 av du Général de Gaulle, 94010 Créteil Cedex, France;* [b]*VŠB - Technical University of Ostrava, Faculty of Safety Engineering, Lumírova 13, 700 30 Ostrava-Výškovice, Czech Republic;* [c]*FB C—Anorganische Chemie, Bergische Universität Wuppertal, Gaußstrasse 20, D-42097 Wuppertal, Germany;* [d]*J. Heyrovský Institute of Physical Chemistry, v.v.i., Academy of Sciences of the Czech Republic, Dolejškova 3, 182 23 Prague, Czech Republic*

(*Received 10 November 2009; final version received 24 November 2009*)

The infrared spectrum of the fluorocarboxyl radical, FCO_2, was recorded at high resolution (0.0035 cm^{-1}) in the 600–1400 cm^{-1} region on a Bruker IFS 120 HR Fourier transform spectrometer of the University of Wuppertal. The analysis of the A-type ν_2 band of FCO_2 (CF stretching mode) centred at 970.208 cm^{-1} was performed making use of the ground state parameters achieved by [L. Kolesniková, J. Varga, H. Beckers, M. Šimečková, Z. Zelinger, L. Nová Stříteská, P. Kania, H. Willner, and Š. Urban, J. Chem. Phys. **128**, 224302/1 (2008)]. For the FCO_2 radical, the ν_2 transitions are, in principle, split into two spin–rotation subcomponents corresponding to $J = N \pm 1/2$. However the spin–rotation parameters in the 2^1 vibrational state have values similar to those of the ground state, and spin–rotation doublings are observable only for the weaker transitions involving medium K_a or K_c values in the P and R branches. The ν_2 fundamental band is weakly perturbed by the $2\nu_5$ dark overtone band at 965.4 cm^{-1} and the 2^1 and 5^2 energy levels of FCO_2 are coupled through Fermi type resonances. The final energy level calculation was performed accounting both for the spin–rotation interaction within the 2^1 and 5^2 vibrational states, and the $2^1 \Leftrightarrow 5^2$ Fermi-type resonances.

Keywords: fluoroformyloxyl radical; high resolution IR spectrum; rotational analysis; spin–rotation interactions; Fermi resonances

1. Introduction

Recent interest in the fluorocarboxyl radical, FCO_2, is motivated because it is assumed to participate in atmospheric processes such as the degradation of hydrofluorocarbons that have been considered as chlorofluorocarbon substitutes [1–4]. On the other hand, FCO_2 is isoelectronic to NO_3 and the spectroscopic and thermodynamic properties of these free radicals are expected to be governed by vibronic interactions to low-lying electronic excited states [5–7]. The Born–Oppenheimer approximation breaks down for NO_3 [6,7], while there still exists little information on the spectroscopic properties of the FCO_2 radical.

Several results were achieved through *ab initio* calculations, like for example, the equilibrium structure of the FCO_2 radical which possesses C_{2v} symmetry in its ground state ($X\ ^2B_2$) and in the next highest states [5,8,9]. Also the standard enthalpy of formation of FCO_2 was calculated [9]. The highly structured absorption in the visible originating at 13,150 cm^{-1} was assigned, by comparison with *ab initio* calculations, to the $B^2A_1 \leftarrow X\ ^2B_2$ electronic transition by Maricq *et al.* [5,10], and from the observed progressions of hot bands, the ν_3 vibrational mode of FCO_2 in the $X\ ^2B_2$ ground state was measured at 520 cm^{-1}. From the study of photodetachment of the FCO_2^- ion, the ν_1, ν_2 and ν_3 mode of FCO_2 in $X\ ^2B_2$ are measured at 1465, 950 and 500 cm^{-1}, respectively [11]. In addition, the visible spectrum and the IR spectrum of natural FCO_2, $FC^{18}O_2$ and $F^{13}CO_2$ isolated in noble gas matrices was reported [12]. In this study the free FCO_2 radical was prepared by vacuum flash pyrolysis of bis(fluoroformy1) peroxide, FC(O)OOC(O)F, diluted in N_2, Ar, or Ne and, the six fundamental vibrational states for FCO_2 in the ground $X\ ^2B_2$ electronic state were assigned. For FCO_2 isolated in Ne

*Corresponding author. Email: agnes.perrin@lisa.univ-paris12.fr

ISSN 0026–8976 print/ISSN 1362–3028 online

DOI: 10.1080/00268970903514579
http://www.informaworld.com

the ν_1, ν_2 and ν_3 modes are at 1475, 960, and 519 cm^{-1} (A_1 symmetry), ν_4 and ν_5 at 1098 and 474 cm^{-1} (B_1 symmetry), and ν_6 at 735 cm^{-1} (B_2 symmetry). Tables 1 and 2 give the symmetry properties of the FCO_2 radical and a short description of the vibrational modes in the ground state $X\ ^2B_2$, respectively.

In [13] the first gas-phase detection of the FCO_2 radical by millimetre wave and high resolution infrared spectroscopy was performed guided by *ab initio* calculations. In this way the observed infrared bands ν_1 (1478 cm^{-1}), ν_2 (970 cm^{-1}) and ν_4 (1094 cm^{-1}) were identified. In this paper a detailed analysis of the FCO_2 radical was performed by microwave techniques, leading to a first set of ground state parameters including rotational, quartic centrifugal distortion, fine and hyperfine constants. Indeed FCO_2 is an open-shell molecular species, the coupling of the electron spin with rotation splits the rotational levels into two sublevels, and each of them is further split into a doublet by the hyperfine interaction due to the fluorine nuclear spin. The analysis of the millimeter wave measurements [13] was performed in the coupling scheme $\boldsymbol{J}=\boldsymbol{N}+\boldsymbol{S}$ and $\boldsymbol{F}=\boldsymbol{J}+\boldsymbol{I_F}$ between the rotational $\boldsymbol{N}$, electron spin $\boldsymbol{S}$, and ^{19}F nuclear spin $\boldsymbol{I_F}$ angular momenta. These ground state parameters were later improved by a subsequent millimetre wave analyses [14,15]. Finally, the electron paramagnetic resonance spectra of the fluoroformyloxyl radical FCO_2 isolated in noble gas matrices have been investigated leading to the determination of principal g values and ^{19}F hyperfine coupling constants of FCO_2 [16].

Little information exists on gas phase infrared band analysis of FCO_2. To our knowledge, there is only one ongoing infrared study, which concerns the ν_4 band (antisymmetric CO stretching) centered at 1094.1422 cm^{-1} [17]. One surprising result of the analysis of this rather unperturbed B-type band are the significant differences between the spin rotational constants of the 4^1 and those of the ground state.

The present study concerns the ν_2 band, centred at 970.20822 cm^{-1} (CF stretching mode) using high resolution spectra recorded at Wuppertal. This A-type

Table 1. Symmetry properties of FCO_2 in the $X\ ^2B_2$ ground electronic state. Vibration–rotational levels $(v_1v_2\ldots v_6)[N\ K_a\ K_c]$ exist only are for K_a odd if $v_4+v_5+v_6=$ even (resp. K_a even for $v_4+v_5+v_6=$ odd).

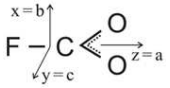

	I	C_{2z}	σ_{xz}	σ_{yz}	Polar vector	Axial vector	Ground electronic state	Vibration
A_1	1	1	1	1	T_z			ν_1, ν_2, ν_3
A_2	1	1	−1	−1		R_z		
B_1	1	−1	1	−1	T_x	R_y		ν_4, ν_5
B_2	1	−1	−1	1	T_y	R_x	$X\ ^2B_2$	ν_6

Table 2. List of the vibrational modes for FCO_2 in the $X\ ^2B_2$ ground electronic state.

Mode symmetry	Mode number		Experimental (Ne matrix)[a]	Experimental (gas phase)[b]
A_1	1	Symmetric CO stretch	1475	1478[c]
	2	CF stretch	960	970.2082[e]
	3	OCO scissor	519	
B_1	4	Antisymmetric CO stretch	1098	1094.42207[d]
	5	OCO rock	474	
B_2	6	OCO wagging	735	

Notes: [a]Fundamental vibration wavenumber (in cm^{-1}), Ref. [12].
[b]Band centres in cm^{-1}.
[c]Ref. [12].
[d]Ref. [17].
[e]This work.

band is perturbed for the high N values due to Fermi resonances involving the 5^2 overtone state. Contrary to what is observed during the ν_4 band study, the spin–rotational constants in the 2^1 excited vibrational state differ only marginally from those of the ground state.

2. Experimental details

FCO_2 radicals were generated in a flow system by pyrolysis of the peroxide FC(O)OOC(O)F at the entrance of a 1 m long White cell. The optical path length between the gold plated mirrors was adjusted to 36 m. The White cell was equipped at the entrance with the pyrolysis device consisting in a quartz tube (6 mm o.d.; 4 mm i.d.) with an electrical heating coil (Kantal wire) at the open end over a length of 20 mm. At the middle of the cell a capacitance pressure gauge (10 mbar MKS Baratron) and at the end a pump exit (flange diameter 40 mm) was attached. The cell was pumped through a 1 m long stainless steel bellow tube (40 mm i.d.) by a roots pump (500 m^3/h, Leybold Ruvac WS 501) to less than 10^{-3} mbar. At the pyrolysis device a cold U-trap containing the precursor and a needle valve for adjusting an argon gas flow was connected. Typical conditions for the generation of FCO_2 radicals were a flow rate of Ar of 30 to 100 mmol h^{-1} over the FC(O)OOC(O)F sample held at temperatures between −75 and −65°C.

During maximal pumping speed the resulting total pressure of the pyrolysis products together with excess of argon was in the range of 0.03 to 0.1 mbar inside the White cell. Under these conditions the residence time of the gas mixture in the cell is estimated to be about one second. It was found that pyrolysis temperatures of 300 to 350°C resulted in the highest concentration of FCO_2. At lower temperatures less precursor were dissociated and at higher temperatures FCO_2 were depleted. It was not possible to increase the concentration of FCO_2 to saturate the most intensive IR bands. By reducing the pump speed with a valve, the pressure and residence time of FCO_2 in the White cell increased, but dimerization occurred and its unimolecular dissociation became more important.

During the measurements a few grams of FC(O)OOC(O)F were needed in 1 h. FC(O)OOC(O)F was prepared by reacting a flow of a $F_2/O_2/CO$ (1 : 3 : 1) gas mixture at room temperature according to the literature procedures [12].

The IR spectra of FCO_2 were recorded on a Bruker HR 120 spectrometer at an apodized resolution (1/maximum optical path difference) of 0.003 cm^{-1} in the order of the Doppler width, and in the region 600 and 1400 cm^{-1} using a KBr beam splitter, an MCT600 detector, and an cut-off filter (>1400). Altogether 60 scans were co-added to obtain the final spectrum. The signal to noise ratio of the spectrum was ca. 20 : 1. Calibration was done by comparison with CO_2 lines [18].

3. Analysis

The fluorocarboxyl radical, FCO_2, is a planar oblate asymmetric rotor molecule of C_{2V} symmetry. Its symmetry axis is the a inertial axis, and the ν_2 mode is of A_1 symmetry type (see Table 1). The total wavefunction (involving the electronic, vibrational, rotational and nuclear spin contributions) remains unchanged under symmetry operations equivalent to the permutation of the two oxygens (with a zero nuclear spin $I(^{16}O) = 0$). Due to the symmetry ($X\,^2B_2$) of the ground electronic state, the existing vibration–rotation energy levels $(v_1 v_2 \ldots v_6)[N\ K_a\ K_c]$ in the ground electronic state are K_a = odd if $(v_4 + v_5 + v_6) =$ even (resp. K_a = even for $(v_4 + v_5 + v_6)$ = odd). Therefore for the ground and the 2^1 vibrational states, only rotational levels with odd values of K_a are allowed [12,15].

As expected from symmetry considerations (see Table 1), the ν_2 band is an A-type band (see Figure 1), and, as usual for planar oblate molecules, the P and R lines are grouped in clusters of lines keeping a constant value of $(2N–K_c)$, the spacing between two successive clusters being of about $2C$. Examples of such clusters

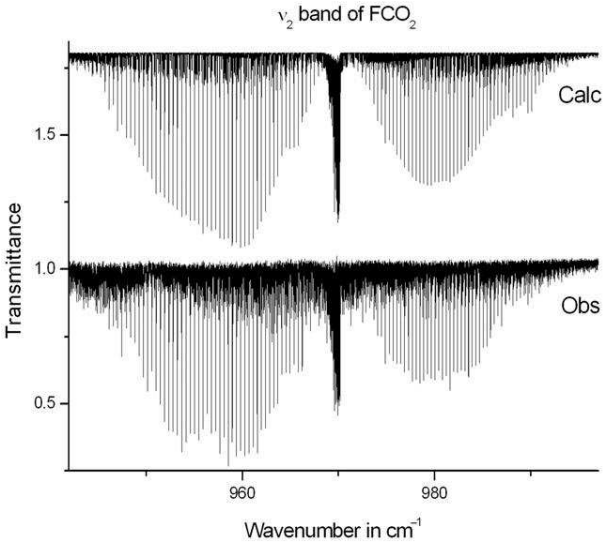

Figure 1. Overview of the 940–999 cm^{-1} spectral region with the ν_2 band of fluorocarboxyl radical, FCO_2. The lower trace corresponds to the experimental spectrum (T = 296 K). The upper trace is the line by line calculation for the ν_2 band of FCO_2.

are given for a portion of the R branch on Figure 2. Within these P and R clusters the strongest transitions which are those involving the low K_a values (starting from $K''_a = 1$) are overlapping, and the assignments within these clusters are often difficult: this is evidenced in Figures 2 and 3. In the Q branch, which is congested, the strongest transitions involve $K_a = J$ and very low K_c values. Series of $N_{N\ 1,0} \leftarrow N_{N\ 0,1}$ ($K_{c''} = 0$ and 1) transitions are easily observed in Figure 4, from which $A' < A''$ can be inferred.

For the FCO_2 radical, each [$N\ K_a\ K_c$] energy levels are split by the electron spin–rotation interactions into two subcomponents corresponding to $J = N \pm 1/2$. However, the spin–rotation parameters in the 2^1 vibrational excited state differ only marginally from those of the ground state. As we are dealing with an A-type band, the spin–rotation splittings have similar values in the upper and lower levels for transitions involving energy levels in the symmetric top limit either for high K_a ($K_a \sim N$, $K_c \ll N$) or for high K_c ($K_a \ll N, K_c \sim N$) values. For this reason, the spin rotation splittings are not observable in the spectrum for strong lines of the P and R branches, or in the Q branch, since these transitions involve very low K_a (P and R branches) and very high K_a values (Q branch), respectively. This is clearly evidenced in Figures 2–5. On the other hand, for weaker lines in the P and R branches involving medium K_a and K_c values ($1 \ll K_a \ll N$, and $0 \ll K_c \ll N$, respectively) the line doublings are clearly observable in the spectrum, since in this case the spin splittings in the upper and lower states differs significantly. Examples of these splittings are given in Figures 2, 3 and 5.

Finally, lets us mention that the hyperfine structure (of a few megahertz only) could not be observed during this infrared study. It is presumed that this hyperfine structure contributes to the apparent line width observed for the ν_2 transitions.

Some low and medium N and K_a transitions in the ν_2 band were first assigned. Then, using the ground state parameters of Ref. [15], the lower state spin–rotational energy levels were calculated and added to the newly observed line positions to get a list of experimental upper state energy levels. The upper state spin–rotational energy levels were inserted in a least squares fit to get an improved set of upper states parameters allowing better predictions and hence more assignments to be made.

This process was repeated iteratively until it appeared that several series were significantly perturbed for $N \geq 40$ values because of resonances involving the energy levels belonging to the 5^2 dark state located near 965 cm^{-1}. A model accounting for these resonances together with the spin–rotation

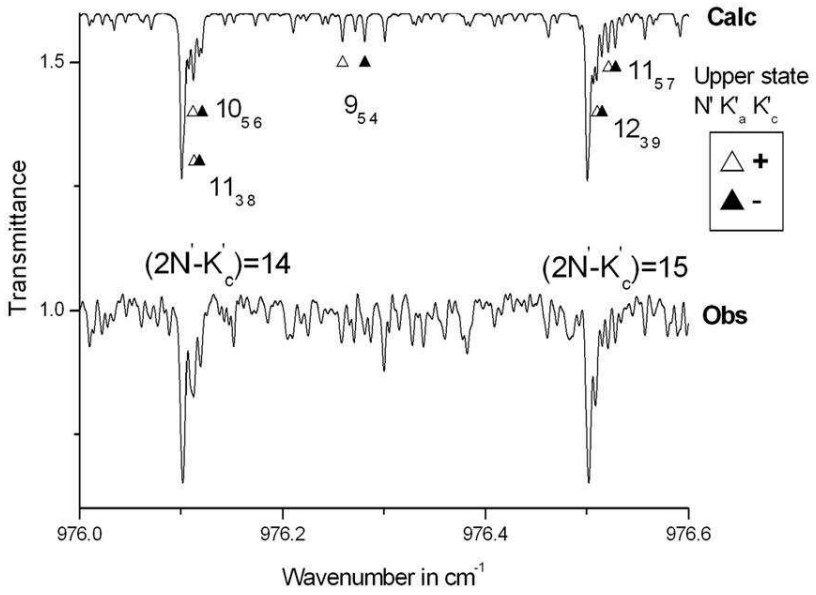

Figure 2. Part of R branch of the ν_2 band of FCO_2 near 976.3 cm^{-1}. Lower trace: experimental spectrum. Upper trace: calculated spectrum. Due to the values of the FCO_2 rotational constants ($A \sim B \sim 2C$) the lines are grouped in stacks of lines corresponding to the same ($2N$–K_c) values (see text). The quoted assignments are given for the upper N', K'_a and K'_c values, with two stacks of lines corresponding to $(2N' - K'_c) = 14$ and 15, respectively. For lines with medium K_a and K_c values, the spin–rotation splittings are observable and doublets of lines involving $J = N + 1/2$ and $J = N - 1/2$ in the upper levels are indicated by open triangles (△) and solid triangles (▲), respectively.

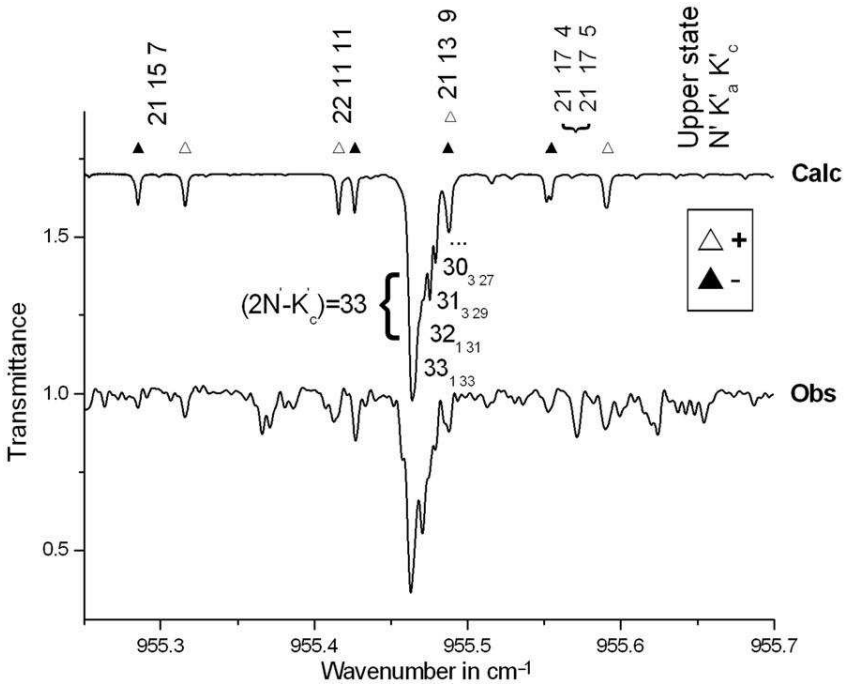

Figure 3. Part of P branch of the ν_2 band of FCO_2 near 955.4 cm^{-1}. Lower trace: experimental spectrum. Upper trace: calculated spectrum. The quoted assignments are given for the upper N', K'_a, and K'_c values for lines belonging to the $(2N' - K'_c) = 33$ stack, and for lines with medium K_a and K_c values. Only for the latter ones the spin-rotation splittings are observable and doublets of lines involving, $J = N + 1/2$ and $J = N - 1/2$ in the upper levels, are indicated by open triangles (△) and solid triangles (▲), respectively.

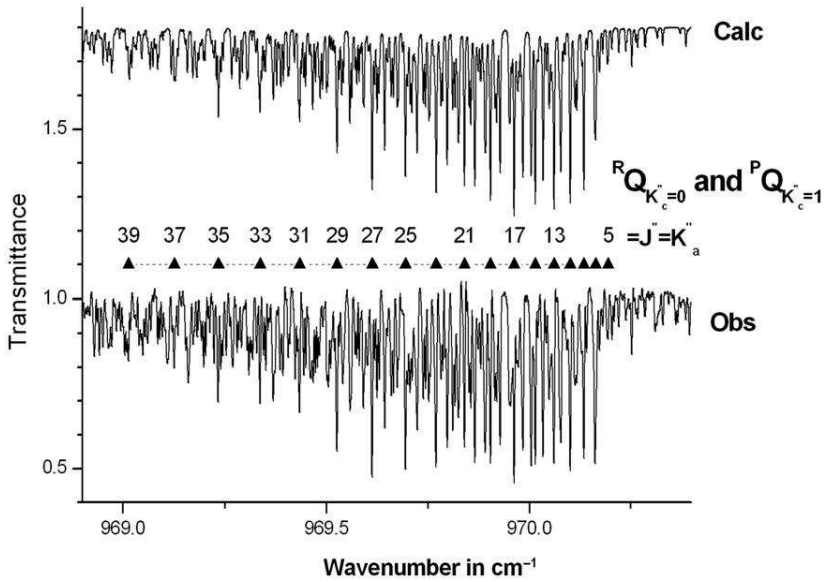

Figure 4. Q branch of the ν_2 band of FCO_2 in the 970.2 cm^{-1} spectral region. Several assignments (solid triangles ▲) are given for the degenerate ${}^{R}Q_{K''_c=0}$ and ${}^{P}Q_{K''_c=1}$ sub-branches, with $J = K_a$ ($\Delta J = \Delta K_a = 0$). In this case, the spin splittings are not observable.

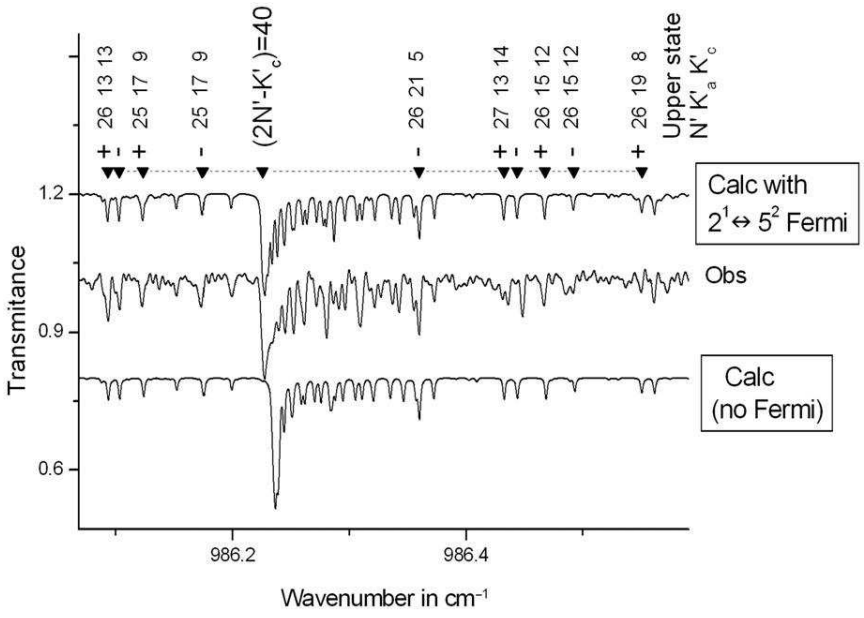

Figure 5. Part of R branch of the ν_2 band of FCO_2 near 986.3 cm^{-1}. The medium trace gives the experimental spectrum at the $(2N' - K'_c) = 40$ stack, and the upper and lower traces give the line by line model accounting and neglecting the $5^2 \Leftrightarrow 2^1$ Fermi resonances. Some transitions are assigned by the upper N', K'_a and K'_c values. The doublets of lines involving, $J = N + 1/2$ and $J = N - 1/2$ in the upper levels, are indicated by plus (+) and minus (−) signs, respectively.

interactions was then set up, which allowed more accurate predictions. To illustrate this point, Figure 5 gives a portion of the R branch at 986.3 cm^{-1}. For the $(2N - K_c) = 40$ stack, the line by line calculation is significantly improved when the $5^2 \Leftrightarrow 2^1$ Fermi type resonances are accounted for by the energy levels calculation. This iterative process was carried out until the ν_2 band was satisfactorily assigned. Table 3 gives an overview of the results of the present analysis. However, as the resonances coupling the 2^1 and 5^2 energy levels occur for rather high N values, the perturbed ν_2 lines are already weak and it was not possible to assign the resonating transitions belonging to the dark $2\nu_5$ band.

Some remaining lines could not be assigned in the spectrum: it is presumed that these lines belong to hot bands. Indeed, since the ν_5 and ν_3 vibrational states are located near 474 and 519 cm^{-1}, respectively, the $\nu_2 + \nu_5 - \nu_5$ and $\nu_2 + \nu_3 - \nu_3$ are assumed to contribute about 10% and 8%, respectively, to the total band intensity. However, the precise band head of these Q branch hot bands could not be located unambiguously.

Table 3. Range of the observed energy levels and the statistical analysis of the results of the energy level calculation.

ν_2 band	
2377 lines,	
1141 levels $N \leq 55$, $K_a \leq 39$	
Statistical analysis of the results	
Number of 2^1 Spin–rotation levels	1141
$0 \leq \delta < 0.001 cm^{-1}$	60.9%
$0.001 \leq \delta < 0.002 cm^{-1}$	22.1%
$0.002 \leq \delta < 0.004 cm^{-1}$	12.7%
$0.004 \leq \delta < 0.008 cm^{-1}$	4.3%
Standard deviation: $1.7 \times 10^{-3} cm^{-1}$ $\delta = \lvert E_{obs} - E_{calc} \rvert$	

4. Energy levels calculation

In order to explain the perturbations which were observed during the analysis of the ν_2 band starting from $N \sim 40$, one has to identify the dark states located in the vicinity of the 2^1 bright state. Indeed, the 5^2, $3^1 5^1$ and 3^2 states of A_1, B_1 and A_1 symmetry type are crudely estimated near 948, 993 and 1038 cm^{-1}, respectively, by extrapolating from the values of the ν_3 and ν_5 vibrational frequencies issued from the

Table 4. Hamiltonian matrix for the $\{2^1,5^2\}$ interacting vibrational states of FCO_2.

		J			
		2^1		5^2	
		$N=J+1/2$	$N=J-1/2$	$N=J+1/2$	$N=J-1/2$
2^1	$N=J+1/2$	$H_{vv}+V_{vv}^{SR}$	V_{vv}^{SR}	$H_{vv'}^{F}$	
	$N=J-1/2$	V_{vv}^{SR}	$H_{vv}+V_{vv}^{SR}$		$H_{vv'}^{F}$
5^2	$N=J+1/2$	c.c.		$H_{vv}+V_{vv}^{SR}$	V_{vvs}^{SR}
	$N=J-1/2$		c.c.	V_{vv}^{SR}	$H_{vv}+V_{vv}^{SR}$

Note: H_{vv}: Watson's A-type reduction, I^r representation Hamiltonian

$$\begin{aligned}H_{vv} = {} & E_v + [A^v - 1/2(B^v + C^v)]N_z^2 + 1/2(B^v + C^v)\boldsymbol{N}^2 + 1/2(B^v - C^v)N_{xy}^2 \\ & - \Delta_K^v N_z^4 - \Delta_{JK}^v N_z^2\boldsymbol{N}^2 - \Delta_J^v(\boldsymbol{N}^2)^2 - \delta_K^v\left\{N_z^2, N_{xy}^2\right\} - 2\delta_J^v N_{xy}^2\boldsymbol{N}^2 \\ & + H_K^v N_z^6 + H_{KJ}^v N_z^4\boldsymbol{N}^2 + H_{JK}^v N_z^2(\boldsymbol{N}^2)^2 + H_J^v(\boldsymbol{N}^2)^3 \\ & + h_K^v\left\{N_z^4, N_{xy}^2\right\} + h_{KJ}^v\left\{N_z^2, N_{xy}^2\right\}\boldsymbol{N}^2 + 2h_J^v N_{xy}^2(\boldsymbol{N}^2)^2 + \cdots\end{aligned}$$

Electron spin–rotation interaction in A-type reduction, I^r representation:

$$\begin{aligned}V_{vv}^{SR} = {} & \varepsilon_{aa}^v S_a N_a + \varepsilon_{bb}^v S_b N_b + \varepsilon_{cc}^v S_c N_c \\ & + \Delta_N^{vS}\boldsymbol{N}^2(\boldsymbol{N}.\boldsymbol{S}) + \frac{1}{2}\Delta_{NK}^{vS}\{\boldsymbol{N}^2 N_z S_z + S_z N_z\boldsymbol{N}^2\} + \Delta_{KN}^{vS}(\boldsymbol{N}.\boldsymbol{S}) \\ & + \Delta_K^{vS} N_z^3 S_z + \delta_N^{vS}(N_+^2 + N_-^2)(\boldsymbol{N}.\boldsymbol{S}) + \frac{1}{2}\delta_K^{vS}\{(N_+^2 + N_-^2)N_z S_z + N_z S_z(N_+^2 + N_-^2)\}.\end{aligned}$$

Fermi-type interactions:

$$H_{vv'}^{F} = h_{vv'}^{0F} + h_{vv'}^{1F}\boldsymbol{N}^2 + h_{vv'}^{2F}N_{xy}^2 + \cdots$$

with: c.c.: complex conjugate, $\{A,B\} = AB + BA$ and $N_{xy}^2 = N_x^2 - N_y^2$.

Ne matrix measurements [12] (see Table 2). We tried several types of energy level calculations depending on the symmetry type of the dark states, which are assumed to be responsible for the observed resonances. Indeed, C-type Coriolis involving the $3^1 5^1 \Leftrightarrow 2^1$ resonating levels, Fermi resonances coupling either the $5^2 \Leftrightarrow 2^1$ or the $3^2 \Leftrightarrow 2^1$ resonating energy levels were considered for these test calculations. It appeared that the resonances are satisfactorily accounted for when considering only the $5^2 \Leftrightarrow 2^1$ Fermi resonances, and this is in agreement with the conclusions of the infrared investigation of the vibrational structure of FCO_2 in noble gas matrices performed by Argüello *et al.* [12].

The final calculation was performed considering the v-diagonal part of the Hamiltonian both spin–rotation [19] and Watson-type rotational operators written in I^r representation with an A-type reduction [20]. This choice of reduction and type of representation for the FCO_2 oblate asymmetric top is justified because it allows a straightforward comparison with the ground state parameters achieved in [13–15]. In addition this Hamiltonian involves Fermi-type operators in the $5^2 \Leftrightarrow 2^1$ off-diagonal blocks. The theoretical details are given in [21], and the final form of the Hamiltonian matrix is given in Table 4.

The experimental 2^1 spin–rotational energy levels obtained in this work were introduced in a least squares fit using this Hamiltonian model. Table 5 lists the Hamiltonian parameters (band centres, rotational, spin–rotation and coupling constants) resulting from the fit, together with their associated statistical uncertainties. Some constants were maintained at their ground state values [15], like for example the spin–rotation constants of the 5^2 dark state. For the 5^2

Table 5. Vibrational energies, rotational, and spin–rotation constants, as well as coupling constants for the $\{2^1, 5^2\}$ interacting vibrational states of FCO_2.

	Band centres and rotational constants		
	0	2^1	5^2
E_v		970.20822(18)	$965 \pm 2\,cm^{-1}$
A	0.4587249990	0.45791846(250)	0.460609(130)
B	0.3772716164	0.37618883(100)	0.379831(110)
C	0.2065695418	0.206146680(570)	0.20887147(910)
Δ_K	5.17792×10^{-7}	$4.2771(620) \times 10^{-7}$	#
Δ_{NK}	-9.67002×10^{-9}	$97.94(450) \times 10^{-9}$	#
Δ_N	2.60737×10^{-7}	$2.08360(400) \times 10^{-7}$	$0.63592(260) \times 10^{-6}$
δ_K	3.58732×10^{-7}	$3.8698(190) \times 10^{-7}$	#
δ_N	1.12616×10^{-7}	$0.81826(300) \times 10^{-7}$	#
H_K		$5.671(770) \times 10^{-11}$	
H_{KN}		$-6.862(990) \times 10^{-11}$	
h_K		$-3.972(500) \times 10^{-11}$	
Spin–rotation constants			
ε^v_{aa}	-2.77982×10^{-3}	$-2.7732(160) \times 10^{-3}$	#
ε^v_{bb}	-2.65044×10^{-2}	$-2.73083(150) \times 10^{-2}$	#
ε^v_{cc}	-1.47348×10^{-3}	$-1.39817(670) \times 10^{-3}$	#
Δ^{vS}_K	5.2036×10^{-7}	#	#
$\Delta^{vS}_{KN} + \Delta^{vS}_{NK}$	-6.5979×10^{-7}	#	#
Δ^{vS}_N	1.3496×10^{-7}	#	#
Δ^{vS}_{NK}	0	#	#
δ^{vS}_K	-1.0064×10^{-7}	#	#
δ^{vS}_N	6.6046×10^{-8}	#	#
Coupling constants			
Fermi		$5^2 \Leftrightarrow 2^1$	
J^2		$h^{1F}_{55,2} = 1.8283(480) \times 10^{-4}$	
J^2_{xy}		$h^{2F}_{55,2} = 4.862(490) \times 10^{-5}$	

Note: The results are in cm^{-1} and the quoted errors are one standard deviation. Constants marked with # were fixed to the ground state values [15] during the least squares fit.

dark state we estimated the accuracy of the vibrational energy to be about $2\,cm^{-1}$, and the achieved rotational constants are rather effective ones: indeed, the resonances coupling the 5^2 and 2^1 energy levels begin to be significant only for $N > 40$, and it is difficult, at this stage, to predict accurately the position of the 5^2 resonating levels. In addition, it is not possible to estimate the rotational constants of 5^2 from those of 5^1 since no high resolution study exists so far for the ν_5 fundamental band.

Finally, as can be seen in Table 5 the spin–rotation parameters in the 2^1 differ marginally from those of the ground state. In contrast, an ongoing study of the ν_4 band [17] revealed a large vibrational dependence of the spin–rotation parameters, which probably can be traced back to a vibronic coupling to a nearby B^2A_1 electronic state via the ν_4 vibrational mode.

As far as the $5^2 \Leftrightarrow 2^1$ Fermi interaction constants are concerned, it was not possible to determine the zero-order constant $h^{0F}_{55,2}$, which was maintained at zero during the calculations.

The results of the energy levels calculations proved to be rather satisfactory, as can be seen from the standard deviation and statistical analysis given in the lower part of Table 3.

Finally, Figures 1–5 give detailed comparisons between the observed and calculated spectra in various spectral regions. For these comparisons, the relative line intensities of the spin–rotational sub-components were computed, using the tensorial method which is described in [22] to account for the spin–rotation interaction.

5. Conclusions

The first high resolution analysis of the ν_2 band of the fluorocarboxyl radical, FCO_2, centred at $970.208\,cm^{-1}$

was performed using spectra recorded at high resolution at Wuppertal. Because the spin–rotation parameters in the 2^1 upper state are similar to the ground state values, spin–rotation doublings for this A-type band are observable only for the weaker transitions involving medium K_a or K_c values in the P and R branches. The ν_2 fundamental band is weakly perturbed by a Fermi-type resonance coupling the 2^1 and 5^2 energy levels. The final energy level calculation was performed accounting both for the spin–rotation resonances within the 2^1 and 5^2 vibrational states, together with the $2^1 \Leftrightarrow 5^2$ Fermi-type interactions.

Acknowledgements

A.P. is grateful to the INSU (Institut national des sciences de l'Univers) of the CNRS for financial support. M.S. is grateful to the three months post-doc position of the 'European Science Foundation' through the 'Interdisciplinary Tropospheric Research: from the Laboratory to Global Change' (INTROP) Project. We appreciate support from the Deutsche Akademische Austauschdienst (DAAD, PPP-Tschechien, D22-CZ 12/09-10) for the German–Czech collaboration, for support from MEYS of the Czech Republic provided via Research program LC06071 and a grant OC09050 (action COST ES0604) and H.B. and H.W. acknowledge financial support from the Deutsche Forschungsgemeinschaft (DFG).

References

[1] J.M. Heras, A.J. Arvia, P.J. Aymonino, and H.J. Schumacher, Z. Phys. Chem. **28**, 250 (1961).
[2] A.J. Arvia, P.J. Aymonino, and H.J. Schumacher, Z. Anorg. Allg. Chem. **316**, 327 (1962).
[3] S. von Ahsen, H. Willner, and G.A. Argüello, J. Fluor. Chem. **125**, 1057 (2004).
[4] J.S. Francisco and M.M. Maricq, Acct. Chem. Res. **29**, 391 (1996).
[5] W.F. Schneider, M.M. Maricq, and J.S. Francisco, J. Chem Phys. **103**, 6601 (1995).
[6] J.F. Stanton, Mol. Phys. **107**, 1059 (2009).
[7] H. Beckers, H. Willner, and M.E. Jacox, Chem. Phys. Chem. **10**, 706 (2009).
[8] J.S. Francisco and A. Ostafin, Mol. Phys. **68**, 255 (1989).
[9] J. Breidung and W. Thiel, J. Phys. Chem. A **110**, 1575 (2006).
[10] M.M. Maricq, J.J. Szente, Z. Li, and J.S. Francisco, J. Chem. Phys. **98**, 784 (1993).
[11] D.W. Arnold, S.E. Bradforth, E.H. Kim, and D.M. Neumark, J. Chem. Phys. **102**, 3493 (1995).
[12] G.A. Argüello, H. Grothe, M. Kronberg, and H. Willner, J. Phys. Chem. **99**, 17525 (1995).
[13] Z. Zelinger, P. Drean, A. Walters, J.R.A. Moreno, M. Bogey, H. Pernice, S. von Ahsen, H. Willner, J. Breidung, W. Thiel, and H. Bürger, J. Chem. Phys. **118**, 1214 (2003).
[14] Z. Zelinger, S. Bailleux, D. Babánková, M. Šimečková, L. Stříteská, L. Kolesniková, P. Musil, P. Kania, Š. Urban, and H. Beckers, J. Mol. Spectrosc. **243**, 292 (2007).
[15] L. Kolesniková, J. Varga, H. Beckers, M. Šimečková, Z. Zelinger, L. Nová Stříteská, P. Kania, H. Willner, and Š. Urban, J. Chem. Phys. **128**, 224302/1 (2008).
[16] H. Beckers, H. Willner, D. Grote, W. Sander, and J. Geier, J. Chem. Phys. **128**, 224301/1 (2008).
[17] S. Bailleux, E. Grigorová, Z. Zelinger, H. Beckers and H. Willner. Poster J28 presented at the 20st International Conference on High Resolution Molecular Spectroscopy, Praha, Czech Republic, 2008.
[18] G. Guelachvilli and K. Narahari Rao, *Handbook of Infrared Standards* (Academic Press, San Diego, 1986).
[19] J.M. Brown and T.J. Sears, J. Mol. Spectrosc. **75**, 111 (1979).
[20] J.K.G. Watson, in *Vibrational Spectra and Structure*, edited by J.R. Durig (Elsevier, Amsterdam, 1977), Vol. 6.
[21] A. Perrin, J.-M. Flaud, C. Camy-Peyret, A.M. Vasserot, G. Guelachvili, A. Goldman, F.J. Murcray, and R.D. Blatherwick, J. Mol. Spectrosc. **154**, 391 (1992).
[22] A. Perrin, J.-M. Flaud, and C. Camy-Peyret, Mol. Phys. **63**, 791 (1988).

The Astrophysical Journal, 679:920–924, 2008 May 20

THE SUBMILLIMETER-WAVE SPECTRUM OF THE CS^+ RADICAL ION

Stéphane Bailleux,[1] Adam Walters,[2] Eva Grigorova,[1] and Laurent Margulès[1]
Received 2007 September 26; accepted 2007 December 1

ABSTRACT

The submillimeter-wave spectrum of the CS^+ radical cation in its ground electronic state ($X\,^2\Sigma^+$) has been observed for the first time, in a flowing positive column discharge in a CS_2-Ar mixture partially cooled with a limited flow of liquid nitrogen. Nine rotational transition frequencies were recorded between 414 and 622 GHz, leading to the determination of accurate molecular constants $B_0 = 25908.8560(41)$ MHz, $D_0 = 41.344(18)$ kHz, and $\gamma_0 = 597.629(41)$ MHz, which we use to predict transition frequencies up to the terahertz region in order to stimulate new attempts at astronomical detection.

Subject headings: methods: laboratory — molecular data — techniques: spectroscopic

1. INTRODUCTION

Many sulfur compounds such as HCS^+ (Thaddeus et al. 1981), C_2S (Saito et al. 1987), C_3S (Yamamoto et al. 1987; Bell et al. 1993), and C_5S (Bell et al. 1993) have been observed in the interstellar medium. The first molecule containing sulfur that was detected in interstellar space was carbon monosulfide (Penzias et al. 1971). CS is present in a variety of astrophysical environments, such as dense clouds and star-forming regions (Hasegawa et al. 1984; Hayashi et al. 1985; Walker et al. 1986; Hauschildt et al. 1993), diffuse clouds (Drdla et al. 1989), circumstellar envelopes (Lindqvist et al. 1988), the shocked molecular gas associated with the supernova remnant IC 443 (van Dishoeck et al. 1993), carbon-rich stars (Bregman et al. 1978), and comets (Smith et al. 1980; Jackson et al. 1982). Although CS has a low ionization potential (11.335 eV; Huber & Herzberg 1979), the CS^+ radical cation has proved elusive and has not been identified in the interstellar medium. No direct experimental measurement of its rotational spectrum has yet been published.

In the laboratory, two electronic band systems of CS^+ are known and have been measured between the near-infrared and UV regions. Coxon et al. (1976) first measured the CS^+ $A\,^2\Pi_i$–$X\,^2\Sigma^+$ system excited by the reaction of metastable He with CS_2. The rotational analysis of observed electronic spectra of CS^+ has revealed that some vibrational levels of the $A\,^2\Pi_i$ state, especially the $v' = 1$, $v' = 5$, and $v' = 6$ levels, are strongly perturbed by high vibrational levels of the $X\,^2\Sigma^+$ state. Gauyacq & Horani (1978) recorded the rotationally resolved emission spectrum and carried out a deperturbation analysis of the (2, 0), (3, 0), (4, 0), and (5, 0) bands. They used a low-pressure hot-cathode discharge through carbon disulfide to create the ion. Later, Horani & Vervloet (1992) reexamined this system using Fourier transform emission spectroscopy between 5800 and 14,000 cm^{-1}. Production was again with metastable He and CS_2. Subsequently, Liu et al. (2000) measured the near-infrared absorption spectrum of the (1, 0) band of the ion using velocity modulation laser spectroscopy. For production they used an AC discharge in a flowing mixture of CS_2 and helium. This was followed by another measure of the (5, 0) band, a new measure of the (6, 0) band, a new deperturbation analysis, and a new set of equilibrium constants for both the *X*- and *A*-states (Liu et al. 2002). Finally, the (7, 1) band was measured (Duan et al. 2003). Cossart (1994) has also recorded the $B\,^2\Sigma^+$–$X\,^2\Sigma^+$ system in the UV region from 230 to 330 nm. Attempts to identify the electronic spectrum of CS^+ in interstellar space by absorption in the line of sight to stars have proved unsuccessful (Ferlet et al. 1986).

Measurement of the submillimeter spectrum provides more precise rotational frequencies but is less sensitive than electronic spectroscopy. The laboratory study of ions is complicated by the difficulty in producing them with a sufficient number density in an absorption cell and because of their short lifetime. Optimal production conditions are often different from those used in electronic and vibrational spectroscopy, since, for example, total cell pressure should be lower in the submillimeter region in order to avoid excessive line broadening. The use of helium as a buffer gas is often reported in electronic and vibrational spectroscopy in discharges used to create ions, whereas it is our experience that argon produces the best results (see, e.g., Civiš et al. 1998). For all these reasons, a certain number of fundamental ions such as CS^+ have not yet been observed in the submillimeter region despite the publication of their electronic and vibrational spectra. For CS^+, two additional experimental difficulties may explain the lack of identification of the laboratory rotational spectrum up to the present. First, the precursor CS_2 is a liquid (melting point $-111\,^\circ$C at atmospheric pressure), so that, a priori, the cell cannot be cooled to liquid-nitrogen temperature (Dixon & Woods 1975) as is often done to increase the signal of ions produced from gaseous precursors. Second, magnetically enlarged negative glow discharges, used to enhance positive ion concentration (De Lucia et al. 1983), cannot be used for CS^+, since it is an open shell. In addition, the low ab initio calculated dipole moment of CS^+ in its ground vibronic state (0.509 D; Blöcker et al. 1990) is not favorable for its detection by conventional absorption-spectroscopy techniques.

We report here first measurements of the millimeter-wave spectrum of CS^+, produced in a flowing positive column discharge in a CS_2-Ar mixture. The objective is mainly to provide precise frequencies for astrophysical work, which should aid detection of the ion or help to confirm upper limits on its number density.

Quarta & Singh (1981) suggested that CS^+ could be a potential interstellar molecule and suggested some reactions in which it could be produced. Horani & Vervloet (1992) also discussed this. An involvement of the cation in the formation of CS in diffuse clouds has also been proposed (Drdla et al. 1989). An extensive compilation of reactions involving CS^+ (for both its formation and destruction) is given in the UMIST database (Woodall et al.

[1] Laboratoire de Physique des Lasers, Atomes et Molécules, UMR CNRS 8523, CERLA, Université des Sciences et Technologies de Lille, F-59655 Villeneuve d'Ascq Cedex, France; stephane.bailleux@univ-lille1.fr.
[2] Centre d'Etude Spatiale des Rayonnements, CNRS, Université Paul Sabatier, F-31028 Toulouse Cedex 4, France.

2007),[3] where its chemistry can be compared with CO^+, a similar reactive ion that has already been detected in space. There are a number of formation routes for CS^+ that have rate constants similar overall to those quoted for CO^+. For example, the ion can be formed by a reaction between H^+ and CS. Analogously to CO^+, CS^+ reacts with H_2, the dominant collision partner in space, to form HCS^+ (McAllister 1978; Decker et al. 2001) and could be an important intermediate in the formation of the latter. As is the case for CO^+, CS^+ could have a detectable abundance in sources where the formation is rapid and hydrogen is mostly in the H^+ ionized atomic form. CO^+ has been detected in various photodissociation regions (NGC 7027 and M17 SW [Latter et al. 1993; Störzer et al. 1995; Fuente et al. 2003], the Orion bar [Störzer et al. 1995; Fuente et al. 2003], NGC 7023 [Fuente & Martín-Pintado 1997; Fuente et al. 2003], Mon R2 and G29.960−02 [Rizzo et al. 2003], and S140 and NGC 2023 [Savage & Ziurys 2004]), including toward the prototypical starburst galaxy M82 (Fuente et al. 2006). Observations indicate that its total column density remains roughly constant for a wide range of densities and UV radiation fields (Rizzo et al. 2003). CO^+ has also been tentatively detected in the X-ray–dominated region toward the nucleus of the galaxy Cygnus A (Fuente et al. 2000), and the formation of CO^+ in M82 has also been attributed principally as being due to X-ray radiation (Spaans & Meijerink 2007). In general, chemical models fail to account for the observed reactive ions' column densities (Black 1998; Fuente et al. 2000), which are generally much higher than predicted. Modeling of gas-phase chemistry in translucent, dark and dense, and diffuse clouds also fails to predict correct abundances of sulfur-bearing molecules (Lucas & Liszt 2002). Hence, a search for the elementary sulfur-containing reactive ion CS^+ is particularly interesting, to verify and refine chemical models and to provide additional information, for example, on possible missing mechanisms.

As expected, we failed to find lines of CS^+ in the spectral survey of the solar-type protostar IRAS 16293−2422 (Castets et al. 2005) to which we had immediate access. Frequencies were also sent to J. Cernicharo in Madrid, who checked in both his 2 mm and 3 mm spectral surveys. Lines of CS^+ were not seen in the spectra of IRC +10216, and no firm identification could be made in the spectrum of Orion. The possibility has also been evoked that the spectra of CS^+ could be observed in comets (Smith et al. 1980; Leach 1987).

Accurate predictions may now be made over the whole range of Earth-based millimeter and submillimeter telescopes, as well as within the range of the high spectral resolution HIFI instrument (Heterodyne Instrument for the Far-Infrared) of the *Herschel Space Observatory*, due for launch in 2008. The relatively small dipole moment of CS^+ may also complicate its astrophysical detection. The ALMA (Atacama Large Millimeter Array) international interferometer will come into service in the next decade, providing unprecedented sensitivity and allowing new searches to be made for previously unidentified potential astrophysical species.

2. EXPERIMENTAL OBSERVATIONS

The spectrometer used in this experiment has been described extensively elsewhere (Bailleux et al. 2002). Measurements were taken between 414 and 622 GHz. The submillimeter-wave radiation was provided by two phase-locked backward-wave oscillators (a Thomson-CSF carcinotron below 470 GHz and a tube from the Istok company [Russia] above 518 GHz). A liquid-helium–cooled InSb bolometer (QMC Instruments) was used as detector. For improved sensitivity, we used frequency modulation at 42 kHz and lock-in detection at twice the modulation frequency, resulting in a second-derivative line shape.

In order to search for the CS^+ ion, we set up a positive column discharge in CS_2. The absorption cell was a 2 m long, 5 cm internal diameter, double-jacketed Pyrex tube, allowing liquid-nitrogen flow through the outer jacket to cool the plasma. The precursor CS_2 was introduced together with argon, allowing in situ production of reactive species. Liquid CS_2 was provided by Sigma-Aldrich (spectrophotometric grade, with purity of 99%) and used without further purification. It was degassed by using freeze-pump-thaw cycles and stored in darkness. The precursor gas (vapor pressure 296 torr at 20°C) was mixed with the carrier gas flow before it entered the absorption cell's inlet.

For the measurement of the near-infrared spectrum of CS^+, discharge currents in the range 140–200 mA were used by Liu et al. (2000, 2002), and the absorption cell was kept at room temperature. Liu et al. also reported that CS_2 should be present in a trace amount and that its partial pressure was rather critical for the detection of the cation.

In order to observe the millimeter-wave spectrum of CS^+, we found it necessary to cool the cell using a limited flow of liquid nitrogen, that is to say, with the outer jacket of the cell partially filled. The optimum discharge current was 200 mA, and the partial pressures (measured at room temperature) giving the best signal-to-noise ratio were respectively 6 and 2 mtorr for Ar and CS_2. We first searched for the two strongest fine-structure components ($J = 9\frac{1}{2} \leftarrow 8\frac{1}{2}$ and $J = 8\frac{1}{2} \leftarrow 7\frac{1}{2}$) of the $N = 9 \leftarrow 8$ transition using predictions based on the work of Liu et al. (2002). We identified both transitions (around 466 GHz) close to the predictions. The frequency interval of 597.7 MHz between the transitions matched accurately the value of γ_0, the fine-splitting constant (597.696 ± 0.420) MHz given in the aforementioned work. An example of the $(N, J) = (9, 9\frac{1}{2}) \leftarrow (8, 8\frac{1}{2})$ line is depicted in Figure 1. Following a further measurement of the two strongest $N = 8 \leftarrow 7$ lines around 414 GHz, we were able to make a new preliminary fit leading to accurate predictions (±400 kHz) for the transitions falling in the 518–622 GHz frequency range. Five new lines were accordingly identified within ±200 kHz of the predictions, securing the identification of the CS^+ ion. In total, nine transitions have been measured in the range 414–622 GHz, corresponding to $7 \leq N'' \leq 11$; Table 1 lists the observed frequencies. Because of the weak signal-to-noise ratio, each line was measured three times, and the experimental uncertainty indicated in Table 1 was deduced from the reproducibility of the measurements. The uncertainty also corresponds to that typically determined in similar measurements with comparable signal-to-noise ratio.

Even under optimum conditions, lines of the cation were near the detection limit of our spectrometer, and the conditions used were critical for their observation. For comparison, the major isotopologue of CS saturated our detection system under the same conditions, and the intensity of the $J = 9 \leftarrow 8$ $C^{34}S$ line (433750.984 MHz; Gottlieb et al. 2003) is around 2 orders of magnitude higher than the lines of the CS^+ ion. At room temperature, lines of CS^+ were not observed. If the cell was cooled beyond the optimum value, lines diminished and disappeared. This is due to a rapid reduction of partial pressure of CS_2, as evidenced by a similar extinction of the line of $C^{34}S$. Our present experimental setup does not allow precise control of the temperature inside the cell, which would be an extensive technical challenge. Hence, the temperature was adjusted dynamically by increasing and reducing liquid-nitrogen flow to optimize line intensity.

Ions produced in a discharge have an axial drift velocity that may Doppler-shift line frequencies in single-pass setups such as used here. This shift, used for velocity modulation detection in

[3] See http://www.udfa.net.

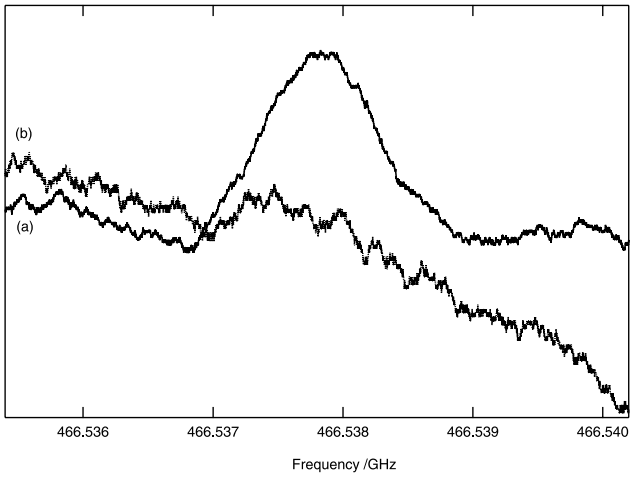

FIG. 1.—Recording of the $(N, J) = (9, 9\frac{1}{2}) \leftarrow (8, 8\frac{1}{2})$ rotational transition of CS^+ in the ground electronic state $X\,^2\Sigma^+$ (averaged over 48 acquisitions with 10 ms of lock-in time constant) (*a*) without and (*b*) with a magnetic field applied.

the infrared, is much smaller in millimeter-wave measurements but may in certain cases be large enough to be detected (Civiš et al. 1998). The shift was not measurable for lines attributed to CS^+; however, there are several explanations. First, the shift is small (typically tens to hundreds of kilohertz) and difficult to identify in cases of low signal-to-noise ratio as here. Second, ion mobility is related to molecular weight and is expected to be most significant for light ions; it is relevant to compare the value of the shift of 12 kHz at 560 GHz obtained by Cazzoli & Puzzarini (2005) for the lighter ion N_2H^+ with our experimental uncertainties of over 50 kHz. Third, it has been our experience in previous measurements of other ions that the size of the Doppler shift is strongly dependent on discharge conditions (as the electric field "seen" by the ions changes); in this case it was not possible to change the conditions without the lines disappearing. Fourth, the method available to us to show this shift was to reverse the polarity of the discharge; however, this led to noisy discharge conditions and even worse signal-to-noise ratio. Finally, for the ions that are produced in the negative glow region, which is a nearly field-free region, no frequency shift due to drift velocity would be expected to be observed (De Lucia et al. 1983; Hirao & Amano 2003 and references therein). Since no magnetic field can be used, this region is small but is that in which a far higher concentration of cations is expected; hence, it is difficult to determine the relative contribution of the negative glow and positive column regions to the observed signal.

We are nevertheless confident that the identification of CS^+ is secure for several reasons, listed below. For the first two lines observed no others were seen in a 20 MHz range, and subsequent lines were seen where predicted. All pairs of lines of the same J have the correct fine splitting and, as expected, similar intensities. All nine new measured lines fit correctly and with the infrared results, giving similar constants to those already published for the cation. With a single precursor molecule (CS_2), the number of species that can be formed is limited, even allowing for oxygen-containing species resulting from small air leaks. The observed transitions do not correspond to known frequencies for species such as CS, C_2S, C_3S, SO, and SO_2. The cell was equipped with a solenoid coil to generate an axial magnetic field (100 G, typically) in the discharge plasma in order to distinguish between paramagnetic and nonparamagnetic absorption signals. All lines attributed to the ion were, as expected, paramagnetic, which rules out all nonradical species.

TABLE 1
OBSERVED TRANSITION FREQUENCIES OF CS^+ IN THE GROUND $X\,^2\Sigma^+$ STATE

N''	J''	Observed[a] (MHz)	Obs. − Calc. (MHz)
7	$6\frac{1}{2}$	414158.125(80)	−0.092
	$7\frac{1}{2}$	414755.898(80)	0.058
8	$7\frac{1}{2}$	465940.013(50)	−0.028
	$8\frac{1}{2}$	466537.696(50)	0.033
9	$8\frac{1}{2}$	517712.932[b]	...
	$9\frac{1}{2}$	518310.565(80)	0.008
10	$9\frac{1}{2}$	569475.989(60)	0.086
	$10\frac{1}{2}$	570073.514(60)	−0.012
11	$10\frac{1}{2}$	621227.961(60)	0.004
	$11\frac{1}{2}$	621825.509(60)	−0.070

[a] Values in parentheses are 1 σ experimental error on the last digits.
[b] Calculated line.

3. RESULTS AND DISCUSSION

Each rotational level (except $N = 0$) of CS^+ is split into two sublevels ($N + \frac{1}{2}$ and $N - \frac{1}{2}$) by coupling with the spin of the unpaired electron. For each rotational transition, a triplet of lines is possible: two corresponding to $\Delta J = \Delta N = 1$ and one to $\Delta J = 0$ (2 orders of magnitude weaker in our frequency range). The observed absorption lines were all found approximately 4 MHz higher in frequency than predictions made using the molecular constants obtained by Liu et al. (2002). The accurate predictions were very valuable for us, owing to the low signal-to-noise ratio of the rotational spectrum combined with the critical experimental conditions to produce the CS^+ cation. All lines were found within 1 σ uncertainty of the predictions, permitting an obvious identification in laboratory measurements with a limited number of possible species in the cell. However, this offset could cause confusion in astrophysical spectra resulting from many different species, especially for weaker lines making up the spectrally dense "grass" of close-lying lines observed in objects showing chemical complexity.

Our new measured frequencies were then included in a global analysis including the 852 ground-state combination differences deposited as an EPAPS document by Liu et al. (2002). The program SPFIT (Pickett 1991) was used for the weighted linear least-squares fitting procedure, which gave a standard deviation of 50 kHz. The measured lines fit well with the ground-state combination differences, and the determination of the molecular parameters has, as expected, improved. Parameters are given in Table 2, together with the constants derived previously by Horani & Vervloet (1992) and Liu et al. (2002) for comparison. It is interesting to note that our results for the rotational and centrifugal parameters B_0 and D_0 are closer to the former (earlier) published work, although taking into

TABLE 2
MOLECULAR CONSTANTS FOR THE GROUND $X\,^2\Sigma^+$ STATE OF CS^+

Constant (MHz)	Horani & Vervloet[a]	Liu et al.[b]	This Work[c]
B_0	25908.99(34)	25908.57(22)	25908.8560(41)
$10^3 D_0$	41.07(30)	40.94(17)	41.344(18)
γ_0	596.89(90)	597.70(42)	597.629(41)

NOTE.—Values in parentheses are 1 σ errors in units of the last digits.
[a] Horani & Vervloet 1992.
[b] Liu et al. 2002.
[c] Values obtained from a global fit including 852 ground-state combination differences.

TABLE 3
SELECTION OF PREDICTED ROTATIONAL LINES OF CS^+ ($X\,^2\Sigma^+$)

$N' \leftarrow N''$	$J' \leftarrow J''$	Frequency[a] (MHz)	$\log A_{21}(s^{-1})$[b]	Energy Level (cm^{-1})
1 ← 0	1/2 ← 1/2	51219.917(42)	−6.869	0.0000
	3/2 ← 1/2	52116.361(22)	−6.847	0.0000
2 ← 1	3/2 ← 1/2	103335.287(27)	−5.955	1.7085
	5/2 ← 3/2	103932.916(25)	−5.868	1.7384
3 ← 2	5/2 ← 3/2	155149.857(31)	−5.346	5.1554
	7/2 ← 5/2	155747.486(30)	−5.311	5.2052
4 ← 3	7/2 ← 5/2	206961.450(36)	−4.941	10.3306
	9/2 ← 7/2	207559.079(34)	−4.921	10.4004
5 ← 4	9/2 ← 7/2	258769.074(39)	−4.634	17.2341
	11/2 ← 9/2	259366.703(37)	−4.621	17.3238
6 ← 5	11/2 ← 9/2	310571.737(41)	−4.386	25.8657
	13/2 ← 11/2	311169.366(39)	−4.377	25.9754
7 ← 6	13/2 ← 11/2	362368.447(41)	−4.179	36.2253
	15/2 ← 13/2	362966.076(39)	−4.172	36.3549
8 ← 7	15/2 ← 13/2	414158.125(80)[c]	−4.000	48.3126
	17/2 ← 15/2	414755.898(80)[c]	−3.995	48.4621
9 ← 8	17/2 ← 15/2	465940.013(50)[c]	−3.843	62.1274
	19/2 ← 17/2	466537.696(50)[c]	−3.838	62.2969
10 ← 9	19/2 ← 17/2	517712.932(31)	−3.703	77.6695
	21/2 ← 19/2	518310.565(80)[c]	−3.699	77.8589
11 ← 10	21/2 ← 19/2	569475.989(60)[c]	−3.576	94.9386
	23/2 ← 21/2	570073.514(60)[c]	−3.573	95.1479
12 ← 11	23/2 ← 21/2	621227.961(60)[c]	−3.461	113.9342
	25/2 ← 23/2	621825.538(60)[c]	−3.458	114.1635
13 ← 12	25/2 ← 23/2	672968.115(62)	−3.355	134.6562
	27/2 ← 25/2	673565.745(62)	−3.353	134.9054
14 ← 13	27/2 ← 25/2	724695.368(90)	−3.258	157.1040
	29/2 ← 27/2	725292.997(90)	−3.255	157.3731
15 ← 14	29/2 ← 27/2	776408.729(125)	−3.167	181.2772
	31/2 ← 29/2	777006.358(125)	−3.165	181.5663
16 ← 15	31/2 ← 29/2	828107.206(166)	−3.082	207.1754
	33/2 ← 31/2	828704.835(167)	−3.080	207.4844
17 ← 16	33/2 ← 31/2	879789.807(215)	−3.002	234.7981
	35/2 ← 33/2	880387.436(216)	−3.000	235.1270
18 ← 17	35/2 ← 33/2	931455.540(271)	−2.927	264.1447
	37/2 ← 35/2	932053.170(272)	−2.925	264.4936
19 ← 18	37/2 ← 35/2	983103.413(336)	−2.856	295.2148
	39/2 ← 37/2	983701.042(336)	−2.854	295.5835
20 ← 19	39/2 ← 37/2	1034732.433(408)	−2.788	328.0076
	41/2 ← 39/2	1035330.063(409)	−2.787	329.3963

[a] Values in parentheses are 1 σ errors in units of the last digits
[b] Base-10 logarithm of the Einstein coefficient for spontaneous emission with $\mu = 0.509$ D.
[c] Measured frequency.

account the uncertainties, this may be coincidental. However, the value we determined for the spin-rotation constant γ_0 was closer to that of Liu et al. (2002). We also performed a fit including solely our submillimeter-wave transitions, and the molecular constants obtained are nearly identical.

The parameters can be used to predict accurate transition frequencies of astrophysical interest up to the terahertz region. Selected calculations are reported in Table 3 up to just over 1 THz. The significantly weaker $\Delta J = 0$ transitions are not given except for $N = 1 \leftarrow 0$, where only two transitions are possible. Also, the difference in intensity between $\Delta J = 0$ and the other transitions increases rapidly with N and is not significant for the first rotational transition. We have also included 1 σ uncertainties, as well as energy levels and Einstein A-coefficients, which can be used to predict astrophysical spectra in various conditions. To situate in the commonly used astrophysical unit, the 1 σ estimated uncertainty of around 35 kHz at 207 GHz corresponds to around 0.05 km s^{-1}.

Additional rotational transition frequencies or predictions of astrophysical intensities are available upon request to the authors.[4] During this work, we also observed transitions of CCS and CCCS. These molecules are also of astrophysical interest, and presently spectra are only reported to 300 GHz (Lovas et al. 1992). We hence plan to publish measurements up to 650 GHz in the near future.

4. SUMMARY

We have measured nine lines of the rotational spectrum of the CS^+ radical cation in its ground electronic and vibrational state, allowing accurate determination of the molecular parameters, which have been used to calculate precise transition frequencies up to the terahertz region. Other information needed for simulating astrophysical spectra is provided. It is hence hoped to stimulate searches

[4] At adam.walters@cesr.fr.

for the rotational spectrum of this species, in particular in photodissociation regions and X-irradiated molecular gas.

CERLA is partly supported by the French Research Ministry, the Nord-Pas-de-Calais Region, and the European Funds for Regional Economic Development. S. B. and E. G. thank the ARCUS (Actions en Régions de Coopération Universitaire et Scientifique) program and the QUASAAR network for financial support of this project. A. W. thanks the Observatoire Midi-Pyrénées for financing his travel to Lille for the measurements. An undergraduate project student, Audrey Coutens, also participated in the experimental work.

REFERENCES

Bailleux, S., Bogey, M., Demuynck, C., Liu, Y., & Walters, A. 2002, J. Mol. Spectrosc., 216, 465
Bell, M. B., Avery, L. W., & Feldman, P. A. 1993, ApJ, 417, L37
Black, J. H. 1998, Faraday Discuss., 109, 257
Blöcker, J. H., Reinsch, E.-A., Rosmus, P., Werner, H.-J., & Knowles, P. J. 1990, Chem. Phys., 147, 99
Bregman, J. D., Goebel, J. H., & Strecker, D. W. 1978, ApJ, 223, L45
Castets, A., et al. 2005, in ASP Conf. Ser. 344, The Cool Universe: Observing Cosmic Dawn, ed. C. Lidman & D. Alloin (San Francisco: ASP), 212
Cazzoli, G., & Puzzarini, C. 2005, J. Chem. Phys., 123, No. 041101
Civiš, S., Walters, A., Tretyakov, M. Yu., Bailleux, S., & Bogey, M. 1998, J. Chem. Phys., 108, 8369
Cossart, D. 1994, J. Mol. Spectrosc., 167, 11
Coxon, J. A., Marcoux, P. J., & Setser, D. W. 1976, Chem. Phys., 17, 403
Decker, B. K., Adams, N. G., & Babcock, L. M. 2001, Int. J. Mass Spectrom., 208, 99
De Lucia, F. C., Herbst, E., Plummer, G. M., & Blake, G. A. 1983, J. Chem. Phys., 78, 2312
Dixon, T. A., & Woods, R. C. 1975, Phys. Rev. Lett., 34, 61
Drdla, K., Knapp, G. R., & van Dishoeck, E. F. 1989, ApJ, 345, 815
Duan, C., Wu, L., Chen, Y., & Liu, Y. 2003, J. Mol. Spectrosc., 217, 146
Ferlet, R., Roueff, E., Czarny, J., & Felenbok, P. 1986, A&A, 168, 259
Fuente, A., Black, J. H., Martín-Pintado, J., Rodríguez-Franco, A., García-Burillo, S., Planesas, P., & Lindholm, J. 2000, ApJ, 545, L113
Fuente, A., García-Burillo, S., Gerin, M., Rizzo, J. R., Usero, A., Teyssier, D., Roueff, E., & Le Bourlot, J. 2006, ApJ, 641, L105
Fuente, A., & Martín-Pintado, J. 1997, ApJ, 477, L107
Fuente, A., Rodríguez-Franco, A., García-Burillo, S., Martín-Pintado, J., & Black, J. H. 2003, A&A, 406, 899
Gauyacq, D., & Horani, M. 1978, Canadian J. Phys., 56, 587
Gottlieb, C. A., Myers, P. C., & Thaddeus, P. 2003, ApJ, 588, 655
Hasegawa, T., et al. 1984, ApJ, 283, 117
Hauschildt, H., Güsten, R., Phillips, T. G., Schilke, P., Serabyn, E., & Walker, C. K. 1993, A&A, 273, L23
Hayashi, M., Omodaka, T., Hasegawa, T., & Suzuki, S. 1985, ApJ, 288, 170
Hirao, T., & Amano, T. 2003, ApJ, 597, L85
Horani, M., & Vervloet, M. 1992, A&A, 256, 683
Huber, K.-P., & Herzberg, G. 1979, Molecular Spectra and Molecular Structure IV: Constants of Diatomic Molecules (New York: Van Nostrand Reinhold)
Jackson, W. M., Halpern, J. B., Feldman, P. D., & Rahe, J. 1982, A&A, 107, 385
Latter, W. B., Walker, C. K., & Maloney, P. R. 1993, ApJ, 419, L97
Leach, S. 1987, A&A, 187, 195
Lindqvist, M., Nyman, L.-Å., Olofsson, H., & Winnberg, A. 1988, A&A, 205, L15
Liu, Y., Duan, C., Liu, J., Wu, L., Xu, C., Chen, Y., Hamilton, P. A., & Davies, P. B. 2002, J. Chem. Phys., 116, 9768
Liu, Y., Liu, H., Gao, H., Duan, C., Hamilton, P. A., & Davies, P. B. 2000, Chem. Phys. Lett., 317, 181
Lovas, F. J., Suenram, R. D., Ogata, T., & Yamamoto, S. 1992, ApJ, 399, 325
Lucas, R., & Liszt, H. S. 2002, A&A, 384, 1054
McAllister, T. 1978, ApJ, 225, 857
Penzias, A. A., Solomon, P. M., Wilson, R. W., & Jefferts, K. B. 1971, ApJ, 168, L53
Pickett, H. M. 1991, J. Mol. Spectrosc., 148, 371
Quarta, M. L., & Singh, P. D. 1981, A&A, 98, 384
Rizzo, J. R., Fuente, A., Rodríguez-Franco, A., & García-Burillo, S. 2003, ApJ, 597, L153
Saito, S., Kawaguchi, K., Yamamoto, S., Ohishi, M., Suzuki, H., & Kaifu, N. 1987, ApJ, 317, L115
Savage, C., & Ziurys, L. M. 2004, ApJ, 616, 966
Smith, A. M., Stecher, T. P., & Casswell, L. 1980, ApJ, 242, 402
Spaans, M., & Meijerink, R. 2007, ApJ, 664, L23
Störzer, H., Stutzki, J., & Sternberg, A. 1995, A&A, 296, L9
Thaddeus, P., Guélin, M., & Linke, R. A. 1981, ApJ, 246, L41
van Dishoeck, E. F., Jansen, D. J., & Phillips, T. G. 1993, A&A, 279, 541
Walker, C. K., Lada, C. J., Young, E. T., Maloney, P. R., & Wilking, B. A. 1986, ApJ, 309, L47
Woodall, J., Agúndez, M., Markwick-Kemper, A. J., & Millar, T. J. 2007, A&A, 466, 1197
Yamamoto, S., Saito, S., Kawaguchi, K., Kaifu, N., Suzuki, H., & Ohishi, M. 1987, ApJ, 317, L119

Journal of Molecular Spectroscopy 256 (2009) 99–101

Contents lists available at ScienceDirect

Journal of Molecular Spectroscopy

journal homepage: www.elsevier.com/locate/jms

Allan variance for optimal signal averaging—monitoring by diode–laser and CO_2 laser photo-acoustic spectroscopy

Jan Skřínský [a,b], Radmila Janečková [a,b], Eva Grigorová [a,b], Michal Střižík [b,c], Pavel Kubát [a], Lenka Herecová [b], Václav Nevrlý [b,c], Zdeněk Zelinger [a,*], Svatopluk Civiš [a]

[a] J. Heyrovský Institute of Physical Chemistry, v.v.i., Academy of Sciences of the Czech Republic, Dolejškova 3, 182 23 Prague 8, Czech Republic
[b] Faculty of Safety Engineering, VSB-Technical University of Ostrava, Lumírova 13, 70030 Ostrava 3-Výškovice, Czech Republic
[c] Institute of Thermomechanics, v.v.i., Academy of Sciences of the Czech Republic, Dolejškova 5, 18200 Prague 8, Czech Republic

ARTICLE INFO

Article history:
Received 30 December 2008
In revised form 28 January 2009
Available online 21 February 2009

Keywords:
Allan variance
Diode laser spectroscopy
Photo-acoustic spectroscopy

ABSTRACT

The concept of the Allan variance has been utilized to test the detection abilities of two powerful experimental methods for trace gas monitoring: IR diode–laser and CO_2 laser photo-acoustic spectroscopy. The detection of stable molecules (OCS, allene, CH_3OH), and unstable species (ozone, short-lived free radical CN and molecular ion ArD^+) have been compared. An approach for studies of the influence of the reactivity on the optimal averaging time for the minimum detectable concentration is demonstrated.

Usually the output data are mean values from an averaging process and the detection limit is calculated on the basis of the variance of this mean. Increasing the stability of the system provides improvements in the detection limit. Stability tests based on the Allan variance method have become a standard procedure for the evaluation of the quality of an instrument. The Allan variance distinguishes high frequency random noise from drifts at longer time scales. An important characteristic of the Allan variance analysis is that it is insensitive to the deterministic content of the analyzed signal (e.g., bias, linear slope, and sine component). The stabilities of the IR diode–laser and the CO_2 laser photo-acoustic spectrometer are analyzed in this paper in terms of the Allan variance [1,2].

Diode–laser absorption spectroscopy is frequently used for monitoring very small concentration levels [3–5] of different stable and unstable species, including radicals and molecular ions. CO_2 laser photo-acoustic spectrometry is a very powerful tool for monitoring trace gases. The achievement of high sensitivity by a diode–laser system requires a long pathway due to a multi-pass absorption cell. An improvement in sensitivity of a CO_2 laser photo-acoustic spectrometry system depends on the reduction of noise levels. Further sensitivity improvement of these detection schemes by signal averaging is limited by the stability of the whole experimental system [4]. The characterization of trace gas analyzers has been performed by Allan variance and this concept has become a well-established tool for researchers to describe the performance of laser-optical trace gas sensors [6,7].

The Allan variance σ_A^2 is calculated for a set of ***m-1*** subgroups of ***k*** classes (where $k = N/m$) that contain ***x*** values of measured data (N) and is plotted over the integration time ***t***:

$$\langle \sigma_A^2(k) \rangle_t = \frac{1}{2(m-1)} \sum_{s=1}^{m-1} (A_{2,s} - A_{1,s})^2 \quad (1)$$

$$A_s(k) = \frac{1}{k} \sum_{L=1}^{k} x_{(s-1)k+L} \quad (2)$$

The Allan-plot shows how the noise influences the measurement, i.e., at low integration time white noise dominates and the Allan variance decreases proportionally to the integration time, while the drift influence begins to dominate after the optimum integration time. The optimum integration time is in the minimum of the Allan-plot.

The concept of the Allan variance has been utilized to test the detection abilities of both frequently used detection systems for trace gas monitoring: the IR diode–laser and the CO_2 laser photo-acoustic spectrometer. Selected observed molecules such as C_3H_4, OCS, CH_3OH, O_3, ArD^+ and CN radical are examples of stable and unstable species. They have different levels of reactivity and different "lifetimes" in the measured medium. We tried to demonstrate the influence of reactivity on the optimal averaging time for the minimum detectable concentration.

The description employed for the diode laser spectrometer was presented in [8,9]. The diode laser (Laser Components GmbH) was placed in a laser head cooled by a He cryostat. The laser was temperature and current controlled using Laser Photonics units, model

* Corresponding author. Fax: +420 2 86582307.
E-mail address: zelinger@jh-inst.cas.cz (Z. Zelinger).

0022-2852/$ - see front matter © 2009 Elsevier Inc. All rights reserved.
doi:10.1016/j.jms.2009.02.006

L5731, at a temperature of 30–70 K. A lens was used to focus the laser beam into a (Czerny–Turner) monochromator to separate the single laser modes from the spectrum. The radiation leaving the monochromator was directed into either a reference cell, a Ge etalon (0.04 cm^{-1}), or into an absorption cell loaded with the gas being studied. The absorption spectrum was recorded with a photoconductor InSb detector operated at liquid nitrogen temperature. The signal from the detector was fed into a lock-in amplifier. The diode–laser spectrometer was tested by means of the Allan variance of stable molecules (OCS, C_3H_4), a short-lived free radical (CN radical) and a molecular ion (ArD^+).

Experimental set-ups aimed at the application of CO_2 laser photo-acoustic spectrometry are described in our previous works [10–12]. The photo-acoustic cell was a thermally stabilized brass tube with a length of 38 cm and a diameter of 8 mm. Detection was performed on longitudinal acoustical resonance (modulation frequency 1.2 kHz; the phase is set on the maximum of the photo-acoustic signal). The CO_2 laser photo-acoustic spectrometer was tested by means of the Allan variance of a stable molecule (CH_3OH) and a reactive molecule (O_3).

At low integration times, white noise ($\langle\sigma_A^2(k)\rangle_t \sim 1/t$) dominates (decreasing dashed lines—seen in Figs. 1 and 2). After the optimal integration time, the influence of the linear drift ($\langle\sigma_A^2(k)\rangle_t \sim t^{\alpha}$, $\alpha = 1$–2) starts (increasing dashed lines—seen in Figs. 1 and 2). The Allan plots of Figs. 1 and 2 are the main results of the stability testing of both detection systems considered: the diode laser and the CO_2 laser photo-acoustic spectrometer. The lack of substantial differences in the Allan plots of both experimental systems proves the universality of the concept of the Allan variance. However, there are interesting differences in the linear drift of ArD^+ (Fig. 1b) and other species (Figs. 1a, c, d and 2). The optimal integration times for other species, with the exception of the molecular ion, are in good agreement with published results [6]. The main difference between the molecular ion and other species is the difference in the "lifetimes" of the observed species in the measured medium. The "lifetime" is on the level of microseconds for the molecular ion and on the level milliseconds to seconds for other species, including the CN radical and stable molecules. The time constant of the lock-in amplifiers used was 1 s. The Allan variance was obtained at a time interval of 1000 s. The optimal integration times for stable molecules (C_3H_4, OCS, CH_3OH, O_3) and the CN radical are approximately 100 s, in contrast to the molecular ion (ArD^+), which indicates the most sensitive measurements at about 400 s. The optimal integration times (determined on the basis of the Allan variance) are on a similar level for stable molecules and for reactive ozone using both detection systems (Figs. 1a, c, d and 2). The only substantial difference is found for the molecular ion used (Fig. 1b). The explanation of this difference lies in the substantial variation in the lifetime of ArD^+ (one order and more) in comparison to other measured species.

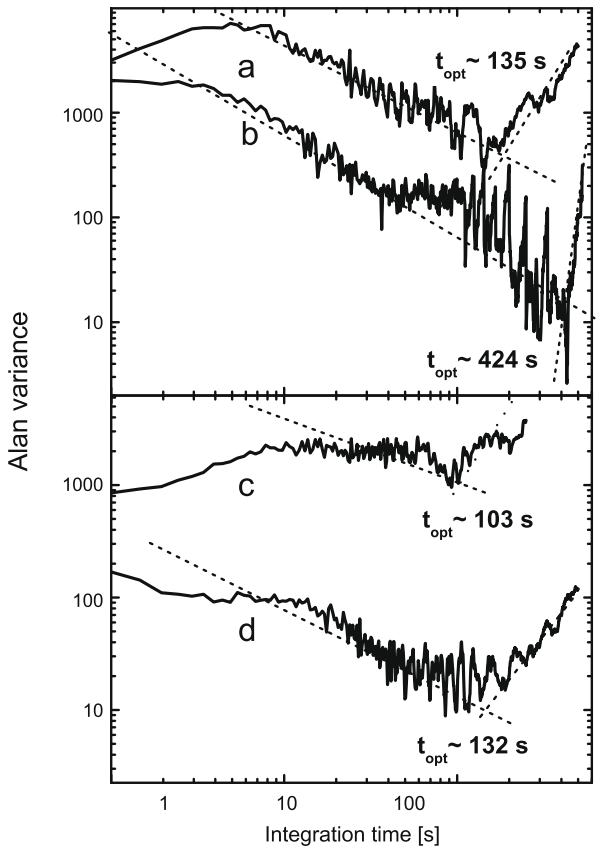

Fig. 1. Results of the diode–laser spectrometer tests by means of the Allan variance for unstable molecules: (a) short-lived CN radical, (b) and molecular ion ArD^+, and for stable molecules: (c) C_3H_4, (d) OCS.

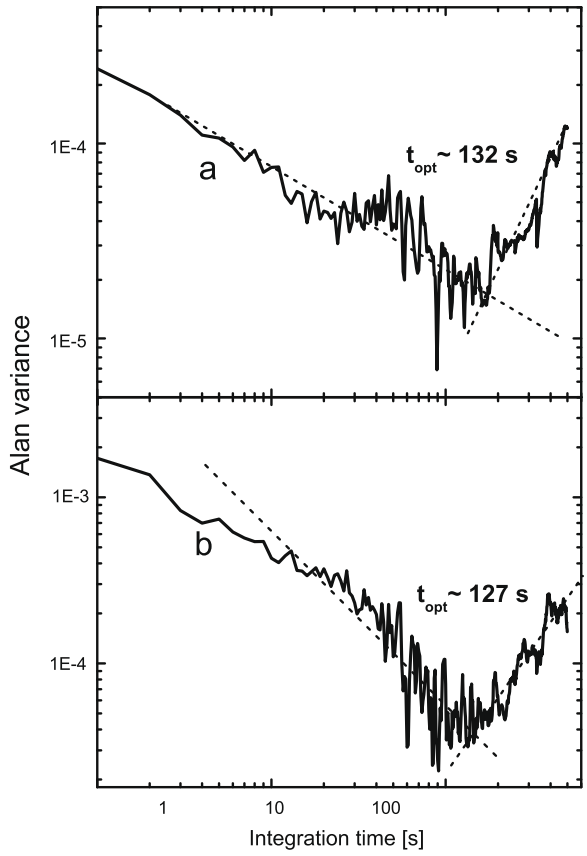

Fig. 2. Results of the CO_2 laser photo-acoustic spectrometer tests by means of the Allan variance (a) for a stable molecule (CH_3OH) and (b) for a reactive molecule (O_3).

The Allan plot provides information about the optimum averaging time. This study shows that the Allan variance can also be used to analyze the performance of a detection system in the case of detection of species with substantially different reactivity and therefore different lifetimes.

Acknowledgments

The authors gratefully acknowledge the financial support from the Ministry of Education, Youth and Sports of the Czech Republic

provided via Grants Nos. OC111, OC186 (within the frame of the EU COST 729 Action) and the Research program LC06071, the support from the Czech Science Foundation (grant no. 202/06/0216) and the European Community Research Infrastructure Action under the FP6 Structuring the European Research Area Programme, EUSAAR Contract N RII3-CT-2006-026140.

References

[1] D.W. Allan, IEEE Trans. Ultrason. Ferr. 34 (1987) 647–654.
[2] D.W. Allan, Proc. IEEE 54 (1966) 221–230.
[3] D.D. Nelson, B. McManus, S. Urbanski, S. Herndon, M.S. Zahniser, Spectroch. Acta A 60 (2004) 3325–3335.
[4] H. Cattaneo, T. Laurila, R. Hernberg, Appl. Phys. B 85 (2006) 337–341.
[5] A. Fried, B. Henry, B. Wert, S. Sewell, J.R. Drummond, Appl. Phys. B 67 (1998) 317–330.
[6] P. Werle, R. Mucke, F. Slemr, Appl. Phys. B 57 (1993) 131–139.
[7] L. Joly, B. Parvitte, V. Zeninari, G. Durry, Appl. Phys. B 86 (2007) 743–748.
[8] Z. Zelinger, S. Civiš, P. Kubát, P. Engst, Infrared Phys. Technol. 36 (1995) 537–543.
[9] Z. Zelinger, P. Kubát, J. Wild, Chem. Phys. Lett. 368 (2003) 532–537.
[10] Z. Zelinger, M. Střižík, P. Kubát, Z. Jaňour, P. Berger, A. Černý, P. Engst, Opt. Lasers Eng. 42 (2004) 403–412.
[11] Z. Zelinger, I. Jančík, P. Engst, Appl. Opt. 31 (1992) 6974–6975.
[12] Z. Zelinger, M. Střižík, P. Kubát, S. Civiš, Analytica Chimica Acta 422 (2000) 179–185.